



Climatology of sediment flux and composition in the subarctic Northeast Pacific Ocean with biogeochemical implications



D.A. Timothy, C.S. Wong[†], J.E. Barwell-Clarke, J.S. Page, L.A. White, R.W. Macdonald^{*}

Institute of Ocean Sciences, Fisheries and Oceans Canada, 9860 West Saanich Road, Sidney, BC V8L 4B2, Canada

ARTICLE INFO

Article history:

Received 21 March 2011
Received in revised form 7 April 2013
Accepted 14 June 2013
Available online 24 June 2013

ABSTRACT

Sequentially sampling conical sediment traps were maintained at Ocean Station Papa (OSP; 50°N, 145°W) in the Alaska Gyre from September 1982 to June 2006. The time series began with a single trap at 3800 m and traps were added at 1000 m and 200 m in March 1983 and May 1989, respectively. A trap at 3500–3700 m also was moored 5° north of OSP from May 1990 to August 1992. Total mass, biogenic silica (BSi), calcium carbonate (CaCO₃), particulate organic carbon (POC) and particulate nitrogen (PN) were routinely measured. In this paper, we develop climatologies of sediment flux and composition at OSP, describing the characteristic features for comparison to sedimentary conditions globally. We then expand our use of the climatologies to arrive at four main conclusions regarding ecology and geochemistry at OSP. Fluxes of BSi and CaCO₃ at 200 m and 1000 m lag by one month the annual cycle of irradiance and arrive at 3800 m ~16 d later, with maximum export occurring several months later for POC. Next, the annual cycle of BSi flux shows that diatom production in late winter and spring is higher than indicated by spring decline of surface nutrients. We then show that the annual cycle of POC flux implies a net community production of organic carbon (NCP_{OC}) of 3.6–5.3 mol m⁻² y⁻¹, double estimates based on mixed layer tracers but similar to estimates unaffected by mixing. NCP_{OC}, combined with a CaCO₃:POC production ratio of 0.18 determined from trap fluxes, gives a net community production of CaCO₃ (NCP_{IC}) of 0.65–0.95 mol m⁻² y⁻¹, in agreement with CaCO₃ dissolution in the water column plus abyssal CaCO₃ flux. Lastly, the flux climatologies at 1000 m and 3800 m are used to infer particle transformations in the bathypelagic zone including disaggregation and remineralization. Fluxes at 3800 m are best described as the sum of a primary flux sinking rapidly and a slowly-sinking secondary flux. Disaggregation of the primary flux is the likely source of secondary fluxes, with a lithogenic component transported horizontally also reaching the 3800-m traps. A detailed description of the sampling also is provided so future experiments can benefit from the successes and failures encountered at OSP.

Crown Copyright © 2013 Published by Elsevier Ltd. All rights reserved.

1. Introduction

1.1. Setting

The sequestration of sinking particles into the ocean's interior is a critical marine biogeochemical pathway that can be continuously monitored using bottom-tethered sediment traps, but only a few time series span more than 15 years (Honjo et al., 2008). The longest trap record, from the Sargasso Sea in the North Atlantic Ocean (Ocean Flux Program; 31.8°N, 64.1°W) (Conte et al., 2001; Deuser, 1996), has been maintained since 1978, and in the Arabian Sea (Haake et al., 1996) and the Bay of Bengal (Ittekkot et al., 1991) traps have been maintained since 1987. Another long time series was collected in the California Current upwelling region (34.8°N,

123.0°W) between 1989 and 2004 (Smith et al., 2006), and traps have been maintained since 1997 in the subarctic Northwest Pacific Gyre (Honda et al., 2002). These and other sediment-trap collections (Buesseler et al., 2007; Honjo et al., 2008) have shown that deep particle flux is closely linked to surface processes (Deuser and Ross, 1980; Fischer et al., 1988; Wong et al., 1999), that transformations including organic matter attenuation occur as particles sink (Bacon et al., 1985; Bishop, 1989; Lee et al., 2004), and that long-term trends may be observed in deep-ocean particle flux (Deuser et al., 1995; Smith and Kaufmann, 1999).

At Ocean Station PAPA (OSP; 50°N, 145°W) in the southern portion of the Alaska Gyre (Fig. 1), traps were moored from 1982 to 2006. The deep waters here are among the longest removed from the surface in the global thermohaline circulation (Broecker and Peng, 1982; Sarmiento et al., 2007), making the Alaska Gyre a cornerstone for monitoring long-term responses of the oceans to natural and anthropogenic forcing. OSP is well located within this domain, since regionally low mesoscale variability (Cummins

^{*} Corresponding author. Tel.: +1 250 363 6409.

E-mail address: Robie.macdonald@dfp-mpo.gc.ca (R.W. Macdonald).

[†] Deceased on June 6, 2013.

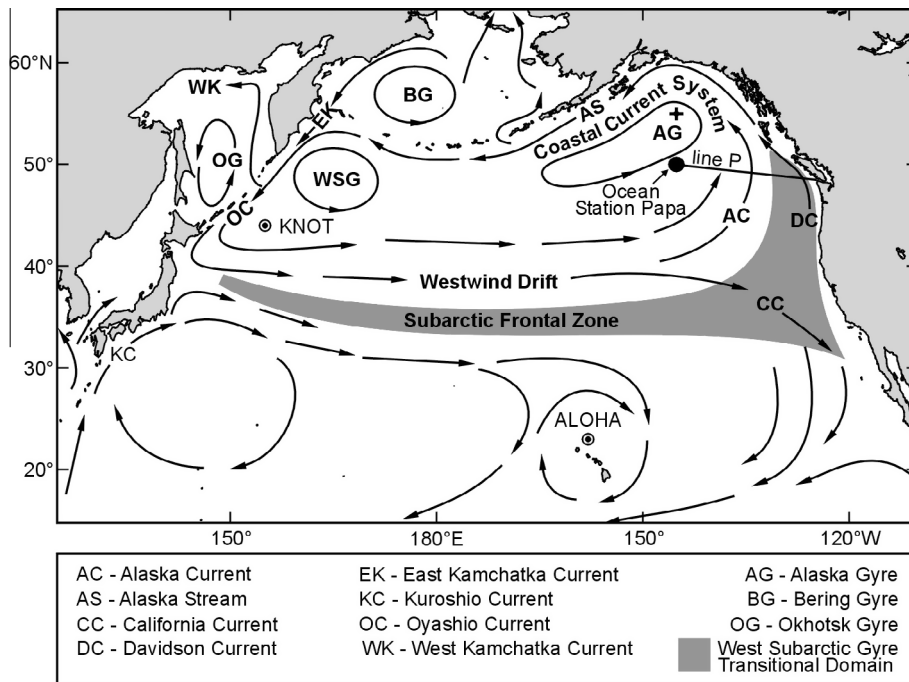


Fig. 1. Mooring locations.

and Lagerloef, 2004) allows records from OSP to be extrapolated to a large area. Oceanographic and atmospheric data were collected routinely from weatherships at OSP between 1951 and 1981 (McCain et al., 1996). Since then, oceanographic sampling has occurred ~three times a year along Line P from the continental shelf to OSP (Fig. 1). The flux characteristics presented here are compared to oceanographic and atmospheric climatologies (Fig. 2) determined largely from data collected during the weathership era.

The cyclonic Alaska Gyre is a high-nitrate low-chlorophyll (HNLC) iron-limited region (Harrison, 2006; Martin and Fitzwater, 1988) with weak wind-driven upwelling ($\sim 10\text{--}20\text{ m yr}^{-1}$) (Tabata, 1961) and prevailing winds and surface currents from the west (Bograd et al., 1999). Primary production and export flux at OSP follow the annual cycle of surface irradiance (Wong et al., 1999), which peaks about a month before the summer solstice because cloud cover is greater in June, July and August than in the spring (Fig. 2a). Marine fog is an important component of summer clouds, whereas in winter clouds are associated with storms of the Aleutian low (Fig. 2b). Precipitation and continental runoff exceed evaporation, creating a permanent halocline at about 100 m depth. The surface mixed layer (Fig. 2e), which extends to the halocline in winter, begins shoaling after April due to seasonal warming and decreased winds. The mixed layer is shallowest ($\sim 20\text{ m}$) during July–September when sea-surface temperature is highest and winds are weakest. Lowest surface salinity lags the shallow mixed layer by about a month (Fig. 2d). Primary production shows a bimodal pattern (Fig. 2i) that may be an artifact of sparse measurements in July and August. The peak in mesozooplankton biomass occurs on average in June (Fig. 2j), but it has fluctuated over the decades occurring in late May–early June in the 1950s, mid-late July in the 1970s and early–mid May in the 1990s (Mackas et al., 1998).

1.2. Previous plankton identifications

Biogenic silica (BSi) and calcium carbonate (CaCO_3) together comprise about 90% of the trapped material in deep waters at OSP. Identifications of mineral-bearing plankton in the trap sam-

ples from portions of this time series thus provide an invaluable background for linking these trap fluxes to surface ocean conditions and plankton growth. Identifications of siliceous plankton, reported as a group (Takahashi, 1997a; Takahashi et al., 1990; Takahashi et al., 1989) and individually as diatoms (Takahashi, 1986; Takahashi, 1987b), radiolarians (Takahashi, 1987a,b) and silicoflagellates (Takahashi, 1987c; Takahashi, 1989), are available for 1982–1986. Identifications of foraminifera are also available for 1982–1986 (Reynolds and Thunell, 1985; Reynolds and Thunell, 1986; Sautter and Thunell, 1989; Thunell and Honjo, 1987). Pteropods were identified in samples collected from 1983 to 2000 (Tsurumi et al., 2005). Coccolithophores are the only mineral-bearing plankton yet to be described for any portion of this time series.

Diatom frustules comprise the majority of BSi fluxes at OSP, with radiolarian tests constituting about 10% of this flux (Takahashi, 1987a) and silicoflagellate skeletons a negligible amount (Takahashi, 1987c). Radiolarians caught in the deep traps are primarily epipelagic, and their fluxes together with those of silicoflagellates resemble the seasonal flux patterns of diatoms (Takahashi, 1997a; Takahashi et al., 1989). Takahashi (1986) describes five groups of diatoms reaching the deep traps at OSP. The first group is of the most abundant species, led by *Neodenticula seminae* which numerically comprises >70% of diatom frustules year-round. Fluxes of this group match the total mass flux, peaking in spring (March and May), summer (July–August) and fall (October). The summer and fall peaks are sometimes punctuated by fluxes of the second group, the large pennate *Rhizosolenia styliformis*, which does not bloom every year but dominates BSi fluxes when it does. Smaller, weakly-silicified species comprise a third group of diatoms with a significant flux-maximum also during July–August. Takahashi's (1986) fourth group consists of fall diatoms that are rare in spring and summer and include the large species *Rhizosolenia* spp. and *Chaetoceros concavicornis*. Fluxes of this group are highest in October and gradually decline into winter. Lastly, a winter group is represented by *Coscinodiscus marginatus* and *C. oculus iridis*, with maximum fluxes between November and March (Takahashi et al., 1989). Based on the composition of sediment caught at 1000 m and 3800 m at OSP (Haake et al., 1993a), the bulk of

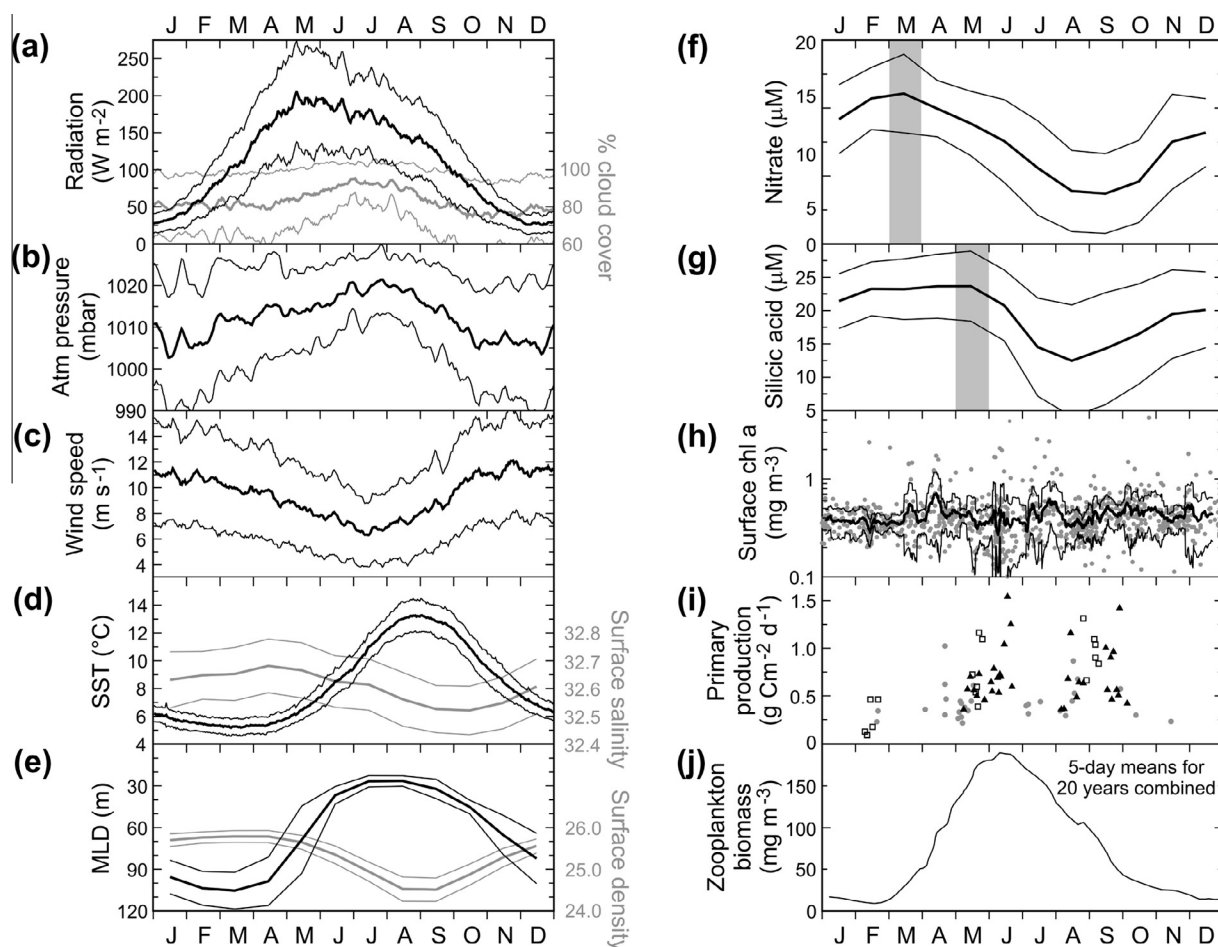


Fig. 2. Climatology of physical, chemical and biological parameters at OSP, ± 1 standard deviation where available. Unless otherwise noted, source is IOS archive of data collected daily from weatherships 1951–1981 and opportunistically afterwards. (a) Radiation (1959–1981) and cloud cover (1951–1980; octas converted to percent of sky). (b) Atmospheric pressure at sea level (1951–1980). (c) Wind speed (1951–1980) converted from 17 m or 28 m above sea level to 10 m above sea level (Benschop (1996) as per Thomas et al. (2005)). (d) Monthly mean salinity (1956–1990) at 10 m from Tabata and Weichselbaumer (1992), and temperature at 10 m (1951–1980). (e) Monthly-mean surface density from (d) and mixed-layer depth for 2002–2009 from Argo floats (<http://www.argo.ucsd.edu>, <http://argo.jcommops.org>). (f) and (g) Monthly-mean surface nutrient concentrations from Peña and Varela (2007). Grey indicates onset of decline. (h) Surface Chl a (1959–2009). Dots are the shallowest value of profiles, or single-depth measurements provided depth < 10 m. (Subsurface chlorophyll maxima are minor at OSP (Peña and Varela, 2007).) Heavy line is an 18-point (~ 1 week) running average. Seven points > 2 mg m^{-3} are plotted but not included in averaging. Eight points < 0.1 mg m^{-3} are out of range. (i) Primary production from Welschmeyer et al. (1993) (black triangles), Wong et al. (1995) (grey circles) and Boyd and Harrison (1999) (open squares). (j) Biomass of zooplankton > 350 μm for the upper 150 m (Fulton, 1983; Miller et al., 1984).

organic matter originates from diatoms and other phytoplankton during most of the year. From July to October, however, a significant portion of POC trapped at 3800 m was the sinking remains of copepods, which descend to 1000–2000 m in fall and winter (Miller et al., 1984).

Coccoliths likely make up the bulk of CaCO_3 fluxes, since they comprise most of the CaCO_3 in the < 63 μm size fraction (Thunell and Honjo, 1987) which dominates when CaCO_3 fluxes are high (Wong et al., 1999). *Emiliania huxleyi* is the most abundant coccolithophore at OSP, usually contributing $< 10\%$ but up to 67% of surface phytoplankton biomass (Putland et al., 2004), and *Syracosphaera* sp. and *Gephyrocapsa oceanica* are sometimes abundant (Lipsen et al., 2007). Assessments of coccolithophore production corroborate their significance to CaCO_3 fluxes at OSP. Wong and Crawford (2002) concluded the major source of CaCO_3 fluxes to OSP traps in June 1998 was a bloom of *E. huxleyi*, and Fabry (1989) estimated that 59–77% of CaCO_3 production at OSP is by coccolithophores. Foraminifera, most abundant in the > 63 μm size fraction, also contribute significantly to CaCO_3 fluxes. The calcite tests of five species of epipelagic foraminifera (*Globigerina quinque-*

loba, *Neoglobobulimina pachyderma*, *Globigerinita glutinata*, *Globigerina bulloides* d'Orbigny and *Orbulina universa*) comprise about 10% of the CaCO_3 flux to the bathypelagic traps (Reynolds and Thunell, 1985), and during sporadic episodes in spring (April–June) and fall (October–January) contribute upwards of 30–50% of total CaCO_3 (Sautter and Thunell, 1989; Thunell and Honjo, 1987). Deep-dwelling *Globorotalia scitula* is a negligible portion of the foraminifera flux at OSP (Reynolds and Thunell, 1985) so that, like BSi, the majority of CaCO_3 fluxes originate from above the 200-m trap. Unlike the planktonic sources of BSi that tend to occur in concert, however, sinking fluxes of foraminifera and coccolithophores are decoupled (Sautter and Thunell, 1989; Thunell and Honjo, 1987). Pteropod aragonite shells comprise most of the remainder of CaCO_3 fluxes. Fabry (1989) estimated that 4–13% of CaCO_3 production is by the two predominant pteropods *Limacina helicina* and *Clio pyramidata*, and Tsurumi (2005) found that *C. pyramidata* makes up 17% of the CaCO_3 flux to the bathypelagic trap. Pteropod shells are usually > 1 mm in length (Fabry, 1989; Tsurumi et al., 2005), so all but the smallest individuals and shell fragments have been removed as swimmers during the program reported here.

2. Sampling and analyses

2.1. Sediment traps and field design

The OSP time series began in September 1982 with a sediment trap moored in the bathypelagic zone at 3800 m, 440 m above the bottom (mab). In March 1983 a mesopelagic trap was added at 1000 m and beginning May 1989 an epipelagic trap was positioned at 200 m. Deployments at all depths ended in June 2006. A trap was also moored at station AG (55°N, 145°W) 5° north of OSP, at 3700 m (200 mab) from May 1990 to February 1992, and at 3500 m (400 mab) from April 1992 to August 1992. Conical PARFLUX sediment traps (Honjo and Doherty, 1988) with sequential sampling bottles and a baffle grid at the mouth to reduce internal turbulence (Gardner, 1980a) were used throughout. The polyethylene sampling bottles are attached to a carousel which rotates at prescribed intervals by a motor and electronic interface. The carousel has one open hole without bottle attachment designed to be in the sampling position during deployment and recovery. Sample interval was always about two weeks. MARK5 sediment traps (collection area = 1.17 m²; bottom diameter = 59 mm; 12 × 500-mL sampling bottles; ~6 month deployments) were deployed until October 1989, with servicing usually in the spring and late summer. From October 1989 until September 1992, either MARK6 (collection area = 0.503 m²; bottom diameter = 30 mm; 13 × 500-mL sampling bottles; ~6 month deployments) or MARK7 (collection area = 0.503 m²; bottom diameter = 28 mm; 21 × 250-mL sampling bottles; ~12 month deployments) traps were deployed at OSP and at station AG. From September 1992 onward, MARK7 traps were used, with the exception that MARK6 traps were deployed at 1000 m in June 2000 (PA29) and at 3700 m in July 2002 (PA31A). After their initial deployments, the epipelagic and mesopelagic traps were occasionally not deployed, but bathypelagic traps were a part of all moorings.

The transitional period between 1989 and 1992 coincided with a series of lost moorings (PA18 and PA20) and a mechanical failure (PA19, 3800 m), such that fluxes were not measured at OSP from November 1990 to September 1992 (Fig. 3). After 1992, clogging of MARK7 traps at 3800 m became problematic (Table A5). Considering the coverage at station AG (May 1990 to August 1992) and

the relatively complete 1000-m time series after 1992, however, the longest period for which there is no flux record from the Alaska Gyre is the 281 days from 14 August 1995 to 21 May 1996.

2.2. Sample handling

Sample bottles were filled with seawater collected from depths between 1500 m and 3000 m. 0.85 g NaN₃ L⁻¹ were added as a poison except during the first two mooring deployments, and 4.15 g NaCl L⁻¹ were added to minimize losses of poison and sediment due to mixing. NaN₃ inhibits aerobic but not anaerobic bacterial respiration. It poisons zooplankton swimmers attracted to the trapped material, but does not prevent disintegration of biological tissues. Upon recovery of the traps, the bottles were removed from the carousel, capped and kept at 4 °C in the dark until processed at the Institute of Ocean Sciences. Qualitative descriptions of the bulk sediments (e.g., color and odor) and semi-quantitative microscopic analyses were made and, after June 1997, bottles from each deployment were photographed as a set. Prior to October 1989, samples were filtered sequentially through 1000 μm and 63 μm mesh and the three resulting size fractions were separately analyzed as described below. From October 1989 onward, samples were filtered through 1000 μm mesh to remove swimmers and chemical analyses were performed only on the <1000 μm size fraction. Using 3.2% NaCl solution as a rinse and forceps where needed, small debris was removed from swimmers and added to the <1000 μm sample. Zooplankton >1000 μm were identified under magnification and stored in 10% formalin and 3.2% NaCl. The results presented here are for only the <1000 μm size fraction, which for samples collected until September 1989 is the sum of the <63 μm and the 63–1000 μm size fractions. This treatment differs from previous studies (Wong and Crawford, 2002; Wong et al., 1999) where the >1000 μm size fraction is included as part of the total flux prior to October 1989.

2.3. Laboratory analyses

After sieving, samples were split into 1/4, 1/16 or 1/64 aliquots using an Erez-Honjo rotary splitter (Honjo, 1978) or a Folsom plankton splitter (McEwen et al., 1954). Aliquots were filtered

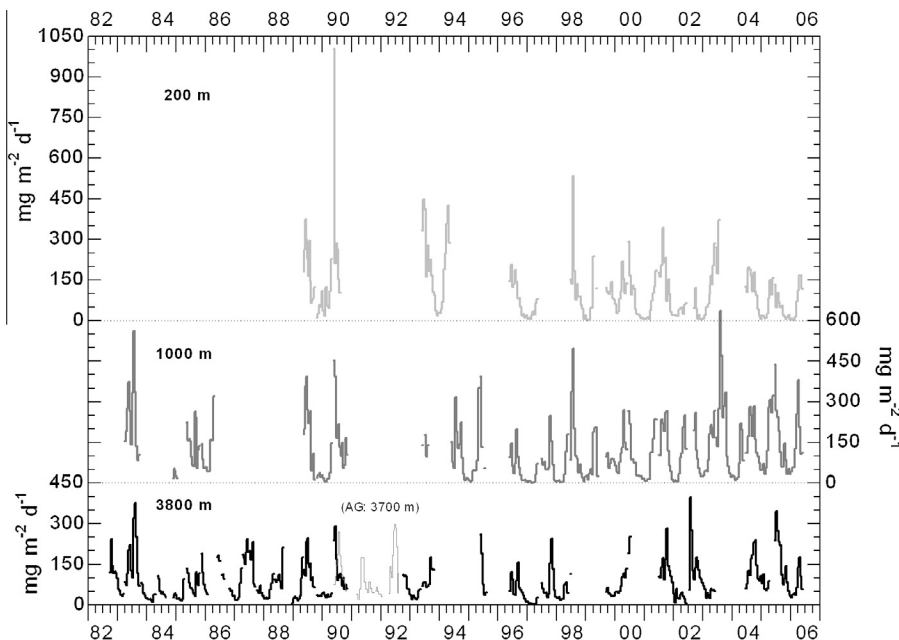


Fig. 3. Total mass flux at OSP and station AG.

onto pre-weighed polycarbonate filters (0.8 or 1.0 μm) or pre-combusted and pre-weighed silver filters (0.8 μm), rinsed with deionised water and dried at 50–60 °C for 24 h. Dried filters were weighed to determine the total mass of the sediment. Samples were then decalcified by soaking in 4% HCl for 20 min, rinsed with distilled water and dried. CaCO_3 was determined as the difference in weight before and after decalcification. The decalcified samples were analyzed for POC and PN by combustion at 980 °C using a Perkin-Elmer 240 or a CEC 440 Elemental Analyzer. A modified version of the alkaline extraction method (DeMaster, 1981) was used for BSi ($\text{SiO}_2 \cdot n\text{H}_2\text{O}$) analysis. 5–50 mg sediment were placed into polypropylene centrifuge tubes containing 40 mL of 1% Na_2CO_3 (pH 11.2), digested in a water bath at 85 °C for 2 h, then centrifuged at 2000 rpm for 5 min. 1 mL of the supernatant diluted with 25 mL distilled water was analyzed for reactive silicate using a Technicon Autoanalyzer (Barwell-Clarke and Whitney, 1996). Aluminum (Al) was measured by graphite furnace atomic absorption spectrometry on 260 selected samples collected between October 1987 (deployment PA12) and May 1999 (deployment PA27).

2.4. Laboratory precision

Duplicate analyses were run on different splits throughout the time series. Laboratory precision, here defined as the average coefficient of variation ($cv = \text{standard deviation} / \text{mean}$) of these duplicates, thus incorporates splitting error, instrument error, calibration error and handling error. The average cv of duplicates for total mass is 4.7% ($n = 388$), for percent PN is 7.1% ($n = 110$), for percent POC is 4.4% ($n = 118$), for percent CaCO_3 is 4.4% ($n = 130$) and for percent BSi is 2.8% ($n = 80$).

2.5. Flux reproducibility

Bathypelagic traps on moorings PA31A and PA31, separated by 6.2 km, collected simultaneously for seven 15-d sampling periods from 7 September 2002 to 21 December 2002. The trap (MARK6; 3700 m) on mooring PA31A was recovered in December 2002 while the trap (MARK7; 3800 m) on mooring PA31 was recovered in June 2003. Samples from both sets were analyzed in the winter of 2003–2004. Flux differences between sets potentially include contributions from variability in: flux to the traps; trapping efficiency ($TE = \text{measured flux} / \text{true flux}$); remineralization within bottles; and laboratory analyses. Fluxes to the trap on mooring PA31A were usually higher than fluxes to the trap on mooring PA31. Differences in total mass were usually less than 10% and always less than 20%, with differences in constituent fluxes sometimes higher. The means of the absolute values of the flux differences ($\% \pm \text{standard error}$) are: POC = 15.0 (± 4.8); BSi = 12.6 (± 2.4); total mass = 8.3 (± 1.9); CaCO_3 7.4 (± 1.4).

2.6. Quality assessment

Detailed chronologies of the successful sampling periods and the unsuccessful or inactive periods are given in Tables A1–A4. All data associated with bottles in the open position when the mooring was recovered have been removed, as well as data from bottles affected by clogs (Table A5), including the last sediment-bearing bottle preceding the series of empty bottles characteristic of clogs. A thorough quality assessment of the data also has been conducted, referring to the original laboratory results and field notes, to remove discrepancies and ensure that fluxes and compositions were calculated uniformly throughout. Accordingly, a number of corrections have been made and the data set archived as a prelude to this paper.

3. Data treatment

The results presented here are based on discrete samples collected sequentially over a 24-year period, but with irregular and sometimes large gaps in the time series (Fig. 3). In this section, we describe the analytical methods used to translate the time series into forms that allow comparisons of flux and composition between depths and to other environmental parameters.

3.1. Climatological curves

3.1.1. Calculation and biasing

Climatological curves of flux (Figs. 4 and 5) and composition (Figs. 6–8) are created by assigning to each day of successful sampling the appropriate calendar day, 1 through 365. (Data from day 366 of leap years are not used.) Data collected on each of the calendar days are then averaged together.

$$X_d = (x_{d1} + x_{d2} + \dots + x_{dn})/n \quad (1)$$

X_d is the average flux or composition for calendar day d , and x_{dn} is the measured flux or composition on calendar day d of year n . Annual and seasonal fluxes and compositions are then calculated by averaging X_d for the appropriate group of calendar days; e.g., annual averages are the average of X_d for calendar days 1 through 365. This method of calculating annual and seasonal averages (Table 1) gives equal weight to all calendar days regardless of sampling frequency for each calendar day.

The gross duration of each time series including periods when data are missing was 17.07 y, 23.19 y and 23.70 y at 200 m, 1000 m and 3800 m, respectively. Subtracting data gaps from the gross durations gives net durations of 9.51 y, 13.57 y and 14.52 y for the time series at subsequently deeper traps (Tables A1–A3). Gross and net durations at Station AG were 2.24 y and 1.72 y, respectively (Table A4). The number of successful deployments for any calendar day varied between 5 and 10 at 200 m, and between 9 and 17 at 1000 m and 3800 m (Fig. 4). Early June was under sampled at all depths because of mooring turnover, and May was under sampled at 3800 m due to mooring turnover and trap failures. At 1000 m and 3800 m, the small sampling decrease in fall is due to twice-yearly mooring turnover during deployments PA1–PA17.

Climatologies of flux and composition for the entire time series are presented in Tables 1 and 2 to ensure averages are based on the maximum number of data available. When comparing fluxes at two or three depths, however, only data collected simultaneously at the depths were used to avoid biasing caused by interannual variability and long-term trends. Table 3 summarizes the climatologies created from simultaneously-collected data. Net durations of simultaneous sampling were 8.72 y at 200 m and 1000 m, 9.45 y at 1000 m and 3800 m, and 6.72 y at all three depths. Annual estimates of total and constituent fluxes for these unbiased climatologies (Table 3) are within 13% of the Table 1 values.

3.1.2. Flux frequency distribution and extreme events

Flux frequency is skewed right (Fig. A1). Log transformation (Fig. A2) results in flux frequencies that are skewed left for fluxes at 200 m and 1000 m and ~normally distributed for fluxes at 3800 m because low winter fluxes are less frequent at the deepest trap (see Section 5.7.3). Our climatologies are generated from mean fluxes without data transformations (Eq. (1)) to include the signals of rare events. The peaks and valleys of climatological curves are similar for the different treatments discussed here (Fig. A3), so the choice of treatment does not affect descriptive conclusions. Fig. A1 gives ratios of arithmetic mean fluxes and median fluxes, and Fig. A2 gives ratios of arithmetic mean fluxes and means of

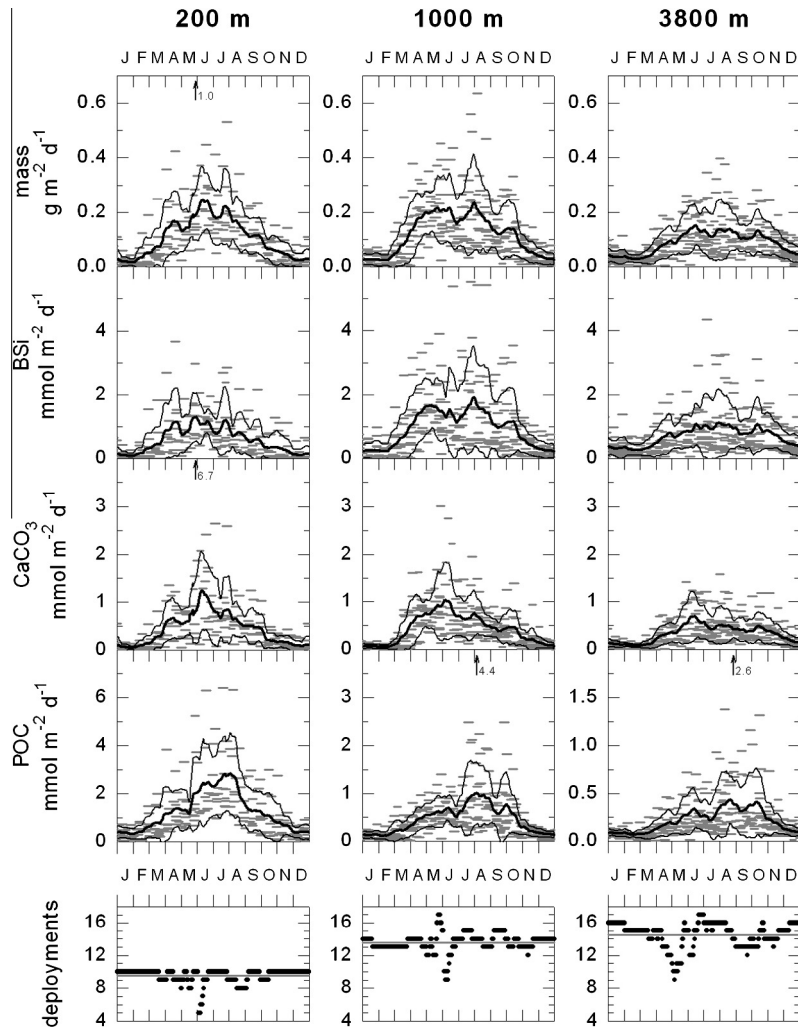


Fig. 4. Total and constituent fluxes at OSP (grey bars) plotted against calendar day. Climatological averages \pm one standard deviation from Eq. (1) also are plotted with a seven-day smooth applied. Bottom panels are the number of years traps were successfully operating on each calendar day, with grey lines depicting the average. Extreme fluxes (Section 3.1.2) not included in the curves are indicated by arrows. Note scale changes for POC fluxes.

log transformed fluxes. These ratios allow conversion from mean fluxes (Table 1) to the most likely flux condition at OSP.

Three extreme flux events are included with minor impact in the annual and seasonal means of Table 1, but they are not used for the climatological curves of Figs. 4 and 5. Very high POC fluxes were recorded in the second half of August 1983 at 3800 m (Wong and Crawford, 2002; Wong et al., 1999) (we do not include the >1 mm size fraction (Section 2.2) so our fluxes are lower than previously reported) and in the first half of August 2003 at 1000 m. Removing these events from POC flux climatologies reduces the August POC peak at 3800 m by 25% and, at 1000 m, by 19%, without affecting the timing of either peak. A third extreme event, also reported by Wong et al. (1999), occurred May 1990 when the highest CaCO_3 and mass fluxes at 200 m were recorded. Removing this event from the climatologies reduces the May peaks at 200 m by 13% and 7% for CaCO_3 and total mass, respectively, and causes both peaks to occur 11 days later. One extreme %POC value at 1000 m from February 1997 is similarly included in averaging (Table 2) but excluded from climatological curves (Figs. 6 and 7).

3.1.3. Flux ratios

The average of flux ratios for constituents a and b can be calculated either as a weight ratio ($\text{WR} = [a_1 + a_2 + \dots + a_n] / [b_1 + b_2 + \dots + b_n]$) or as the average of ratios ($\text{AR} = [a_1/b_1 + a_2/b_2 + \dots + a_n/b_n] / n$).

For continuous periods over which sinking fluxes are ecologically or geochemically related, WR ensures that anomalous ratios during low-flux periods do not bias ratio calculations. In generating climatological averages across years (independent fluxes), however, the use of AR avoids biasing towards conditions of high-flux years. Differences between WR and AR are sometimes large for this data set, so both are given in Table 2. AR is used for the climatological curves of Figs. 6–8.

3.2. Seasonal delineation

Four flux seasons of equal length are delineated by passing a 91-day running average through the climatological curve of total mass flux, setting 'summer' and 'winter' seasons where the 91-day flux averages are maximally different from one another (Fig. 9). For fluxes at 200 m, 1000 m and 3800 m, the maximum difference occurs when 'summer' begins, respectively, on calendar days 141 (21 May), 140 and 157 (6 June). The beginning of climatological summer is therefore set at 21 May for 200 m and 1000 m, and at 6 June (16 d later) at 3800 m. The lag to 3800 m matches sinking rates between 1000 m and 3800 m estimated next. 91-day running averages also have been passed through the climatological curves

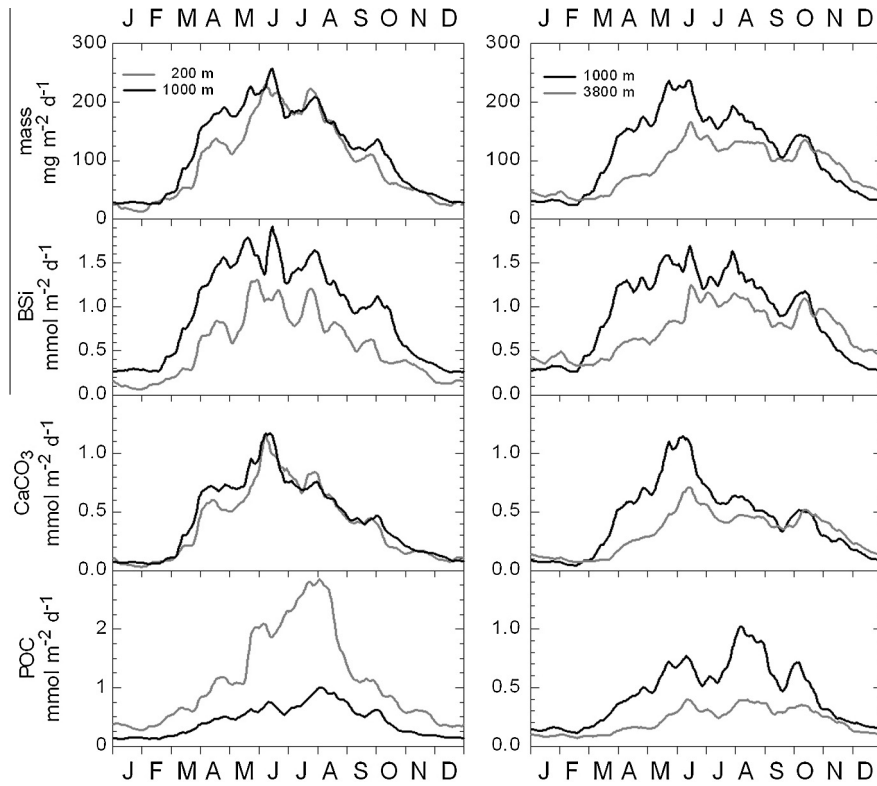


Fig. 5. Climatological fluxes at OSP. Climatologies on left from fluxes collected simultaneously at 200 m and 1000 m; climatologies on right from fluxes collected simultaneously at 1000 m and 3800 m (Table 3). Extreme fluxes (Section 3.1.2) are not included. Note scale changes for POC fluxes.

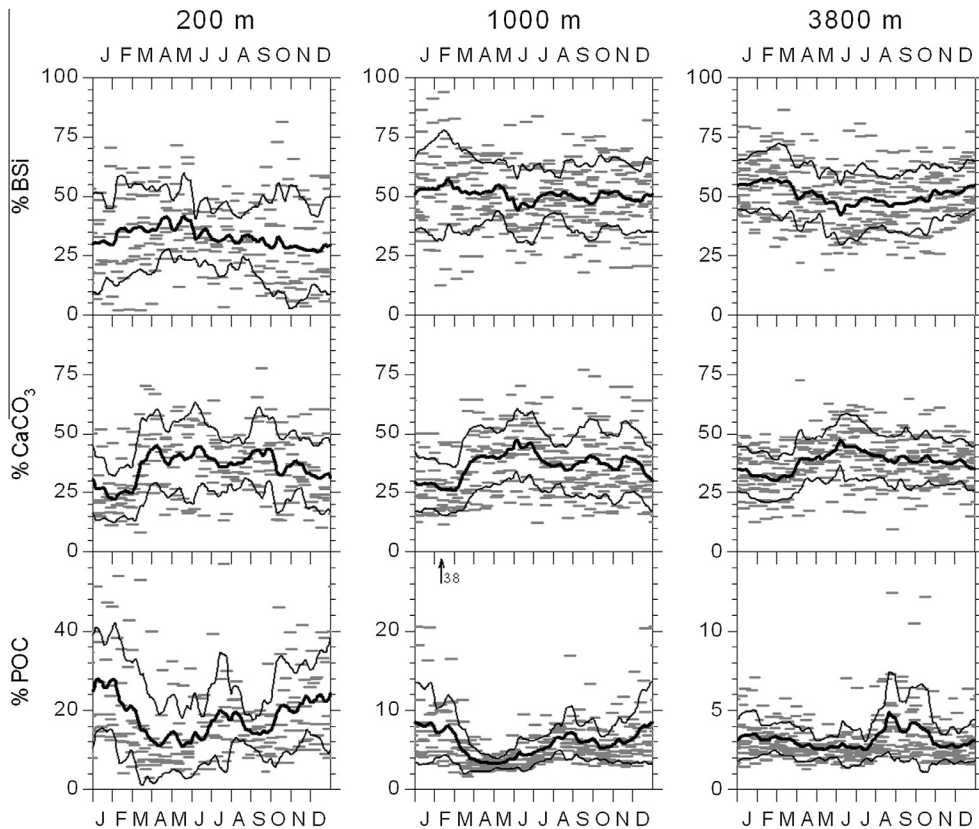


Fig. 6. Sediment composition at OSP. See caption to Fig. 4. Climatologies are calculated from average ratios instead of weight ratios (Sections 3.1.3). One extreme %POC value at 1000 m not included in the curves (Section 3.1.2) is indicated by an arrow. Note scale changes for %POC.

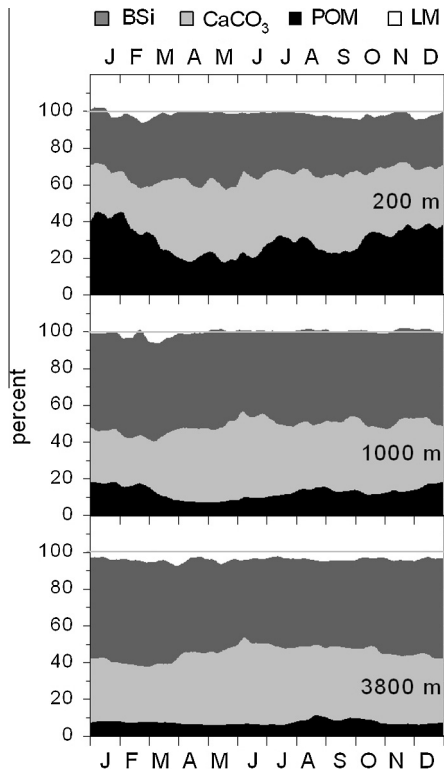


Fig. 7. Climatology of sediment composition at OSP based on the curves of Fig. 6.

without the constraint of having four equal seasons, with the result that the 91-d window of maximum flux matches to within several days the summer windows defined above. However, the 91-d windows of minimum flux lags by 1–3 weeks the winter windows, and this lag increases with depth. The choice of the winter window has a small affect on average winter fluxes (Table 1) because temporal flux gradients are small at this time of year. A secondary flux of bathypelagic sediments (Section 5.7.3) is probably the main reason the flux minimum at 3800 m is shifted towards spring.

A 91-d running average passed through the climatological curve of irradiance at OSP (Fig. 2a) shows that solar summer begins on calendar day 111 (21 April), one month before maximum fluxes to the traps at 200 m and at 1000 m. Persistent cloudiness in June–August results in solar summer beginning 16 d earlier than if there were no clouds at OSP. The 91-d sunshine minimum begins day 312 (8 November) and matches the beginning of solar winter (day 310) under cloud-free conditions.

3.3. Average sinking rates

To estimate the average time required for sediments to pass from shallow to deep traps, fluxes at deep traps were incrementally shifted backwards to determine the best correlation in total mass and constituent fluxes (Fig. 10). Shifting 1000-m fluxes relative to 200-m fluxes does not improve correlations, implying an average transit time ≤ 0.5 bottle durations (8 d) and thus an average sinking rate (sr) greater than 100 m d^{-1} . For the 1000–3800 m depth interval, flux correlations are maximized with a lag of one bottle duration, which gives transit times of 0.5–1.5 durations (8–24 d) and an average sr of 120 m d^{-1} to 350 m d^{-1} . Similar sinking rates of $175\text{--}300 \text{ m d}^{-1}$ were determined based on distinct flux events at OSP (Wong et al., 1999). Also from this time series, a lag of one bottle duration for a range of diatom species sinking between 1000 m and 3800 m has been attributed to aggregates as the primary vector of export instead of different

species sinking separately (Takahashi, 1986). Correlation coefficients for the upper depth interval are lower than for the deep interval (Fig. 10), possibly because a fraction of material caught at 1000 m was missed at 200 m (Section 5.7.2).

3.4. Lithogenic content

A tracer for lithogenic material (LM) was not regularly measured on the samples collected at OSP. We thus estimate %LM by subtracting the contents of the biogenic components from 100%.

$$\%LM = 100 - \%CaCO_3 - (POM : POC)\%POC - (BSi : Si)\%Si \quad (2)$$

POM is particulate organic matter. %LM includes minor contributions by authigenic and biogenic minerals other than BSi and $CaCO_3$. POM:POC and BSi:Si can be obtained from the literature, but %LM is sensitive to these ratios especially at locations such as OSP where %POC and %Si are both high.

Al was determined on selected samples collected from 1987 to 1999, allowing estimates using Eq. (3) of the weight ratios POM:-POC, BSi:Si and LM:Al specific to sediment caught at OSP (Table 4). Not only do these ratios allow better estimates of %LM than if literature values were used, but also POM:POC reflects the types of organic compounds present and BSi:Si indicates the water content of the opal.

$$\begin{aligned} (\text{total flux} - CaCO_3 \text{ flux}) &= (POM : POC)POC \text{ flux} \\ &+ (BSi : Si)Si \text{ flux} + (LM : Al)Al \text{ flux} + d \quad (3) \end{aligned}$$

Eq. (3) has the form: $y = ax_1 + bx_2 + cx_3 + d$, where fluxes y , x_1 , x_2 and x_3 are known. The weight ratios a , b and c , and the intercept d , are solved by least-squares regression. The independent variables (x_1 , x_2 and x_3) show a low degree of multicollinearity, indicating the data subsets applied to Eq. (3) are good representations of the entire data set collected from OSP.

Beginning February 1990, Al fluxes were much higher than the background of $<7\text{--}14 \mu\text{mol m}^{-2} \text{ d}^{-1}$, possibly because of an atmospheric dust event (e.g., Wong and Matear, 1999). Eq. (3) regressions with and without these samples give similar POM:POC and BSi:Si ratios. Nevertheless, the high-Al samples heavily weight results, so only samples with background Al fluxes are included in the regressions used to characterize OSP sediment. Resulting POM:POC weight ratios range from 1.62 to 2.33, and BSi:Si weight ratios from 2.28 to 2.39, depending on depth (Table 4). Error in the LM:Al ratios of samples from 200 m and 1000 m is higher than the ratios, indicating LM fluxes at these depths are not statistically different than zero in this regression model. The LM:Al ratio of samples from 3800 m (13 ± 5) is not statistically different from samples affected by the dust event presented next. The high error again may be caused by poor characterization of LM due to the low LM fluxes. Estimates of %LM from Eq. (2) can be compared to %Al measured on this subset of data most characteristic to OSP. Average %Al for these samples is 0.070% at 200 m, 0.080% at 1000 m and 0.32% at 3800 m. Using a LM:Al weight ratio of 10 (see regression presented next) to 13 (LM:Al at 3800 m), LM content is 0.7–1% at 200 m and 1000 m and 3–4% at 3800 m, confirming the annual average estimates of Table 2.

Eq. (3) also was fit to the Al-affected samples pooled from all depths. The resulting LM:Al ratio of 9.7 ± 0.56 ($n = 26$) compares reasonably with those of pelagic clay (11.9) and of Post-Archean Australian shale (PAAS) (7.96–12.2; mean = 10.2) (Taylor and McClennan, 1985). The POM:POC and BSi:Si ratios of this sample group are not statistically different than those of Table 4.

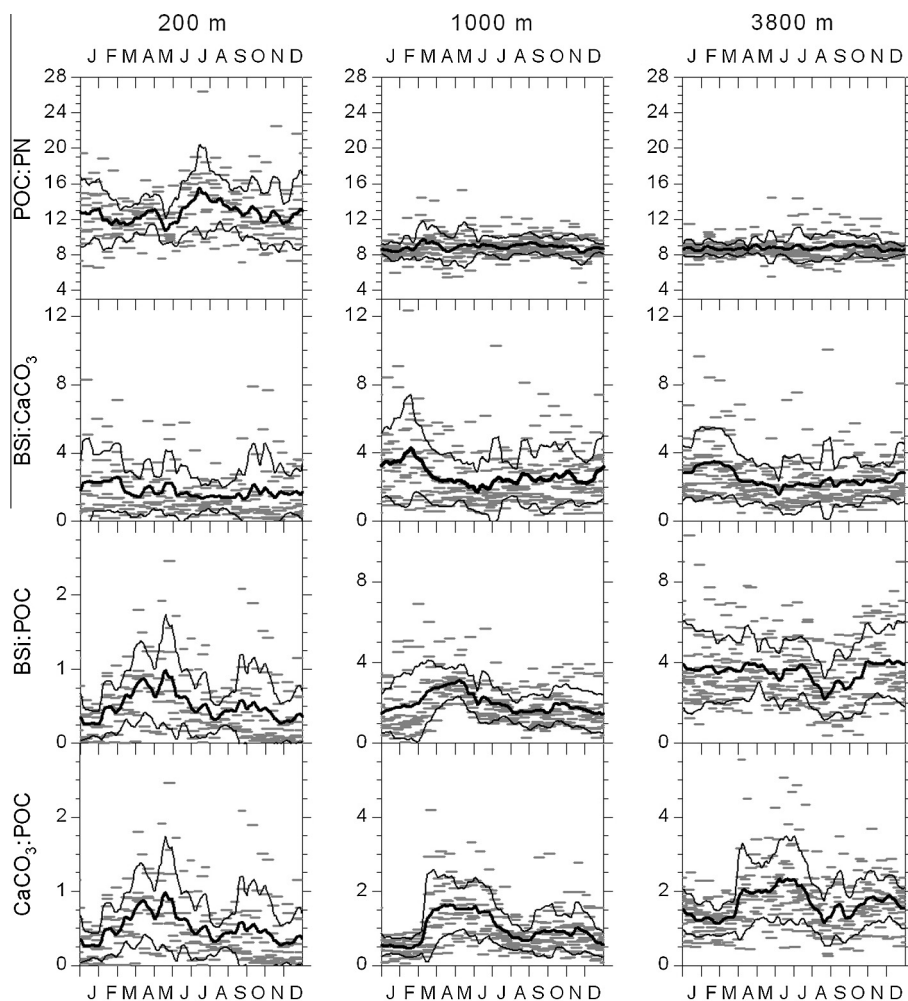


Fig. 8. Flux ratios (molar) at OSP. See caption to Fig. 4. Climatologies are calculated from average ratios instead of weight ratios (Section 3.1.3). Note scale changes for BSi:POC and CaCO_3 :POC.

4. Results

4.1. Flux and composition at OSP

Annually-averaged mass flux (Table 1) is virtually the same at 200 m ($111 \text{ mg m}^{-2} \text{ d}^{-1}$) and 1000 m ($119 \text{ mg m}^{-2} \text{ d}^{-1}$) and decreases to $88.0 \text{ mg m}^{-2} \text{ d}^{-1}$ at 3800 m. Fluxes of CaCO_3 mirror those of the total mass, changing little from 200 m ($451 \mu\text{mol m}^{-2} \text{ d}^{-1}$) to 1000 m ($438 \mu\text{mol m}^{-2} \text{ d}^{-1}$) and decreasing to 3800 m ($338 \mu\text{mol m}^{-2} \text{ d}^{-1}$). As a result, annually-averaged CaCO_3 content (35–40%; Table 2) varies little with depth. BSi fluxes increase significantly from 200 m ($586 \mu\text{mol m}^{-2} \text{ d}^{-1}$) to 1000 m ($948 \mu\text{mol m}^{-2} \text{ d}^{-1}$), but decrease from 1000 m to 3800 m ($694 \mu\text{mol m}^{-2} \text{ d}^{-1}$) similarly to total mass and CaCO_3 flux declines in the bathypelagic zone. BSi content thus increases from ~35% at 200 m to ~50% at 1000 m and 3800 m. POC fluxes decrease with depth, from $1256 \mu\text{mol m}^{-2} \text{ d}^{-1}$ (200 m) to $471 \mu\text{mol m}^{-2} \text{ d}^{-1}$ (1000 m) to $226 \mu\text{mol m}^{-2} \text{ d}^{-1}$ (3800 m), causing average POC content to decrease from ~15% to ~5% to ~3% at consecutively deeper traps.

Peaks in the biogenic fluxes at 200 m occur in April, June and July–August (Figs. 4 and 5). The three BSi peaks are of similar magnitude, while highest CaCO_3 fluxes occur during the second peak in early June. POC fluxes progressively increase throughout the summer and are highest in early August. A fourth peak in the fluxes of all constituents at 200 m occurs in late September and is notable

because it translates into prominent maxima in early October at 1000 m and 3800 m. Peaks are less resolved in the deeper traps. At 1000 m, BSi fluxes are high from April until June, then peak in July–August and again in October. This pattern corresponds to fluxes of diatom frustules collected at OSP from 1982–1986 (Section 1.2). Fluxes at 3800 m reflect those at 1000 m, with high BSi and CaCO_3 flux attenuation between these depths from March until early June (Fig. 7).

Based on the seasonal fluxes of Table 1, the summer:winter flux ratio at 200 m is greatest for CaCO_3 (11), less for BSi (7.6) and least for POC (6.1), while spring:fall ratios show BSi and CaCO_3 fluxes are higher in the spring and POC fluxes are higher in the fall. The summer:winter flux ratios decrease as particles sink. At 3800 m, summer:winter flux ratios are 4.2, 2.9 and 4.0 for CaCO_3 , BSi and POC, respectively, such that the loss of seasonality with depth is greatest for CaCO_3 and BSi, and least for POC. Also, the timing of deposition is shifted, with the flux of all constituents higher in the fall than in the spring at 3800 m. Of the three biogenic components, %POC shows the greatest variability, both within (cv's of Table 2) and between seasons (seasonal compositions of Table 2). At 200 m, %POC is highest in winter, lowest in spring and intermediate in summer and fall (Figs. 6 and 7). High wintertime %POC is also seen at 1000 m, but at 3800 m %POC peaks in late summer and fall. % CaCO_3 is lowest in winter at all depths. %BSi varies little by season, but at 200 m is highest in spring and at 3800 m is highest in winter.

Table 1
Annual and seasonal fluxes (Eq. (1)) at OSP and station AG. *n* is the number of years of sampling on each calendar day. Coefficients of variation (*cv* = standard deviation/mean) in parentheses, are calculated for each calendar day then averaged over the appropriate period. *cv* for station AG is not shown because of low *n*. Seasons (Section 3.2) begin 16 days later at 3800 m than at 200 m and 1000 m.

Averaging period		avg <i>n</i>	mass (mg m ⁻² d ⁻¹)	BSi (μmol m ⁻² d ⁻¹)	CaCO ₃ (μmol m ⁻² d ⁻¹)	POC (μmol m ⁻² d ⁻¹)	PN (μmol m ⁻² d ⁻¹)	LM (mg m ⁻² d ⁻¹)
<i>OSP: 200 m</i>								
Annual	Jan 1–Dec 31	9.5	111 (0.8)	586 (1.0)	451 (0.9)	1260 (0.7)	96.4 (0.6)	1.9 (>10)
Winter	Nov 20–Feb 19	10.0	26.1 (1.0)	134 (1.3)	82.5 (1.2)	401 (0.7)	32.0 (0.6)	1.1 (>10)
Spring	Feb 20–May 20	9.4	113 (0.8)	710 (1.1)	431 (0.8)	1030 (0.7)	83.8 (0.7)	1.7 (>10)
Summer	May 21–Aug 19	9.1	214 (0.6)	1020 (0.6)	948 (0.8)	2440 (0.6)	182 (0.6)	3.1 (>2)
Fall	Aug 20–Nov 19	9.5	90.8 (0.7)	480 (1.1)	342 (0.7)	1160 (0.7)	87.9 (0.7)	1.8 (>2)
<i>OSP: 1000 m</i>								
Annual	Jan 1–Dec 31	13.6	119 (0.7)	948 (0.8)	438 (0.7)	471 (0.6)	52.9 (0.6)	0.0 (>10)
Winter	Nov 20–Feb 19	13.6	30.5 (0.8)	264 (1.0)	94.3 (0.8)	147 (0.5)	17.4 (0.6)	0.0 (>10)
Spring	Feb 20–May 20	13.2	130 (0.7)	1070 (0.8)	492 (0.7)	372 (0.6)	42.5 (0.7)	0.6 (>10)
Summer	May 21–Aug 19	13.8	198 (0.6)	1500 (0.8)	778 (0.7)	798 (0.6)	89.1 (0.6)	0.2 (1.4)
Fall	Aug 20–Nov 19	13.7	117 (0.7)	963 (0.8)	390 (0.6)	567 (0.7)	62.6 (0.7)	0.0 (0.8)
<i>OSP: 3800 m</i>								
Annual	Jan 1–Dec 31	14.5	88.0 (0.6)	694 (0.7)	338 (0.6)	226 (0.7)	25.7 (0.7)	3.5 (1.6)
Winter	Dec 6–Mar 6	15.6	39.1 (0.6)	347 (0.7)	125 (0.5)	89.0 (0.4)	10.4 (0.4)	1.9 (1.3)
Spring	Mar 7–Jun 5	13.4	80.8 (0.6)	625 (0.7)	318 (0.7)	175 (0.7)	20.0 (0.6)	4.1 (2.1)
Summer	Jun 6–Sep 4	15.2	131 (0.6)	1000 (0.8)	524 (0.6)	355 (0.8)	41.0 (0.8)	4.6 (1.7)
Fall	Sep 5–Dec 5	13.9	101 (0.5)	801 (0.6)	383 (0.6)	283 (0.7)	31.2 (0.7)	3.5 (1.3)
<i>AG: 3700 m</i>								
Annual	Jan 1–Dec 31	1.7	85.6	524	301	228	26.1	16
Winter	Dec 6–Mar 6	0.6	35.6	200	105	112	13.0	9.2
Spring	Mar 7–Jun 5	1.8	87.3	480	345	181	20.9	17
Summer	Jun 6–Sep 4	2.8	140	893	512	403	46.0	21
Fall	Sep 5–Dec 5	1.6	61.3	405	174	174	19.8	13

Table 2
Annual and seasonal composition and molar ratios at OSP and station AG. See Table 1 for *n* and seasonal delineations. Weight ratios (WR) are from the fluxes of Table 1 and average ratios (AR) are from Eq. (1). *cv* of AR, in parentheses, is not shown for station AG because of low *n*. %LM is from Eq. (2). %BSi, %CaCO₃ and %POC at station AG are LM-free for comparison to sediments at OSP.

	%BSi		%CaCO ₃		%POC		%LM		POC:PN		BSi:CaCO ₃		BSi:POC		CaCO ₃ :POC	
	WR	AR	WR	AR	WR	AR	WR	AR	WR	AR	WR	AR	WR	AR	WR	AR
<i>OSP: 200 m</i>																
Annual	36	33 (0.5)	41	36 (0.4)	14	18 (0.6)	1.7	1.9 (>2)	13	13 (0.2)	1.3	1.8 (0.8)	0.47	0.51 (0.8)	0.36	0.37 (0.7)
Winter	34	30 (0.6)	32	28 (0.4)	18	24 (0.5)	4.2	1.9 (>2)	13	12 (0.3)	1.6	2.0 (0.8)	0.33	0.32 (0.8)	0.21	0.20 (0.8)
Spring	42	37 (0.4)	38	37 (0.4)	11	15 (0.7)	1.5	1.8 (>2)	12	12 (0.2)	1.6	1.9 (0.7)	0.69	0.69 (0.6)	0.42	0.51 (0.8)
Summer	32	34 (0.4)	44	39 (0.4)	14	16 (0.6)	1.4	1.1 (>2)	13	13 (0.2)	1.1	1.6 (0.7)	0.42	0.55 (0.7)	0.39	0.44 (0.7)
Fall	35	30 (0.6)	38	39 (0.4)	15	17 (0.5)	1.9	2.7 (>2)	13	13 (0.2)	1.4	1.6 (1.0)	0.41	0.46 (0.9)	0.30	0.33 (0.5)
<i>OSP: 1000 m</i>																
Annual	53	51 (0.3)	37	36 (0.4)	4.8	5.9 (0.4)	0.0	0.2 (>10)	8.9	8.9 (0.1)	2.2	2.7 (0.6)	2.0	2.0 (0.5)	0.93	0.98 (0.5)
Winter	57	51 (0.3)	31	32 (0.4)	5.8	8.0 (0.6)	0.0	0.0 (>10)	8.5	8.6 (0.1)	2.8	3.1 (0.6)	1.8	1.7 (0.7)	0.64	0.63 (0.5)
Spring	54	53 (0.3)	38	36 (0.3)	3.4	4.5 (0.4)	0.5	1.8 (>10)	8.7	9.0 (0.2)	2.2	2.8 (0.6)	2.9	2.6 (0.5)	1.3	1.3 (0.6)
Summer	50	49 (0.3)	39	41 (0.3)	4.9	5.0 (0.3)	0.1	0.0 (>10)	9.0	9.0 (0.1)	1.9	2.2 (0.7)	1.9	2.0 (0.4)	0.98	1.2 (0.5)
Fall	54	50 (0.3)	33	37 (0.4)	5.8	6.1 (0.4)	0.0	0.0 (>10)	9.1	9.0 (0.1)	2.5	2.6 (0.7)	1.7	1.7 (0.5)	0.69	0.85 (0.6)
<i>OSP: 3800 m</i>																
Annual	50	51 (0.2)	38	38 (0.3)	3.1	3.2 (0.4)	4.0	4.1 (>2)	8.8	8.8 (0.1)	2.1	2.5 (0.6)	3.1	3.5 (0.5)	1.5	1.7 (0.4)
Winter	57	55 (0.2)	32	33 (0.3)	2.7	3.2 (0.4)	4.9	3.9 (>2)	8.6	8.6 (0.1)	2.8	3.1 (0.6)	3.9	3.8 (0.5)	1.4	1.4 (0.3)
Spring	49	51 (0.2)	39	38 (0.3)	2.6	2.8 (0.3)	5.0	4.8 (>2)	8.7	8.7 (0.1)	2.0	2.4 (0.5)	3.6	3.7 (0.4)	1.8	1.8 (0.4)
Summer	49	47 (0.3)	40	42 (0.3)	3.3	3.3 (0.4)	3.5	3.8 (>2)	8.7	8.8 (0.2)	1.9	2.1 (0.7)	2.8	3.2 (0.4)	1.5	1.9 (0.5)
Fall	51	50 (0.2)	38	38 (0.3)	3.4	3.4 (0.5)	3.5	4.1 (1.6)	9.1	8.9 (0.1)	2.1	2.3 (0.5)	2.8	3.5 (0.5)	1.4	1.6 (0.4)
<i>AG: 3700 m</i>																
Annual	48	49	43	42	3.9	4.3	18	22	8.7	8.6	1.7	1.9	2.3	2.4	1.3	1.3
Winter	48	49	40	40	5.1	5.1	26	25	8.7	8.7	1.9	1.9	1.8	1.8	0.93	0.93
Spring	44	44	49	47	3.1	3.7	19	23	8.7	8.6	1.4	1.6	2.7	2.4	1.9	1.7
Summer	48	48	43	42	4.0	4.5	15	17	8.8	8.6	1.7	1.9	2.2	2.4	1.3	1.3
Fall	54	53	36	37	4.3	4.2	21	22	8.8	8.4	2.3	2.3	2.3	2.8	1.0	1.2

Consistent with POC attenuation, BSi:POC and CaCO₃:POC both increase with depth (Table 2 and Fig. 8). The ratios of Fig. 8 further demonstrate the relative suppression of winter CaCO₃ fluxes at all depths, the high CaCO₃ fluxes from April to June, the effect of increasing POC fluxes in late summer and fall and the low BSi fluxes at 200 m. BSi:CaCO₃ is notably invariant from 1000 m to 3800 m. POC:PN is highest at 200 m (13) and decreases to 8.8–8.9 at 1000 m and 3800 m.

4.2. Flux and composition at station AG

Lithogenic fluxes to the traps at station AG are estimated using the weight ratios for 3800 m at OSP (Table 4). These fluxes are four to five times higher than at the deepest trap at OSP. They are also about four times higher than at bathypelagic traps in the central Subarctic Pacific Ocean (49°N, 174°W) but comparable to lithogenic fluxes to deep traps moored in the Aleutian Basin (53.5°N,

Table 3

Comparison of climatologies generated from time series of different lengths. The first row of each depth is for the climatology of all data available at that depth. Subsequent rows are for climatologies of data collected simultaneously at the depths indicated in the second column. “200–1000 m” and “1000–3800 m” subsets are used for Fig. 5 and Fig. 10 and Section 5.7. “200–1000–3800 m” subsets are used for Table 5. Net length is number of days of successful data collection. Central date is the temporal average for each time series. Annual fluxes are calculated from Eq. (1).

Depth (m)	Time series	Net length (d)	Central date	Annual flux averages			
				Mass ($\text{mg m}^{-2} \text{d}^{-1}$)	BSi ($\mu\text{mol m}^{-2} \text{d}^{-1}$)	CaCO ₃ ($\mu\text{mol m}^{-2} \text{d}^{-1}$)	POC ($\mu\text{mol m}^{-2} \text{d}^{-1}$)
200	All 200 m	3472	1999 May 30	111	586	451	1260
200	200–1000 m	3183	1999 Nov 25	102	543	422	1130
200	200–1000–3800 m	2452	1999 Sep 10	104	568	409	1190
1000	All 1000 m	4957	1997 Sep 14	119	948	438	471
1000	200–1000 m	3183	1999 Nov 25	117	940	442	430
1000	1000–3800 m	3448	1997 Jan 29	117	927	441	447
1000	200–1000–3800 m	2452	1999 Sep 10	118	979	428	445
3800	All 3800 m	5302	1993 Dec 23	88.0	694	338	226
3800	1000–3800 m	3448	1997 Jan 29	88.9	733	321	228
3800	200–1000–3800 m	2452	1999 Sep 10	90.0	794	304	213

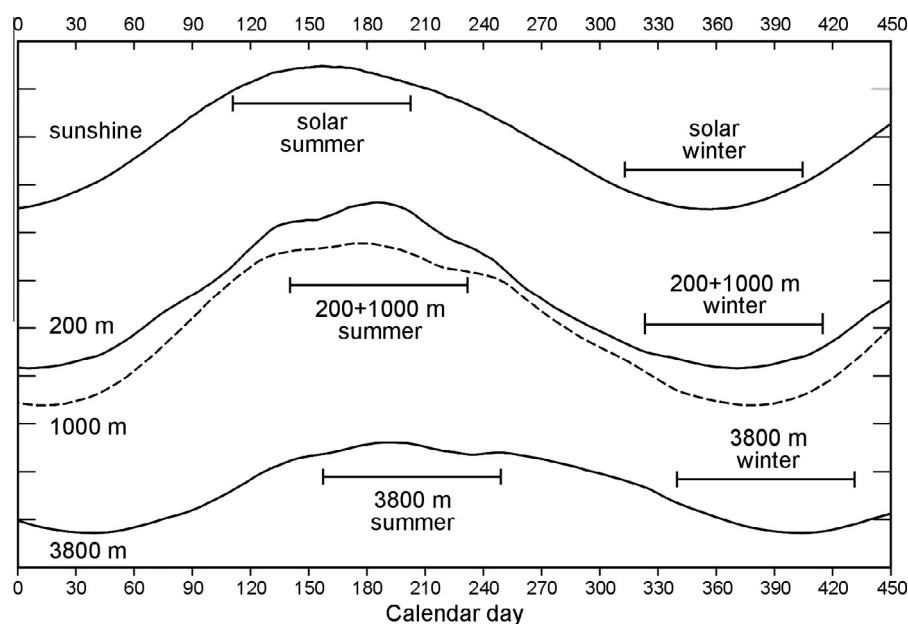


Fig. 9. 91-day running average passed through climatological curves of sunshine and mass flux at 200 m, 1000 m and 3800 m.

177°W) (Takahashi et al., 2000). After removing the lithogenic component, the composition of sediment caught at station AG is similar to sediment from the deep traps at OSP (Table 2). POC fluxes are also similar at both stations (Table 1). Annual fluxes at station AG, however, are ~80% for BSi and ~90% for CaCO₃ of those at 3800 m at OSP, with especially low fluxes in fall and winter. During the 2+ years of deployment at station AG, traps sampled 418 days of spring–summer but only 210 days of fall–winter, so under-sampling may have biased low the estimates of annual flux.

5. Discussion

5.1. Characteristics of sediment flux and composition

The global average sediment-trap flux at 2 km depth is 112–120 $\text{mmol m}^{-2} \text{y}^{-1}$ for each of the biogenic components, BSi, CaCO₃ and POC (Honjo et al., 2008). Assuming exponential flux decline from 1000 m to 3800 m, OSP fluxes (Table 1) interpolated to 2 km are 310 $\text{mmol BSi m}^{-2} \text{y}^{-1}$, 146 $\text{mmol CaCO}_3 \text{ m}^{-2} \text{y}^{-1}$ and 132 $\text{mmol POC m}^{-2} \text{y}^{-1}$. These fluxes are higher than the global averages by factors of 2.7 for BSi, 1.3 for CaCO₃ and 1.1 for POC. Most often BSi or CaCO₃ predominates the settling flux (Honda,

2003; Honjo et al., 2008), allowing the oceans to be classified into siliceous basins, occurring at high latitudes, and calcareous basins, usually found at mid and low latitudes. The ecology and geochemistry at OSP are thus unusual, since they occur in a siliceous basin but where CaCO₃ fluxes are higher than the global average. The small lithogenic fluxes at OSP also are not usual, but they may not extend throughout the Alaska Gyre since lithogenic fluxes were high at station AG. In this section we consider further some of the characteristics of sediment flux and composition at OSP.

5.1.1. POM:POC and BSi:Si weight ratios

The POM:POC weight ratio (Table 4) of sediment collected at 200 m (1.62) is lower than ~1.87 characteristic of fresh plankton (Anderson, 1995; Hedges et al., 2002) likely because of the presence of swimmer-associated lipids (POM:POC = 1.27–1.64 Laws, 1991). Higher POM:POC ratios (2.16–2.33) for sediments from 1000 m and 3800 m, in agreement with the ratio of 2.2 determined by Klaas and Archer (2002), can be explained by preferential loss of lipids from the sinking flux and by synthesis of compounds with high POM:POC ratios. Organic compounds caught by shallow traps (Lee et al., 2004; Wakeham et al., 1997) are similar to those of overlying plankton but, at deep traps, lipids are preferentially lost

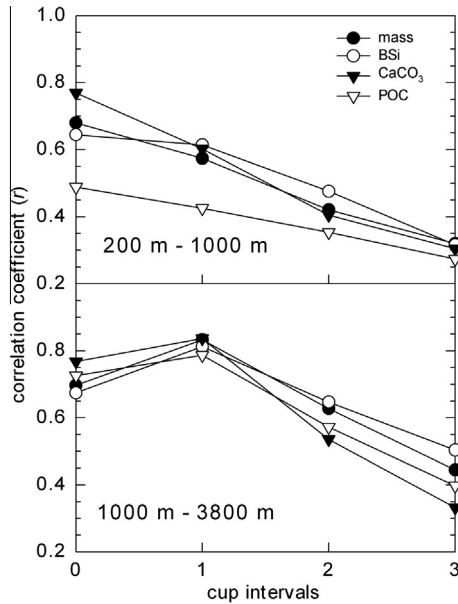


Fig. 10. Correlation coefficient of mass fluxes at 200 m and 1000 m, and at 1000 m and 3800 m, as deep fluxes are shifted backwards by one bottle duration.

Table 4

Weight ratios (\pm standard error) from Eq. (3) fit to data from OSP bottles for which AI was measured, excluding those that sampled an AI flux event beginning February 1990 (Section 3.4). Three outliers from 3800 m also have been removed. $r^2 > 0.99$ and $F > 3000$ for all regressions. Low LM:AI ratios at 200 m and 1000 m with high standard error indicate LM fluxes are too low for detection with this model.

Depth (m)	POM:POC	BSi:Si	LM:AI	Intercept ($\text{mg m}^{-2} \text{d}^{-1}$)	<i>n</i>
200	1.62 ± 0.04	2.39 ± 0.03	3.65 ± 7.2	0.63 ± 1.02	52
1000	2.16 ± 0.10	2.35 ± 0.03	3.18 ± 9.8	-0.82 ± 0.58	96
3800	2.33 ± 0.13	2.28 ± 0.03	13.0 ± 4.7	-0.37 ± 0.81	83

while carbohydrates and amino acids with POM:POC typically >2 (Anderson, 1995; Laws, 1991) are preserved. Lee et al. (2004) also suggest that at least some of the uncharacterized POM, comprising $\geq 70\%$ of total POM at deep traps, consists of transparent exopolymers (Zhou et al., 1998), extracellular polymeric substances (Allison and Sutherland, 1987) and structural macromolecules such as peptidoglycan (Benner and Kaiser, 2003; Hedges et al., 2001). Sugars and amino acids comprise the bulk of these molecular groups, giving the uncharacterized fraction of marine POM a likely POM:POC ratio >2 .

The BSi:Si ratios of Table 4 are in close agreement with 2.4 for BSi that is 10% water by weight as determined for sediments younger than 30 M y (Mortlock and Froelich, 1989). The small decrease from 2.39 at 200 m to 2.28 at 3800 m is consistent with a preferential loss of water from the BSi matrix as it dissolves (Schmidt et al., 2001).

5.1.2. C:N ratios

POC:PN (C:N) ratios of the sinking particles at OSP, as discussed previously (Wong et al., 1999), reflect the variability normally seen in oceanic plankton (Antia et al., 1963; Parsons et al., 1961; Redfield et al., 1963), but decreases in C:N with depth (Table 2 and Fig. 8) contradict the generalization that more rapid N recycling should lead to increases (Toth and Lerman, 1977; Verity et al., 2000). Average C:N (13) at 200 m is likely elevated by lipids carried by copepod swimmers (Wakeham et al., 1993; Wong et al., 1999),

suggested also by the low POM:POC ratio at 200 m and by the higher flux correlations at 200 m for PN than for POC (Table 5). Grazing of trapped particles may have been minimized by the use of NaN_3 poison (Gardner, 2000), but small swimmers and body parts including lipid sacks would have passed the $1000 \mu\text{m}$ screens during sample preparation. Lipid accumulation within the grazer community (Mackas et al., 1998) can explain the July peak in C:N (Fig. 8) lagging maximum copepod biomass by about a month (Fig. 2j). Fig. 2j implies mesozooplankton are absent in winter. However, copepods are active year-round at OSP (Goldblatt et al., 1999), possibly explaining why no 200–1000 m sample pair showed increasing C:N with depth, even in winter (not shown).

The C:N ratio does not increase on going from 1000 m to 3800 m at OSP, again contrary to expectation. However, in the South Atlantic Ocean, C:N decreases from the mesopelagic zone into the bathypelagic zone (Table 3 of Schneider et al., 2003) and below 3000 m the C:N ratio normally decreases with depth (Fig. 5 of Schneider et al., 2003). POM solubilization after sediment has been trapped (Antia, 2005) might affect these changes, as might swimmer contamination by copepods that exceed 1000 m during ontogenic migration (Kobari and Ikeda, 2001; Miller et al., 1984). Sorption of ammonium and/or nitrogen-rich dissolved organic matter also may cause the decline in C:N with depth observed globally below 3000 m, as proposed for deep-sea sediments (Müller, 1977) and in experiments where C:N decreases with increasing BSi and CaCO_3 content for various sediment mixtures suspended in seawater (De La Rocha et al., 2008).

5.1.3. Compositional variability and flux-flux correlations

Compositional variability at OSP (Fig. 6 and cvs of Table 2) is higher than for a similar trap time series in the subtropical Sargasso Sea (Conte et al., 2001), where cvs for %POC are 0.53, 0.21 and 0.15 at 500 m, 1500 m and 3200 m, respectively, and for % CaCO_3 are 0.26, 0.12 and 0.08 at progressively deeper depths (BSi composition not available at all depths). Compositional variability of POC and CaCO_3 thus decreases threefold from shallow to deep traps in the Sargasso Sea, whereas at OSP it decreases by a factor of only ~ 1.5 (Table 2). Conte et al. (2001) attribute most of the depth-homogenization in the Sargasso Sea to an active mesopelagic zooplankton community. Primary production measured by ^{14}C uptake in both the Sargasso Sea and the Alaska Gyre is similar ($40 \pm 15 \text{ mmol m}^{-2} \text{d}^{-1}$ Harrison, 2002; Lohrenz et al., 1992; Lomas et al., 2009), but bathypelagic fluxes at OSP are $2.5\times$ higher for total mass and $1.6\times$ higher for POC, indicating less

Table 5

Flux-flux correlation coefficients (*r*) at each depth, for fluxes collected simultaneously at all three depths (Table 3); *n* = 151.

	Mass	BSi	CaCO_3	POC
<i>BSi</i>				
200 m	0.84			
1000 m	0.90			
3800 m	0.91			
<i>CaCO₃</i>				
200 m	0.95	0.67		
1000 m	0.88	0.59		
3800 m	0.85	0.55		
<i>POC</i>				
200 m	0.67	0.46	0.54	
1000 m	0.81	0.75	0.63	
3800 m	0.85	0.74	0.73	
<i>PN</i>				
200 m	0.83	0.63	0.70	0.93
1000 m	0.80	0.71	0.66	0.98
3800 m	0.87	0.78	0.73	0.97

active water-column recycling in the Alaska Gyre than in the Sargasso Sea.

Despite high compositional variability at OSP, constituent fluxes are well correlated (Table 5) because flux variability is much higher (Fig. 11). Such low variability of POC content, compared to flux, led to the proposal that POC flux is determined by its association with dense minerals (Armstrong et al., 2002), with POC transfer efficiency reasonably predicted by fluxes of CaCO_3 without consideration of BSi fluxes (François et al., 2002; Klaas and Archer, 2002). Klaas and Archer (2002) attributed this to high CaCO_3 density, whereas François et al. (2002) attributed it to tight coupling between primary and secondary producers causing export largely in the form of fecal pellets in low-latitude calcareous oceans, with lower coupling in high-latitude siliceous oceans causing export in the form of aggregates. They proposed the lower POC transfer efficiencies to 2000 m for siliceous ecosystems thus is a packaging effect, since aggregates disintegrate and decompose more readily than do fecal pellets. This latter interpretation is supported by the flux comparisons between high-latitude OSP and low-latitude Sargasso Sea. At OSP, POC fluxes at 1000 m are better correlated with BSi fluxes than with CaCO_3 fluxes, but convergence to $r = \sim 0.7$ for both associations at 3800 m (Table 5) suggests POC passes through the bathypelagic zone more efficiently with CaCO_3 . This may result from differential ballasting between minerals

(Armstrong et al., 2002; Klaas and Archer, 2002), or from changes in package integrity as the ecosystem shifts from siliceous to calcareous (De La Rocha et al., 2008; De La Rocha and Passow, 2007; François et al., 2002; Passow, 2004; Passow and De La Rocha, 2006).

5.1.4. Dilution of POC by BSi and CaCO_3

POC content at OSP tends to be highest in winter when mass flux is low (Fig. 6), except at the deepest trap where it is highest in fall, possibly due to high winter secondary fluxes impoverished in POC (Section 5.7.3). The high seasonality in fluxes of BSi and CaCO_3 , compared to POC flux seasonality (Section 4.1), translates into weak or negative correlations between %POC and POC flux (Fig. 11) and between %POC and mass flux (Fig. 12). One possible reason for these comparative seasonalities is that POC flux is suppressed in summer because a higher proportion of POC production is respired above 200 m. Another possibility is that bio-mineral fluxes are suppressed in winter because the energy demands of buoyancy (Richardson and Cullen, 1995; Smayda, 1970; Smetacek, 1985; Waite et al., 1992) when light and iron co-limit photosynthesis (Maldonado et al., 1999) provide a measurable advantage for the growth of un-armoured phytoplankton.

A positive correlation between %POC and mass accumulation exists when a wide range of depositional regimes is compared

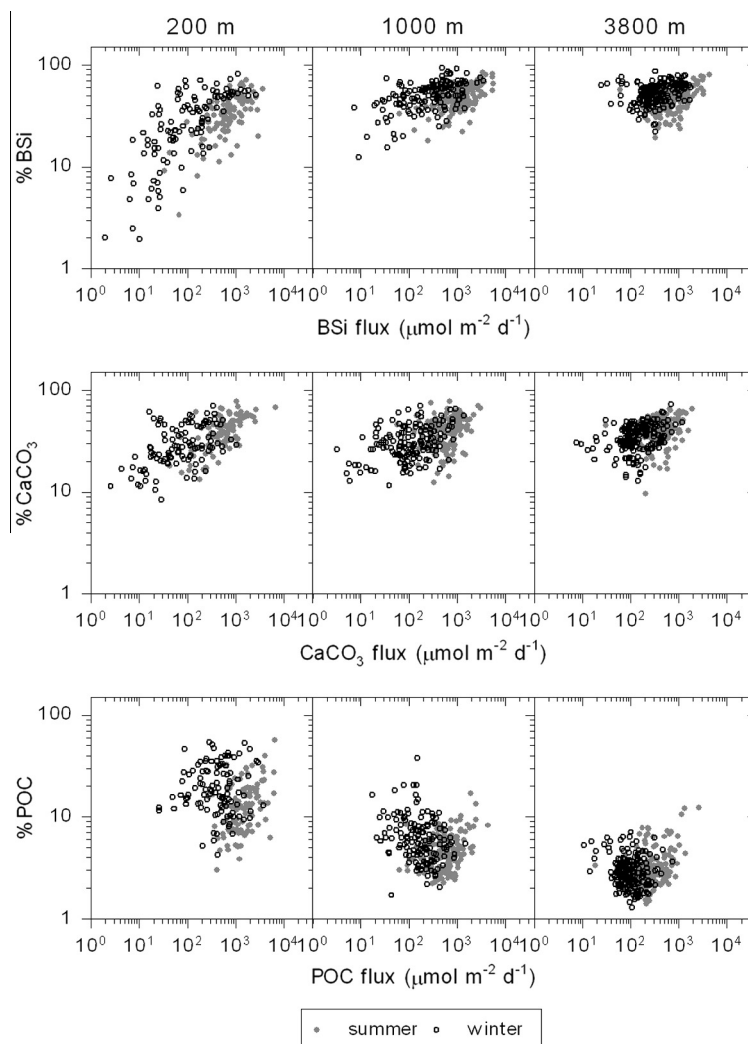


Fig. 11. Content versus flux for BSi, CaCO_3 and POC at each depth at OSP. “Summer” is from mid spring to mid fall and “winter” is from mid fall to mid spring, as defined in Section 3.2.

(e.g., Müller and Suess, 1979), possibly because a component of organic matter escapes degradation when sedimentation rate is high and because the correlation exists in sediment delivered to the seafloor (Emerson and Hedges, 1988). This latter explanation should not be generalized to single oceanic locations, since a positive correlation between %POC and the mass flux caught by traps does not exist in the Sargasso Sea (Conte et al., 2001) or at OSP. Indeed, %POC is inversely proportional to mineral flux when comparing deltaic and non-deltaic continental-shelf sediments (Mayer, 1995) and, in the Alaska Gyre, a sediment core collected by McDonald et al. (1999) shows low %POC in some opal-rich facies deposited during high-flux events.

5.2. Timing and mechanisms of BSi, CaCO₃ and POC export

Export flux follows an annual cycle defined by sunshine (Fig. 9), while surface chlorophyll concentration shows little seasonality (Fig. 2h). Chlorophyll-normalized photosynthesis is proportional to irradiance below light saturation (e.g., Cullen et al., 1993), so export flux tracks changes in the rate of primary production at OSP. In the Northeast Atlantic Ocean, high fluxes to 3100-m traps lagged spring peaks in primary production and chlorophyll biomass by about a month (Newton et al., 1994), and in the Sargasso Sea (Deuser et al., 1990) and at a station near the Canary Islands (Neuer et al., 1997), the lag between peaks in satellite-derived chlorophyll biomass and ~3000-m flux was 1.5 months and one month, respectively. These lags are remarkably similar to the 1.5 months between irradiance and sinking flux at 3800 m at OSP, since the physical conditions and plankton ecology in the Northeast Atlantic Ocean (Savidge et al., 1995) and in the subtropical Atlantic Ocean (Lohrenz et al., 1992) differ considerably from those in the HNLC waters at OSP.

Unlike fluxes of BSi and CaCO₃, POC fluxes progressively increase throughout summer, peaking in July–August (Fig. 7). A number of factors can contribute to the separation of bio-mineral and POC fluxes, including microzooplankton grazing, mesozooplankton mortality and molting, and POC accumulation in the mixed layer. Microzooplankton are thought to maintain low chlorophyll biomass by grazing new phytoplankton growth at OSP (Harrison, 2002; Landry et al., 1993; Miller et al., 1988; Strom and Welschmeyer, 1991; Welschmeyer et al., 1991); for opposing view see Rivkin et al., 1999). Microzooplankton grazing exports phytoplankton shells stripped of organic matter, consistent with flux climatologies of BSi and CaCO₃ that track photosynthesis while POC is retained and respired in the mixed layer. Grazing by mesozooplankton copepods causes <10% of POC export at OSP (Thibault et al., 1999), with trapped material containing few copepod fecal pellets and undamaged diatom frustules (Takahashi, 1986; Takahashi, 1987c) as occurs from grazing by microzooplankton (Buck and Newton, 1995; Jacobson and Anderson, 1986). Copepod death and molting, however, contribute significantly to POC fluxes in the subarctic North Pacific Ocean (Haake et al., 1993a; Kobari et al., 2008), and may cause the high fluxes of large (>1000 μm) particles in August–September at 200 m and at 1000 m, and in fall-winter at the deepest trap (Fig. 13). Lastly, mixed-layer POC concentrations at OSP at least double from spring into summer, based on increases in C:chl*a* ratios (Booth et al., 1993; Peña and Varela, 2007) and invariant chl*a*. These higher POC concentrations must translate into increased POC export and/or recycling, since phytoplankton with high growth rate constitute chlorophyll biomass.

The drop in POC flux in late August and September (Fig. 5) is notable because primary production is still high at this time of year (Fig. 2i). High respiration rates (e.g., Laws et al., 2000; Sakshaug, 1993) by dinoflagellates, large diatoms and microheterotrophs,

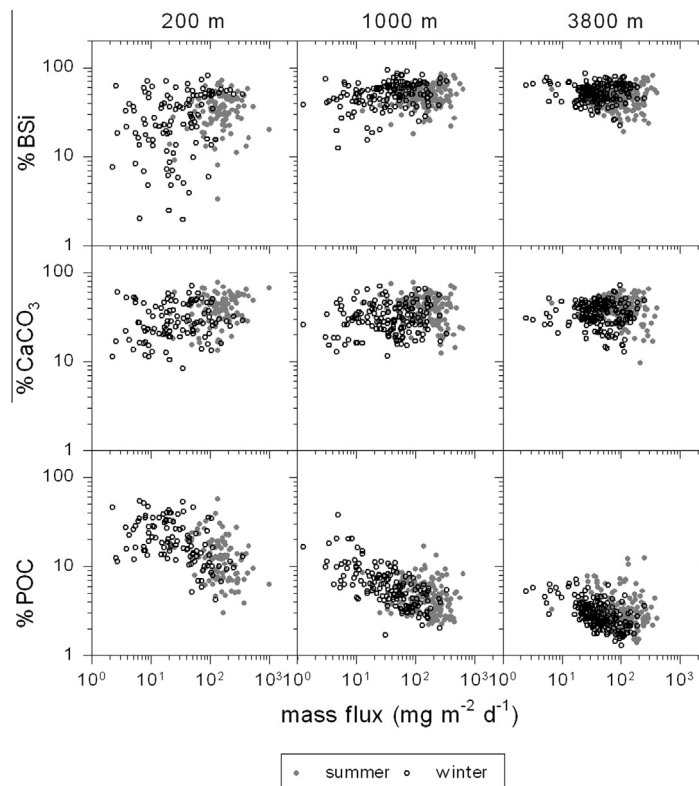


Fig. 12. %BSi, %CaCO₃ and %POC versus total mass flux at each depth at OSP. Caption of Fig. 11 explains “summer” and “winter” delineations.

all common in the warm waters of late summer (Fig. 2d) (Booth et al., 1993; Strom et al., 1993; Takahashi, 1986), may contribute to these low POC fluxes.

5.3. BSi export in relation to $\text{Si}(\text{OH})_4$ climatology

Delayed diatom growth in spring has been inferred from declining mixed-layer concentrations of nitrate (NO_3^-) beginning in ~March followed two months later by declining concentrations of silicic acid ($\text{Si}(\text{OH})_4$) (Fig. 2) (Harrison, 2002; Harrison et al., 1999; Peña and Varela, 2007; Whitney and Freeland, 1999). This inference is not supported by the flux climatologies of BSi, CaCO_3 and POC, however, which all ramp-up at the onset of spring (Fig. 5). Nor is there a scarcity of diatoms in surface waters of the Alaska Gyre in late-winter and spring. Examples from OSP include a sustained population of large diatoms observed in November–February 1980–1981 (Clemons and Miller, 1984); a significant population of *Nitzschia cylindroformis* extending from OSP to at least 170 km to the west in May 1988 (Booth et al., 1993); high mixed-layer abundance of large diatoms identified as *Fragilariopsis* sp. and *Chaetoceros* sp. (and of the coccolithophorid *Emiliana huxleyi*) in February 1996 (Lam et al., 2006); and high diatom contributions to primary production in spring (Boyd and Harrison, 1999).

Weather ship data collected ~daily at OSP (Fig. 14) permit us to examine spring nutrient decline. Within the tremendous inter-annual variability in surface $[\text{NO}_3^-]$ and $[\text{Si}(\text{OH})_4]$ in late-winter and spring, there is no evidence of NO_3^- drawdown unaccompanied by $\text{Si}(\text{OH})_4$ drawdown. Both nutrients declined during spring of some years (e.g., 1972, 1973, 1974, 1979), whereas during spring of other years (e.g., 1975, 1976, 1977, 1980) neither nutrient de-

clined. Additionally, $[\text{Si}(\text{OH})_4]$ was prone to singular drops in spring, likely the result of diatom growth. The reason for the contrast between $[\text{NO}_3^-]$ and $[\text{Si}(\text{OH})_4]$ spring climatologies (Fig. 2), however, lies in the pronounced *rebounds* in $[\text{Si}(\text{OH})_4]$ not matched by $[\text{NO}_3^-]$ (e.g., May–June 1972, March–April 1973, April–June 1976 and April–May 1980), leading at times to $[\text{Si}(\text{OH})_4]$ exceeding pre-spring values (Fig. 14). These events probably result from the steep vertical $[\text{Si}(\text{OH})_4]$ gradient at the base of the mixed layer (Fig. 15), causing storm erosion of the pycnocline during spring when stratification is weak (high surface density and deep MLD; Fig. 2e) to mix more $\text{Si}(\text{OH})_4$ than NO_3^- towards the surface. In contrast, the prolonged $\text{Si}(\text{OH})_4$ depletions of ~July–September (Fig. 14) (Wong and Matear, 1999) are restricted to the period of minimum $\text{Si}(\text{OH})_4$ supply from mixing. Indeed, the May–August decline in surface $[\text{Si}(\text{OH})_4]$ (Fig. 2g) coincides much better with mixed-layer shoaling (Fig. 2e) than with diatom growth occurring ~one month prior to BSi export (Fig. 5), suggesting that only during the short period when the mixed layer is most stratified can it be assumed mixing does not play a significant role in surface $\text{Si}(\text{OH})_4$ mass balance.

5.4. Flux stability index

A seasonality index based on the number of months required for 1/2 of annual production to occur (production half-time), was proposed as a means to account for high export efficiency (export flux / primary production) when primary production is episodic (Berger and Wefer, 1990). The concept of production half-time was later used to define the flux stability index (FSI) as the time required for half of annual sediment-trap fluxes to accumulate (Antia et al., 2001; Lampitt and Antia, 1997). To avoid the problems of generating annual FSI values from multi-year time series with gaps, we have calculated one FSI value for each depth at OSP: $\text{FSI} = (\text{time required for } 1/2 \text{ the flux to accumulate}) / (\text{length of time series})$. Accordingly, FSI (t/t) equals 0.5 for constant flux and decreases as fluxes become more episodic. At OSP, 200-m fluxes of BSi and CaCO_3 are the most episodic ($\text{FSI} \approx 0.16$), with fluxes of POC ($\text{FSI} \approx 0.19$) and total mass ($\text{FSI} \approx 0.20$) slightly less episodic (Fig. 16). This ordering may result from the fluxes of each plankton species having a unique phase, with fewer species contributing to fluxes of BSi and CaCO_3 than to fluxes of total mass and POC.

FSI of total mass, BSi and CaCO_3 increases with depth at OSP (Fig. 16), consistent with the global trend for FSI_{mass} (Lampitt and Antia, 1997), but FSI_{POC} slightly decreases from 1000 m to 3800 m and globally there is no clear trend with depth in FSI_{POC} (Lampitt and Antia, 1997). Increases with depth in FSI_{mass} have been attributed to the larger catchment area of deep traps (Lampitt and Antia, 1997). Interactions between particles of varying settling rates will also increase FSI with depth, and heterotrophic communities can modify FSI by delaying or hastening material transport. In contrast, Greater degradation of POC during periods of low flux at OSP (Haake et al., 1993a) will tend to decrease FSI_{POC} at depth by amplifying the difference between high and low flux events. Combined with the factors that increase FSI_{mass} at depth, this degradation effect might explain the small and irregular depth variability in FSI_{POC} observed at OSP and globally.

An increase in FSI_{mass} of 9.8/182.5 (d/d) per km depth is estimated for the global data set of Lampitt and Antia (1997). At OSP, however, FSI_{mass} increases by only 0.68/182.5 and 1.6/182.5 per km at the shallow and deep depth intervals, respectively, reflective of the compositional heterogeneity that is maintained as particles sink at OSP but not in the subtropical North Atlantic Ocean (Section 5.1.3). Lampitt and Antia (1997) also estimated FSI_{mass} of 0.14, 0.25 and 0.26 for three one-year intervals of the 3800-m time series from OSP, which on average agrees with the long-term FSI_{mass} at 3800 m of 0.23, but indicates considerable interannual variability in the episodicity of bathypelagic fluxes at

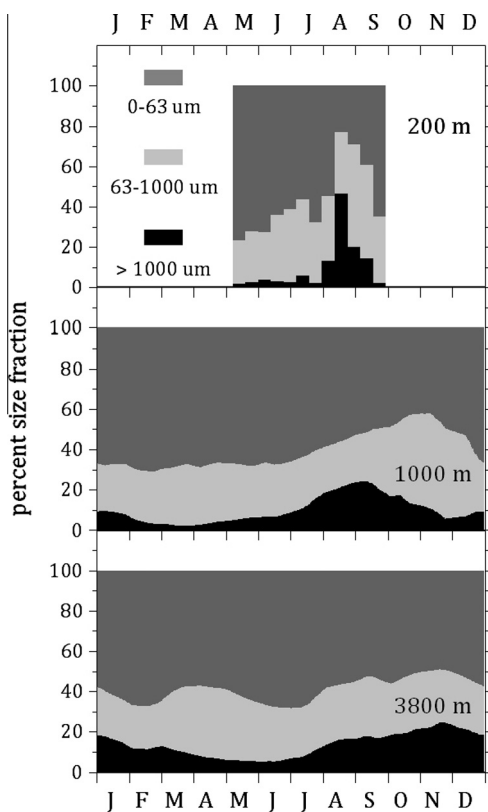


Fig. 13. The proportion of the three size fractions to the total mass flux based on trap fluxes collected from 1983 to 1989. The equivalent of 2.0 and 5.1 years of size-fractionated data were collected and analyzed at 1000 m and 3800 m, respectively, but at 200 m size fractionations were analyzed only for deployment PA15 (8 May 1989–29 September 1989).

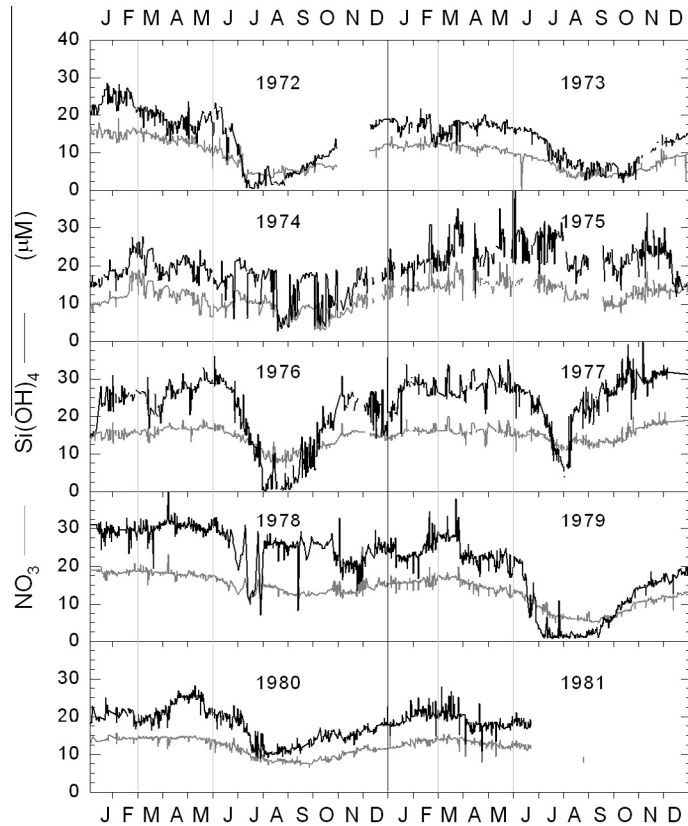


Fig. 14. NO_3^- and $\text{Si}(\text{OH})_4$ concentrations at 5 m during weathership occupation at OSP. The entire time series (1970–1981) is presented by Wong and Matear (1999) who discuss summer $\text{Si}(\text{OH})_4$ depletions of 1972, 1976 and 1979. Data collected prior to 1972 are noisy and not included here. Grey vertical lines highlight the months when climatological curves (Fig. 2f and g) show declines in NO_3^- but not in $\text{Si}(\text{OH})_4$.

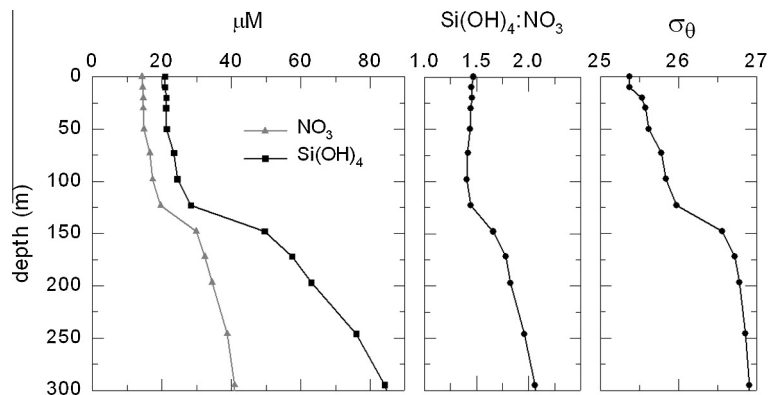


Fig. 15. Vertical profiles of nutrient concentration, the $\text{NO}_3^-:\text{Si}(\text{OH})_4$ molar ratio and density (σ_θ), 17 May 1990 at OSP.

OSP. According to Berger and Wefer's (1990) categorizations, the total flux at OSP is "pulsed" at 200 m and "strongly seasonal" at 3800 m.

5.5. POC export efficiency

POC export efficiency, or the e -ratio (Downs, 1989), again is defined as (POC export flux)/(primary production). Comparing yearly-averaged primary production of $\sim 40 \text{ mmol C m}^{-2} \text{ d}^{-1}$ (Harrison, 2002) to annual POC flux (Table 1), export efficiency at OSP is 3.1%, 1.2% and 0.57% at 200 m, 1000 m and 3800 m, respectively. At steady state, the f -ratio (new nutrient assimilation / total nutrient assimilation) is identical to the e -ratio determined at the base of

the euphotic zone (e.g., Laws et al., 2000). Measures of the f -ratio at OSP range from $\sim 27\%$ (Varela and Harrison, 1999) to $\sim 36\%$ (Wheeler and Kokkinakis, 1990). Export efficiency of 3.1% at 200 m thus appears very low. However, at least half of sinking POC is expected to decay between the base of the euphotic zone and 200 m (Bishop, 1989; Primeau, 2006; Timothy, 2004) and DOC production equivalent to $\sim 25\text{--}50\%$ of primary production at OSP (Bishop et al., 1999) may be an important component of export that escapes sediment traps. Trapping efficiency (Buesseler et al., 2007), solubilisation within traps (Antia, 2005) and swimmers (Michaels et al., 1990) present other uncertainties especially in the epipelagic zone. Results from the deeper traps, less prone to these biases, are consistent with the relationship between FSI_{mass} and ex-

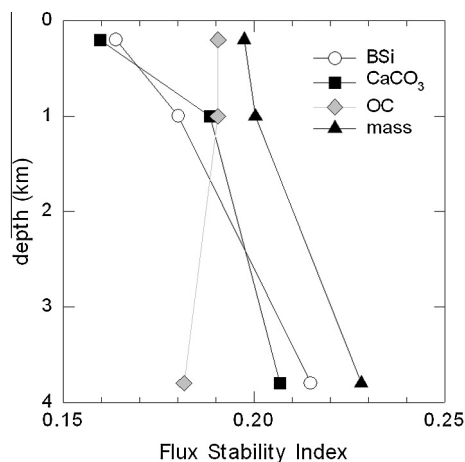


Fig. 16. Flux stability index (FSI) of constituent and total fluxes at OSP.

port efficiency of Lampitt and Antia (1997), which predicts an export efficiency at 2000 m of 1.2% using FSI_{mass} measured at 1000 m or 3800 m at OSP.

5.6. Net production

5.6.1. Organic carbon

Net community production of organic carbon (NCP_{OC}) represents the upper limit of the biological pump of CO_2 into the deep ocean. NCP_{OC} , new production and export production should be equivalent at steady state (Platt et al., 1989), so POC fluxes at 200 m are at least a factor of two lower than expected based on the above comparison of the e -ratio and the f -ratio. Nevertheless, the climatology of POC flux generates a valuable description of the seasonality of NCP_{OC} , provided there is little distortion of the seasonal cycle of POC flux caused by trap biases. In this section, we estimate annual NCP_{OC} at OSP by normalizing the climatological curve of POC flux to a seasonal measure of NCP_{OC} .

Emerson and Stump (2010) estimate NCP_{OC} from O_2 accumulation in the mixed layer at OSP from June 2007 to February 2008. They obtain an O_2 accumulation rate of 0.022 – 0.027 $mol\ m^{-2}\ d^{-1}$ for calendar days 170 to 290 (mid June to mid October), with O_2 accumulation undetectable after October. Assuming O_2 production over 150 d (Emerson, 1987) of 0.024 $mol\ m^{-2}\ d^{-1}$ and an O_2 :OC production ratio of 1.45, they estimate NCP_{OC} is 2.5 $mol\ m^{-2}\ y^{-1}$ at OSP.

Fluxes at 200 m and 1000 m are similarly related to surface production at OSP, with a one-month delay between primary production and trap flux at both depths (Section 3.2). The measures of O_2 accumulation over calendar days 170–290 (Emerson and Stump, 2010) are therefore equivalent to trap fluxes over days 200–320. POC fluxes over days 200–320 constitute 42% of annual POC flux at 200 m and 50% of annual POC flux at 1000 m. Assuming 0.022 – 0.027 $mol\ O_2\ m^{-2}\ d^{-1}$ accumulating over 120 days represents 42–50% of NCP_{OC} and using an O_2 :OC production ratio of 1.45, we estimate NCP_{OC} is 3.6 – 5.3 $mol\ m^{-2}\ y^{-1}$ at OSP. This estimate is about double those based on nutrient and gas tracers within the mixed layer (Emerson and Stump, 2010; Goes et al., 2001; Wong et al., 2002) and based on ^{234}Th mass balance at OSP (Charette and Moran, 1999), probably because the tracer estimates are forced to assign $NCP_{OC} = 0$ to much of the year surrounding winter when surface signals of biological activity do not accumulate. This lack of accumulation must be due to strong mixing (e.g., Large et al., 1986), because winter rates of primary production are high at OSP, equivalent to about 50% of rates in spring and summer (Harrison et al., 2004), and there is no evidence the f -ratio is

low in winter (Varela and Harrison, 1999). Our estimate, however, does match others not affected by mixing. It matches estimates of new production (3.2 – 6.5 $mol\ OC\ m^{-2}\ y^{-1}$) based on bottle measurements of primary production (12 – 18 $mol\ OC\ m^{-2}\ y^{-1}$; Harrison, 2002) and f -ratios of 0.27 – 0.36 (Varela and Harrison, 1999; Wheeler and Kokkinakis, 1990), and it matches export production at OSP (4.2 $mol\ OC\ m^{-2}\ y^{-1}$) determined from global modeling of ocean chemistry (Schlitzer, 2004). It also agrees with the estimate of NCP_{OC} (~ 4.4 $mol\ m^{-2}\ y^{-1}$) based on organic carbon remineralization between 200 m and 900 m in the subarctic Pacific Ocean (2.0 $mol\ m^{-2}\ y^{-1}$; Feely et al., 2004b), assuming 1/2 of OC export degrades above 200 m (e.g., Primeau, 2006) and a small POC flux of ~ 0.2 $mol\ m^{-2}\ y^{-1}$ (as at 1000 m at OSP; Table 1) remains at 900 m. These comparisons show that tracer measures of NCP_{OC} may be accurate when mixing is low, but a realistic model of seasonality such as trap fluxes of POC must be used when translating to annual NCP_{OC} .

5.6.2. CaCO₃

Sediment-trap records can also constrain net community production of $CaCO_3$ (NCP_{IC}), a fundamental baseline measurement as calcifying plankton respond to future ocean acidification (Feely et al., 2004a). Previous estimates of $CaCO_3$ production range over an order of magnitude at OSP, from 0.12 – 0.20 $mol\ m^{-2}\ y^{-1}$ based on plankton growth rates (Fabry, 1989) to 1.5 $mol\ m^{-2}\ y^{-1}$ from bottle measures of $CaCO_3$ production (Lipsen et al., 2007). These estimates do not distinguish between $CaCO_3$ production before and after biologically-mediated dissolution in the euphotic zone, which can be significant (Antia et al., 2008; Bishop and Wood, 2008; Feely et al., 2002; Milliman et al., 1999). Following others, we estimate NCP_{IC} as the product of NCP_{OC} and the $CaCO_3$:OC production ratio. This ratio determines ocean-atmosphere CO_2 flux (Archer et al., 2000; Broecker and Peng, 1982), but it, too, is poorly constrained in the region of OSP, with estimates ranging from 0.05 – 0.1 based on global modeling (Jin et al., 2006; Sarmiento et al., 2002) to 0.5 from measures of fCO_2 and pH during summer-fall 2007 (Emerson et al., 2011). The long-term $CaCO_3$:POC flux ratio to traps at 200 m, 0.37 (Table 2), sets the upper limit of the $CaCO_3$:OC production ratio, since more rapid POC remineralization increases the ratio at depth (our Table 2; Feely et al., 2004b). Fluxes to surface-tethered traps at 200 m at OSP are 32% and 65% for POC and $CaCO_3$, respectively, of the fluxes at 50 m (Wong et al., 1999), giving a $CaCO_3$:POC flux ratio of 0.18 at 50 m. The $CaCO_3$:OC production ratio may be lower, since loss of POC is greater than loss of $CaCO_3$ during storage in trap bottles (Antia, 2005), and OC production exported as DOC also reduces the ratio.

The trap records setting an upper $CaCO_3$:OC production ratio of 0.18 , along with our estimate for NCP_{OC} (3.6 – 5.3 $mol\ m^{-2}\ y^{-1}$), gives 0.65 – 0.95 $mol\ m^{-2}\ y^{-1}$ as an upper estimate for NCP_{IC} at OSP. NCP_{IC} should equal the sum of $CaCO_3$ dissolution in the water column and deep $CaCO_3$ flux. $CaCO_3$ dissolution is estimated to be $0.62 \pm 50\%$ $mol\ m^{-2}\ y^{-1}$ between 200 m and 1500 m in the Pacific Ocean north of $40^\circ N$ (Berelson et al., 2007) and 0.051 $\mu mol\ kg^{-1}\ y^{-1}$ below 1500 m (0.12 $mol\ m^{-2}\ y^{-1}$ between 1500 m and 3800 m) in the Pacific Ocean (Feely et al., 2002), and $CaCO_3$ flux at 3800 m is 0.12 $mol\ m^{-2}\ y^{-1}$ at OSP (Table 1). The required $CaCO_3$ flux at 200 m of 0.43 – 1.2 $mol\ m^{-2}\ y^{-1}$ (the lower bound excludes dissolution attributed to waters below 1500 m since this dissolution might occur at boundary sediments (Berelson et al., 2007)) must be augmented by the amount of dissolution that occurs between the base of the euphotic zone and 200 m. Assigning to dissolution the 35% loss of sinking $CaCO_3$ from 50 m to 200 m measured by surface-tethered traps (Wong et al., 1999), the $CaCO_3$ flux at 50 m required to balance dissolution and abyssal flux, 0.67 – 1.8 $mol\ m^{-2}\ y^{-1}$, overlaps with our estimate of NCP_{IC} .

The CaCO_3 :POC flux ratio of 0.18 at 50 m is virtually identical to the CaCO_3 :POC production ratio of 0.17 estimated from bottle incubations performed over three years at OSP (Lipsen et al., 2007). About 70% of CaCO_3 production determined from incubations, therefore, must dissolve in the euphotic zone to match the POC recycling described by the f -ratio at OSP. High rates of surface CaCO_3 dissolution were observed in a mesocosm experiment where 27–70% of the CaCO_3 stock dissolved daily in the acidic digestive vacuoles of microzooplankton (Antia et al., 2008). Antia et al. (2008) also show that microzooplankton grazing, prominent at OSP (Section 5.2), dissolves more CaCO_3 than mesozooplankton grazing. Below the euphotic zone, less acidic microenvironments caused by a shift towards bacterially mediated and/or slower POC decay would result in less CaCO_3 dissolution relative to POC decay, as indicated by increasing CaCO_3 :POC flux ratios at depth observed at OSP and elsewhere.

5.7. Flux changes with depth

Deployment of shallow and deep sediment traps has led to a better understanding of water-column remineralization (Betzer et al., 1984; Bishop, 1989; Martin et al., 1987; Primeau, 2006; Suess, 1980; Timothy, 2004) and has provided the material to study particle sources, biochemical transformations and interactions between particle size classes (Bacon et al., 1985; Buesseler et al., 1990; Clegg et al., 1991; Haake et al., 1993a; Lee et al., 2004; Murnane, 1994; Murnane et al., 1990). Here, we assess modifications of sinking particles by comparing flux climatologies at two depths created from time series collected simultaneously (Table 3). First, however, we consider whether a one-dimensional (vertical) view of particle flux and transformation is appropriate at OSP by assessing the significance of horizontal gradients in export flux, and of local resuspension.

5.7.1. Horizontal transport and resuspension

Sinking particles transported horizontally between regions of different export production can affect flux changes with depth for a vertical array of traps (e.g., Siegel et al., 2008; Waniek et al., 2000). For horizontal transport to produce long-term biases, export flux from the area sampled by shallow traps must be persistently different than export flux from the area sampled by deep traps. How big an area might this represent? We estimate mean mesopelagic current speeds of $\sim 1 \text{ cm s}^{-1}$ in the region of OSP, from bulk transport between 200 m and 1000 m (Table 2 of Tabata, 1991) for flow from the west–southwest (Bograd et al., 1999). Assuming sinking rates of $100\text{--}350 \text{ m d}^{-1}$ (Section 3.3) and bathypelagic currents $\leq 1 \text{ cm s}^{-1}$, we derive a horizontal transport distance of $\leq 9\text{--}30 \text{ km}$ for particles sinking from 200 m to 3800 m. This result is consistent with modeling of particle trajectories to traps at 4000 m near Hawaii, where mean displacement distances $\leq 54 \text{ km}$ were found for particles with $sr \geq 50 \text{ m d}^{-1}$ (Siegel et al., 2008). Considering mean currents and eddy diffusion, Siegel et al. (2008) further estimated that the 95% surface containment radius (the statistical funnel) for a trap at 4000 m was $\sim 350 \text{ km}$ for material sinking at 50 m d^{-1} . At OSP, an area of this magnitude may be considered biogeochemically uniform, based on sea level data (Cummins and Lagerloef, 2004), satellite imagery (Wang and Shao, 2008) and decades of sampling (e.g., Booth et al., 1993; Clemons and Miller, 1984; Harrison et al., 2004). Thus, we assume that the climatological trends in flux with depth reflect one dimensional processes at OSP.

Resuspended sediments do not appear to reach the bathypelagic traps at OSP, further supporting a one-dimensional view with particles sinking from above. Within the bottom nepheloid layer reaching 500 mab in several ocean basins, trap fluxes increase exponentially and become more enriched in lithogenic material

(LM) as the seabed is approached (Dymond, 1984; Gardner and Richardson, 1992; Honjo et al., 1982; Walsh et al., 1988). At OSP, annually-averaged fluxes decrease from 1000 m to 3800 m (400 mab), but winter fluxes of BSi and CaCO_3 increase to the deepest trap ($F_{3800\text{m}}/F_{1000\text{m}} \sim 1.3$; Table 1). Nevertheless, LM content and its seasonality are low at 3800 m (Fig. 7) indicating resuspension to 3800 m is minor year-round. %LM was high for sediment caught at Station AG (Table 2) where the traps were closer to the bottom than at OSP, but even these traps were probably not in the bottom nepheloid layer. Average LM fluxes were $17 \text{ mg m}^{-2} \text{ d}^{-1}$ during deployments AG1, AG2 and AG3 (25, 16 and $9.5 \text{ mg m}^{-2} \text{ d}^{-1}$, respectively) when traps were at 3700 m (200 mab), and during AG4 were $18 \text{ mg m}^{-2} \text{ d}^{-1}$ when the trap was at 3500 m (400 mab). The similarity in LM flux at the two depths does not support local resuspension as the source of the lithogenic debris at Station AG. Rather, the source may be a chain of seamounts to the north, Surveyor Seamount being the closest (120 km from station AG) and rising to within 340 m of the surface.

5.7.2. Mesopelagic zone

Decreases in POC flux from 200 m to 1000 m (Fig. 17a) agree with empirical models of POC decay (e.g., Primeau, 2006), but the record from OSP is prone to the sediment-trap artifacts discussed in Section 5.5. Actual POM fluxes, especially at 200 m, are probably higher than measured by the traps, such that the true POM flux decline with depth is likely steeper than shown here.

A puzzling feature of Fig. 17a is that BSi fluxes increase by a factor of 1.6 from 200 m to 1000 m, whereas CaCO_3 fluxes remain unchanged and POM fluxes decrease. Radiolarians cannot explain the increase given that they constitute only $\sim 10\%$ of the total BSi flux at 1000 m at OSP (Takahashi, 1987a), with much of this in the $>1 \text{ mm}$ size fraction removed from the data presented here. Significant BSi excretion below 200 m by migrating zooplankton feeding near the surface is also implausible; this vector accounts for an average of only 3% of POC transport past 150 m in the Sargasso Sea (Schnitzer and Steinberg, 2002). Nor can high BSi dissolution in the trap bottles explain the low fluxes at 200 m, since bottle concentrations of BSi ($\sim 10\text{--}100 \text{ mM}$) were much higher than the saturation concentration of Si(OH)_4 ($\sim 1 \text{ mM}$), resulting in $<5\%$ dissolution of trapped BSi at all depths (Timothy and Macdonald, submitted).

Trapping efficiency (TE) might explain the apparent increases in BSi fluxes to 1000 m. For example, if $TE_{200\text{m}} \leq 0.6 TE_{1000\text{m}}$ for all constituents, while water-column dissolution removed much more CaCO_3 than BSi from the sinking flux, CaCO_3 fluxes might appear constant with depth while BSi fluxes appear to increase. An experiment in the subarctic northwest Pacific Ocean (Bishop and Wood, 2008) found 92% of net CaCO_3 production dissolved above 500 m compared to only 65% of net BSi production. Much of the dissolution occurred above 200 m, however, so it remains uncertain whether differential dissolution and TE variability can account for our observations. Another explanation is that BSi fluxes at 200 m are low due to preferential removal of BSi from loosely consolidated aggregates entrained into the traps. Particle sorting at the mouth of sediment traps has long been speculated (Blomqvist and Kofoed, 1981; Buesseler et al., 2000; Butman et al., 1986; Gardner, 1980a,b; Gust et al., 1996; Gust and Kozerski, 2000; Hawley, 1988; Stanley et al., 2004), but sorting is difficult to show conclusively (Buesseler et al., 2007). Nevertheless, sorting is likely the reason for compositional differences between sediments caught by traps with different hydrodynamic properties (Stanley et al., 2004) and is the most straightforward explanation for why BSi fluxes were relatively low at 200 m at OSP. The mechanism could involve diatoms sinking slowly to 200 m, then accelerating below 200 m as they lose buoyancy through senescence (Waite and Nodder, 2001; Waite et al., 1992) and as transparent exopolymers associ-

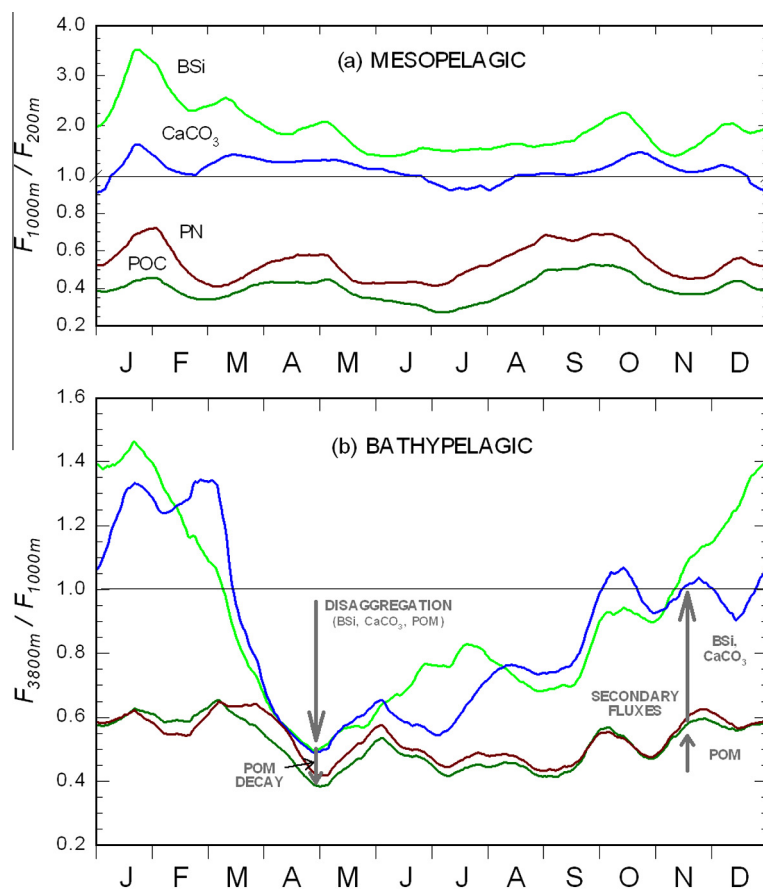


Fig. 17. Ratios of climatological fluxes for the depth intervals (a) 200–1000 m and (b) 1000–3800 m, with the latter forming the basis of the model of Section 5.7.3. Climatologies are from fluxes collected simultaneously at two depths (Table 3). A 16-d shift of the 3800-m fluxes accounts for settling and a 31-d running average is passed through all curves. Note scale change for mesopelagic ratios >1.

ated with diatom aggregates are lost (Engel and Schartau, 1999). Vertically migrating mats of *Rhizosolenia* spp. and other diatoms, which thrive under calm conditions in N-limited gyres (Moore and Villareal, 1996), probably do not play a role since the low BSi fluxes at 200 m occur year-round (Fig. 17a) despite winter turbulence. It is unclear whether these mats would occur in iron limited HNLC waters (McKay et al., 2000), but to our knowledge they have not been observed at OSP.

5.7.3. A model of particle transformation in the bathypelagic zone

The bathypelagic flux ratios (Fig. 17b) show some remarkable features when compared to the flux ratios of the mesopelagic zone. Attenuation of POM fluxes is similar in the two zones, but the patterns of BSi and CaCO_3 flux ratios are considerably different between zones. Bathypelagic flux ratios of BSi and CaCO_3 are low in spring, increase in summer and are maximum in winter. The spring convergence of BSi and CaCO_3 flux ratios with POM flux ratios is striking, as is the growing divergence of BSi and CaCO_3 flux ratios away from POM flux ratios after April. Also curious is that the patterns of BSi and CaCO_3 flux ratios track each other throughout the year. Dissolution kinetics in the deep North Pacific Ocean are comparable for both minerals (Fiadeiro, 1980), but this alone cannot explain why fluxes of BSi and CaCO_3 decrease and increase with depth in a like manner. In the following discussion, we assume the climatological bathypelagic flux ratios are not affected by persistent horizontal gradients in export flux or by local resuspension. As a caveat, however, the bathypelagic flux ratios would be affected by changes in TE with depth. TE for bottom-tethered traps

positioned ≥ 3000 m is $\sim 1 \pm 0.5$ and decreases as water depth decreases at an average rate of 0.16 km^{-1} at five locations where traps were moored at ~ 1000 m and ≥ 3000 m (Figure 5.5 of Buesseler et al. (2007)), giving $\text{TE}_{1000\text{m}} = 0.55 \text{ TE}_{3800\text{m}}$.

Examination of Fig. 17b has led us to a model that incorporates a primary flux of particles passing quickly from 1000 m to 3800 m, and a secondary flux of particles at 3800 m supported by processes within the bathypelagic zone. The presence of a secondary flux builds upon the idea (e.g., Conte et al., 2001) that this component causes increases in flux with depth during low flux periods. We see the need to incorporate four processes to explain Fig. 17b: (1) disaggregative loss of particles from the primary flux; (2) remineralization loss of POM from the primary flux; (3) remineralization loss of POM, BSi and CaCO_3 from particles disaggregated from the primary flux; and (4) supply of secondary fluxes at 3800 m originating from within the bathypelagic zone. We do not prescribe a source or composition to the secondary flux. Rather, these are examined using model results describing secondary fluxes (as per Timothy, 2004; Timothy and Pond, 1997). Aggregation and disaggregation, both critical to sinking, are commonly parameterized in models of particle cycling (e.g., Bacon et al., 1985; Clegg and Whitfield, 1990; Murnane, 1994; Murnane et al., 1990). While our model quantifies disaggregation, it does not solve for aggregation. Nevertheless, the importance of aggregation is assessed from model results.

The total flux at 3800 m is the sum of primary and secondary fluxes.

$$F_{3800\text{m}} = (F_{1000\text{m}} - DF - RPF) + SF \quad (4)$$

Here, F_{3800m} and F_{1000m} are fluxes at these depths, DF is disaggregation of the sinking flux between 1000 m and 3800 m, RPF is remineralization within the primary flux as it passes from 1000 m to 3800 m and SF is the secondary flux at 3800 m. The terms in parentheses comprise the primary flux passing quickly from 1000 m to 3800 m. Normalizing to F_{1000m} translates Eq. (4) into a form that can be related to Fig. 17b.

$$F_{3800m}/F_{1000m} = (1 - DF_{ratio} - RPF_{ratio}) + SF_{ratio} \quad (5)$$

The subscript “ratio” indicates normalization to F_{1000m} .

Of the four processes outlined above, only remineralization between 1000 m and 3800 m of particles disaggregated from the primary flux (RDF_{ratio}) is not considered in Eq. (5). For one-dimensional conditions based on long-term (i.e., steady-state) climatology, the fate of disaggregated particles is either remineralization within the bathypelagic zone or sinking to 3800 m. RDF_{ratio} can thus be quantified as the difference between total remineralization ($1 - F_{3800m}/F_{1000m}$) and remineralization within the primary flux. As such, it accounts for all remineralization in the broad spectrum of particles with sinking rate less than that of the primary flux.

$$RDF_{ratio} = (1 - F_{3800m}/F_{1000m}) - RPF_{ratio} \quad (6)$$

To solve the model, DF_{ratio} and RPF_{ratio} in Eq. (5) are estimated from Fig. 17b and from trap data collected mid-April to mid-May. SF_{ratio} and RDF_{ratio} are then calculated from Eqs. (5) and (6).

We assume disaggregation occurs non-selectively such that the primary flux maintains its bulk composition as it attenuates from disaggregation. Disaggregation is the precursor to most POM decay, since POM consumption occurs largely within the suspended pool (Cho and Azam, 1988; Nagata et al., 2000; Taylor and Karl, 1991). Diatom frustules and radiolarian shells appear unchanged between 1000 m and 3800 m at OSP (Takahashi, 1986; Takahashi, 1987a), so as a first approximation we assume disaggregation also precedes BSi dissolution ($RPF_{ratio} = 0$ for BSi). F_{3800m}/F_{1000m} for BSi shows pronounced seasonality and is lowest at the end of April (Fig. 17b), indicating DF_{ratio} most exceeds SF_{ratio} (Eq. (5)) at this time of year. Assuming for BSi that $SF_{ratio} = RPF_{ratio} = 0$, rearranging Eq. (5) gives $(1 - BSi_{3800m}/BSi_{1000m})$ in late April as a best estimate

of DF_{ratio} at any point of the year. There are 13 bottle pairs from 1000 m and 3800 m (applying a one-bottle shift to account for sinking time from 1000 m to 3800 m) for which >50% of collection occurred within the period mid-April to mid-May. For four of these pairs, $BSi_{3800m}/BSi_{1000m} > 1$ and the mass flux at 1000 m was low ($< 50 \text{ mg m}^{-2} \text{ d}^{-1}$) indicating collection occurred during winter-like conditions when SF_{ratio} was high. We use the average BSi_{3800m}/BSi_{1000m} ratio for the remaining nine pairs, 0.45 ± 0.067 , to represent flux conditions when DF_{ratio} most exceeds SF_{ratio} . The resulting DF_{ratio} of 0.55 (Table 6) is used for the entire year. This estimate is high by the amount BSi dissolves from the primary flux and low by the amount $SF_{ratio} \neq 0$ for BSi in late April. Below we estimate these errors are largely offsetting.

The use of a truly conservative tracer to define DF_{ratio} might allow the model to separate RPF from RDF for all biogenic components. Because BSi fluxes are used to set DF_{ratio} , however, and because F_{3800m}/F_{1000m} in late April is similar for CaCO_3 and BSi (Fig. 17b), the model necessarily sets RPF of these bio-minerals to zero, with all BSi and CaCO_3 dissolution assigned to the disaggregated flux. But the low POM flux ratios, even in April, indicate a loss of sinking POM in excess of disaggregation, which we assign to remineralization within the primary flux ($R_{POM}PF$). After applying three model assumptions (DF_{ratio} is the same for POM and BSi; $RPF_{ratio} = 0$ for BSi; $SF_{ratio} = 0$ in late April), subtraction of Eq. (5) for BSi from Eq. (5) for POM gives:

$$R_{POM}PF_{ratio} = (BSi_{3800m}/BSi_{1000m})_{April} - (POM_{3800m}/POM_{1000m})_{April} \quad (7)$$

This estimate of $R_{POM}PF_{ratio}$ is a minimum, since it represents POM loss from the primary flux in excess of BSi loss from the primary flux. The nine bottle pairs used to estimate $(BSi_{3800m}/BSi_{1000m})_{April}$ are also used for estimates of $(POM_{3800m}/POM_{1000m})_{April}$ (Table 6). As with disaggregation, there is no direct way to determine the seasonality of $R_{POM}PF_{ratio}$, so we use the late-April estimate for the entire year.

Table 6 provides annual, flux-weighted estimates for the four terms of the model based on the shortened time series where

Table 6
In the mesopelagic zone: weighted flux ratios from 200 m to 1000 m and POM remineralization. In the bathypelagic zone: weighted flux ratios from 1000 m to 3800 m, model parameterization, and remineralization. Bathypelagic values are for $TE_{1000m} = TE_{3800m} = 1$ and, in parentheses, for $TE_{3800m} = 1$ and $TE_{1000m} = 0.55$.

	BSi	CaCO_3	POC	PN
<i>Mesopelagic measured ratios</i>				
Annual average F_{1000m}/F_{200m} ^a	1.7	1.0	0.38	0.52
<i>Mesopelagic remineralization ($\mu\text{mol m}^{-3} \text{ y}^{-1}$)</i>				
Total remin. from 200 m to 1000 m ^b	–	–	357	21
<i>Bathypelagic measured ratios</i>				
F_{3800m}/F_{1000m} annual average ^c	0.79 (0.43)	0.73 (0.40)	0.51 (0.28)	0.53 (0.29)
F_{3800m}/F_{1000m} in late-April ^d	0.45 (0.25)	0.46 (0.25)	0.36 (0.20)	0.38 (0.21)
<i>Bathypelagic model parameterization</i>				
Disaggregation of primary flux (DF_{ratio})	0.55 (0.75)	0.55 (0.75)	0.55 (0.75)	0.55 (0.75)
Remin. from primary flux (RPF_{ratio})	0 (0)	0 (0)	0.09 (0.05)	0.07 (0.04)
Remin. from disaggregated flux (RDF_{ratio})	0.21 (0.57)	0.27 (0.60)	0.40 (0.67)	0.40 (0.67)
Secondary flux at 3800 m (SF_{ratio})	0.34 (0.19)	0.28 (0.15)	0.15 (0.08)	0.15 (0.08)
<i>Bathypelagic remineralization ($\mu\text{mol m}^{-3} \text{ y}^{-1}$)</i>				
Remin. from primary flux (RPF) ^e	0 (0)	0 (0)	5.5 (5.5)	0.48 (0.48)
Remin. from disaggregated flux (RDF) ^f	26 (127)	15 (62)	25 (75)	2.8 (8.4)
Total remin. from 1000 m to 3800 m	26 (127)	15 (62)	30 (80)	3.2 (8.9)

^a From deployments collecting simultaneously at 200–1000 m (Table 3).

^b Calculated as the product of F_{1000m}/F_{200m} (a) and all fluxes collected at 200 m (Table 1).

^c From deployments collecting simultaneously at 1000 m and 3800 m (Table 3).

^d See text for late-April ratios; standard error is 15–20% of the ratios presented.

^e Calculated as the product of RPF_{ratio} (this table) and all fluxes collected at 1000 m (Table 1).

^f Calculated as the product of RDF_{ratio} (this table) and all fluxes collected at 1000 m (Table 1).

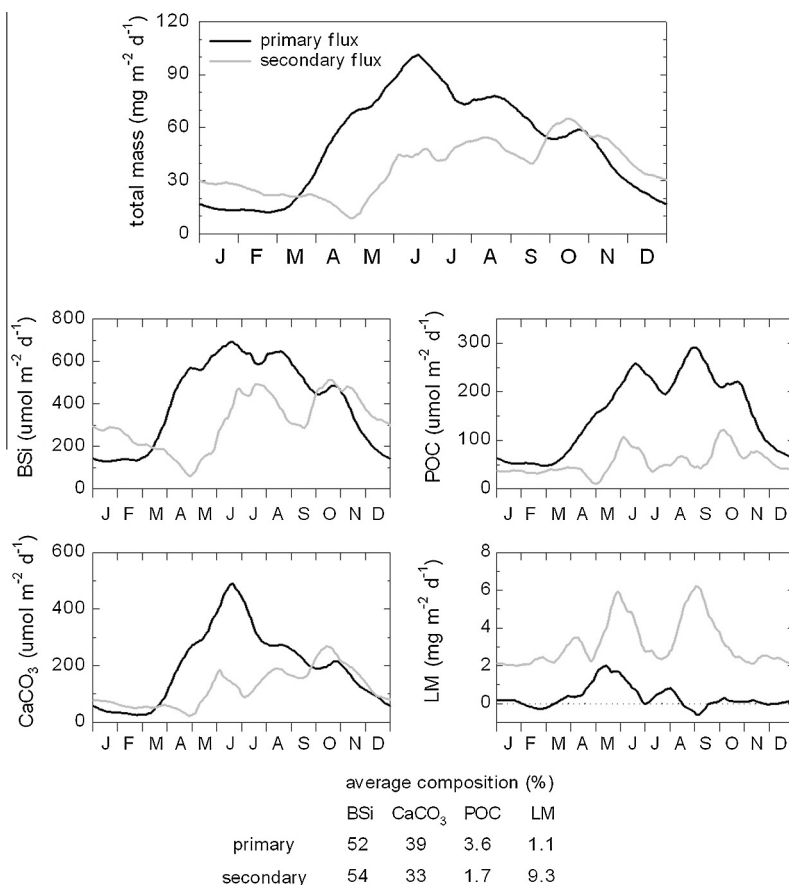


Fig. 18. Primary and secondary fluxes at 3800 m, with tabulation of their average composition.

fluxes at 1000 m and 3800 m were collected simultaneously (net length = 3448 d; Table 3) and on the nine bottle pairs representing conditions from mid-April to mid-May. The seasonality and average composition of primary and secondary fluxes are given in Fig. 18. Results of Table 6 assume $TE_{3800m} = 1$ and that TE_{1000m} ranges from 0.55 to 1, based on the above discussion of depth-changes in TE in the bathypelagic zone. If TE_{1000m} is constant throughout the year, it can be shown through Eq. (4) that the magnitude and composition of primary and secondary fluxes (i.e., Fig. 18) are not affected by uncertainty in TE_{1000m} .

Secondary fluxes are a large portion of the total flux at 3800 m, annually contributing 42% to the mass flux, 43% to BSi fluxes, 38% to CaCO₃ fluxes, 26% to POC fluxes, and 86% to LM fluxes. Secondary fluxes are thus depleted of POM and enriched in LM relative to the total flux at 3800 m. The BSi:CaCO₃ molar ratio of 2.6 for the secondary flux is slightly higher than that of bulk trap material, 2.1 at 1000 m and 2.3 at 3800 m for the shortened climatologies used here. Thus, a key result of the model is that the secondary flux appears to derive from the primary flux, since its composition does not resemble suspended material. For example, BSi:CaCO₃ of the secondary flux is much lower than 7, the BSi:CaCO₃ ratio of the <51 μm particle size class collected by *in situ* filtration at ~800 m in the subarctic Northwest Pacific Ocean (Bishop and Wood, 2008) where BSi:CaCO₃ of sediment caught by bathypelagic traps is ~3.7 (Honda et al., 2002). (We have taken particulate Si concentrations presented as μM in Table 2 of Bishop and Wood (2008) to be nM as indicated by their Fig. 15 and in their text.)

Another key result is that secondary fluxes arrive behind primary fluxes at 3800 m (Fig. 18), again suggesting secondary fluxes have disaggregated from the primary flux. If so, we can estimate from Fig. 18 the sinking rates of disaggregated fluxes reaching

3800 m. At the onset of spring, secondary fluxes begin to increase (~1 April) about 50 d after increases in the primary flux (~10 March). At the end of summer, secondary fluxes begin to decline (~20 October) about 120 d after declines in the primary flux (~20 June). If disaggregation occurs, on average, halfway between 1000 m and 3800 m, and we take into account the 16 days for primary fluxes to sink from 1000 m to 3800 m, then the implied sinking rate of disaggregated fluxes is 11–24 m d⁻¹. These results apply to total mass, BSi and CaCO₃ fluxes, and to POC fluxes in spring. However, the summer-fall lag between primary and secondary fluxes is shorter for POC than for BSi and CaCO₃ (Fig. 18), which can be explained by a high POC decay rate and thus higher proportional loss of POC in the most slowly sinking disaggregated particles. It is difficult to ascertain from Fig. 18 whether the lag between primary and secondary LM fluxes fits this model, since several flux events have high impact on these curves. However, much of the secondary LM flux cannot be explained by disaggregated primary fluxes (discussed below), requiring different mechanisms to deliver LM to the 3800-m traps.

The conclusion that secondary fluxes originate mostly from primary fluxes with a delayed arrival at 3800 m of about one season would explain increases in flux with depth during low-flux periods at OSP without invoking biological production and particle repackaging, the suggested mechanism for similar observations elsewhere (Conte et al., 2001 and references therein). This conclusion allows us to assess the error in DF_{ratio} caused by assuming that, for BSi in late April, SF_{ratio} and RPF_{ratio} of Eq. (5) are zero. Winter BSi fluxes at 1000 m are 264 μmol BSi m⁻² d⁻¹ (Table 1), with 34% of this, or 90 μmol BSi m⁻² d⁻¹, later becoming secondary fluxes at 3800 m (Table 6). Subtracting this amount from the deep bottle of the nine bottle pairs used for

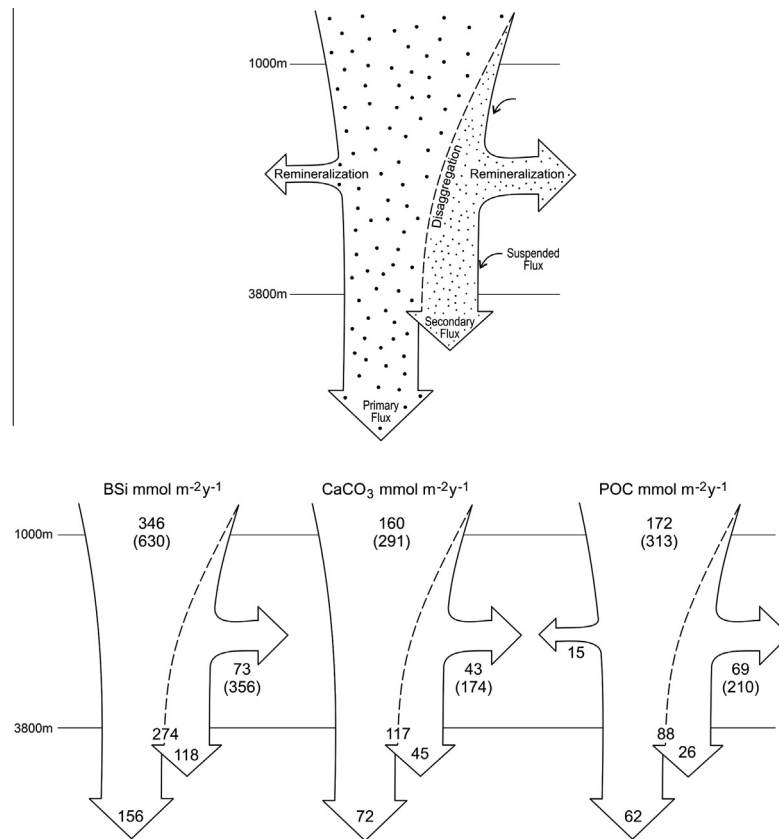


Fig. 19. Schematic of constituent fluxes in the bathypelagic zone, showing the primary flux, disaggregation leading to secondary fluxes, and remineralization. Values are for $TE_{1000m} = TE_{3800m} = 1$ and, in parentheses, for $TE_{3800m} = 1$ and $TE_{1000m} = 0.55$. One value is given for fluxes unaffected by TE_{1000m} . Total flux at 3800 m differs somewhat from Table 1 values because it uses the time series collected simultaneously at 1000 m and 3800 m ($F_{3800} = F_{1000} \times F_{3800}/F_{1000}$, where F_{1000} is from Table 1 and F_{3800}/F_{1000} is from Table 6).

the late-April averages corrects DF_{ratio} for the assumption $SF_{ratio} = 0$ in late April, increasing DF_{ratio} from 0.55 to 0.61 (10%). This is offset by assuming $RPF_{ratio} = 0$ for BSi. Primary (disaggregated) fluxes are 45% (55%) of the 1000-m flux and spend, on average, 16 d (100 d) in the bathypelagic zone. Assuming all sinking BSi dissolves at the same rate and noting 21% of the 1000-m BSi flux is lost in the bathypelagic zone (Table 6), the resulting RPF_{ratio} for BSi, 0.06, is also 10% of DF_{ratio} . This analysis generates a BSi dissolution rate constant of 0.004 d^{-1} that agrees with rates (0.002 d^{-1} to 0.01 d^{-1}) determined from experiments mimicking ocean conditions at 0°C to 5°C (Passow et al., 2011), and thus lends support to the model partitioning of primary and secondary fluxes and their residence times. We can also conclude that using a constant for DF_{ratio} probably does not cause a seasonal bias in the climatological curves of primary and secondary fluxes (Fig. 18). According to Eq. (5), POM flux ratios are affected by DF_{ratio} , $R_{POM}PF_{ratio}$ and SF_{ratio} . $R_{POM}PF_{ratio}$ is a small term and SF_{ratio} for POM is also relatively small because of POM decay from disaggregated particles (summarized below), so the low seasonality in POM flux ratios (Fig. 17b) should indicate low seasonality in DF_{ratio} . Finally, high POM degradation from disaggregated fluxes returns us to the striking seasonality in the BSi and CaCO_3 flux ratios (Fig. 17b) noted at the outset of this section. Whereas disaggregated POM is largely lost in the water column, much of the disaggregated BSi and CaCO_3 eventually must sink past 3800 m to maintain mass balance, causing the amplified seasonality in BSi and CaCO_3 flux ratios.

Disaggregation of primary fluxes was also used to explain spring-summer increases in suspended particle concentrations in

North Atlantic bathypelagic waters, with fall-winter declines attributed to aggregation, remineralisation and solubilisation (POM converted to DOM) of the suspended load (McCave et al., 2001). Primary fluxes thus appear to be a net source, through disaggregation, of the entire spectrum of particles down to fine suspensions, instead of a net sink of finer particles through scavenging as earlier believed (see McCave et al., 2001). This would explain the uncertain results of a thorium cycling model applied to data collected from the bathypelagic zone at OSP (Murnane et al., 1990; Murnane, 1994). Of the three possibilities suggested by Murnane et al. (1990), their simplification of the particle spectrum to two classes most likely caused the uncertainty. Nevertheless, the increase in LM flux from $\sim 0\text{--}1 \text{ mg m}^{-2} \text{ d}^{-1}$ at 1000 m to $\sim 3\text{--}4 \text{ mg m}^{-2} \text{ d}^{-1}$ at 3800 m at OSP (Section 3.4 and Table 1) requires a source of LM in addition to vertical fluxes to 1000 m. Horizontal transport supplies suspended particles to the deep North Atlantic Ocean, leading to a significant lithogenic component in the downward flux (Conte et al., 2001; McCave et al., 2001). Suspended LM in the bathypelagic zone at OSP may be delivered horizontally from the continental margin (Lam et al., 2006) and from seamounts in the Alaska Gyre, then settle to 3800 m through aggregation. Additionally, our argument that locally resuspended sediment does not reach the bathypelagic traps cannot discount the possibility some of the LM flux to 3800 m is delivered this way. Taken in their entirety, our results suggest autochthonous material with residence times of several weeks (primary flux) to several months (secondary flux) comprise the majority of the total flux at 3800 m, with horizontally transported suspended particles with 5–10 y residence time (Bacon and Anderson, 1982) supplying mostly lithogenic

fluxes. Compositional data for bathypelagic suspended particles at OSP, including their lithogenic content, would be of considerable value in testing this conclusion.

Our modeling (Table 6 and Fig. 19) has indicated the following sequence of events when assuming $TE_{1000m} = TE_{3800m}$. Of the total flux at 1000 m, 55% disaggregates within the bathypelagic zone, generating a secondary flux with a mean sinking rate of $\sim 10\text{--}20\text{ m d}^{-1}$ and with similar composition to the rapidly-sinking ($\sim 120\text{--}350\text{ m d}^{-1}$) primary flux. Of the disaggregated POM, 73% decays within the bathypelagic zone with the remainder settling to 3800 m within several months. Additionally, 7–9% of the POM flux at 1000 m degrades from the primary flux. Of the disaggregated BSi and CaCO_3 , 38% and 49%, respectively, dissolves before reaching 3800 m. If $TE_{1000m} = 0.55 TE_{3800m}$, much more of the 1000-m flux must remineralise for the total flux at 3800 m to remain unchanged. In this case, DF_{ratio} increases to 0.75 and RDF of the biogenic components increases by factors of three to five (Table 6). Estimates of remineralization based on water-column tracers in the bathypelagic zone of the Pacific Ocean are 0.058 and $0.0084\ \mu\text{mol kg}^{-1}\text{ y}^{-1}$ for BSi and ON, respectively (Sarmiento et al., 2007), $\sim 0.07\ \mu\text{mol kg}^{-1}\text{ y}^{-1}$ for OC (Chen, 1990; Feely et al., 2004b) and $0.051\ \mu\text{mol kg}^{-1}\text{ y}^{-1}$ for CaCO_3 (Feely et al., 2002), all within the ranges of Table 6. To the extent these estimates can be applied to water-column remineralization at OSP, they imply TE_{1000m} is 0.6 (for OC, ON and CaCO_3) to 0.8 (for BSi) for TE_{3800m} of 1. However it is possible that a portion of bathypelagic remineralization determined from water-column tracers occurs at the seafloor, as proposed for CaCO_3 (Berelson et al., 2007). By assuming $TE_{1000m} = TE_{3800m} = 1$, these trap results constrain the minimum proportion of total remineralization occurring in the water column at about 30% for CaCO_3 , 40% for OM and 45% for BSi.

6. Conclusions

Time series of ocean biogeochemistry are crucial to understanding the ecological consequences of the increased warming, storminess and ocean acidification that are now occurring (Solomon et al., 2007). A major objective of the few sediment-trap time series carried out globally has been to detect biogeochemical trends including shifts in ecology, and compare them with other observed system changes. In this paper, we presented the climatologies of particle flux and composition at OSP that are needed to establish the significance of single events and long-term trends. We then linked these climatologies to surface processes and used them to describe particle transformations as they sink. The primary conclusions are:

1. Fluxes normalized to 2000 m are 2.7, 1.3 and 1.1 times higher than the global averages for BSi, CaCO_3 and POC, respectively. The Alaska Gyre is thus a siliceous basin with unusually high calcareous fluxes. Lithogenic fluxes are minor at OSP, making this site ideal to detect dust-fall events.
2. Fluxes of BSi and CaCO_3 lag surface solar irradiance by about one month at 200 m and 1000 m, and by another \sim two weeks at 3800 m. POM is preferentially retained and recycled in the mixed layer, with maximum export occurring several months after maximum fluxes of BSi and CaCO_3 .
3. Export fluxes are episodic at OSP despite perennially low chlorophyll concentrations showing little seasonality. As a result of episodically high fluxes, 40–50% of MARK7 traps with narrow sampling bottles became clogged during deployment at 3800 m. Given the common occurrence of this problem globally, traps with larger bottom orifices should become standard protocol.

4. Sediment traps provide an excellent opportunity to test sedimentary tracers of past ocean conditions. In this regard, POC content at OSP is a poor indicator of mass or POC flux because POC is diluted by BSi and CaCO_3 when mass flux is high.
5. The annual cycle of BSi flux and a reanalysis of surface nutrient data show the spring delay in $[\text{Si}(\text{OH})_4]$ decline, based on mixed-layer nutrient climatology, results from intense mixing in spring rather than delayed diatom growth as previously proposed.
6. The annual cycle of POC flux, normalized to measures of net community production of organic carbon (NCP_{OC}) in summer-fall (Emerson and Stump, 2010), implies an annual NCP_{OC} of $3.6\text{--}5.3\ \text{mol m}^{-2}\text{ y}^{-1}$. This rate is similar to estimates of new production and of water-column OC remineralization plus deep POC flux, two equivalencies to NCP_{OC} . It is also similar to estimates of export production at OSP made from global modeling, but it is double estimates of NCP_{OC} based on mass balance of mixed-layer tracers.
7. The estimate of NCP_{OC} and a CaCO_3 :OC export ratio of 0.18 determined from trap data gives a net community production of CaCO_3 (NCP_{IC}) of $0.65\text{--}0.95\ \text{mol m}^{-2}\text{ y}^{-1}$ in agreement with water-column CaCO_3 dissolution plus deep CaCO_3 flux.
8. The similarity between the CaCO_3 :POC flux ratio at 50 m and the CaCO_3 :POC production ratio from bottle incubations (Lipsen et al., 2007) requires that $\sim 70\%$ of CaCO_3 production must dissolve in the euphotic zone to match the rate of POC recycling at OSP.
9. Flux climatologies at 1000 m and 3800 m imply sediments caught at 3800 m include a component sinking rapidly (the primary flux; $\sim 120\text{--}350\text{ m d}^{-1}$) and another component sinking slowly (the secondary flux; $\sim 10\text{--}20\text{ m d}^{-1}$). A mass-balance model finds that secondary fluxes contribute $\sim 40\%$ to the annual mass flux at 3800 m. Based on compositional evidence and on the arrival times at 3800 m, the secondary flux likely derives from disaggregated primary fluxes with an additional lithogenic component transported horizontally to the bathypelagic zone at OSP.
10. Remineralization of BSi, CaCO_3 , OC and N estimated from decreasing flux with depth in the bathypelagic zone agrees with estimates for the Pacific Ocean based on water-column tracers provided trapping efficiency at 1000 m is 0.6–0.8 and at 3800 m is 1. Alternatively, the estimates based on tracers may include a component of seafloor remineralization. In this case, remineralization in the water column at OSP is at least 30–45% of the remineralization determined by tracers, with the remainder occurring at the seafloor.

Acknowledgements

This work is the culmination of years of dedication by sea-going and laboratory technicians, mooring experts, visiting scientists, the captains and crews of the *CSS Parizeau* and the *CSS Tully* and Canadian funding agencies. Sus Honjo and Kazuo Iseki were instrumental to establishing the time series. Ron Bellegay, Tim Soutar and Darren Tuele maintained and deployed the traps. Frank Whitney oversaw sample handling and chemical analyses during much of the program. Marie Robert arranged cruises, assisted at sea and freely shared water-quality data. Roy Hurston and Isaac Fine helped to retrieve OSP weather ship data and Angelica Peña provided nutrient climatology. Conversations with Patrick Cummins and Bill Crawford have given insight into physical conditions at OPS. Moira Galbraith helped with plankton identification. Carol Arnosti gave useful comments on POM:POC weight ratios. Com-

ments by two anonymous reviewers significantly improved the final manuscript. ARGO data were collected and made freely available by the International Argo Project and the national programs contributing to it (<http://www.argo.ucsd.edu>, <http://argo.jcomm-ops.org>). Argo is a pilot program of the Global Ocean Observing System. The operational grant to C.S. Wong funded the field and laboratory program. Data quality control and analyses were supported under the Department of Fisheries and Oceans' International Governance Science Program targeted funding for ocean variability and marine ecosystems.

Appendix A.

A.1. Sampling schedules at OSP and station AG

Tables A1 through A4 give sampling schedules at OSP and Station AG.

A.2. Clogs

Clogging of MARK7 traps was problematic during this time series. The extent of the problem is documented here to aid future experiments in the choice of trap design.

The traps at OSP sometimes had empty bottles, beginning at bottle b_1 and continuing to the last bottle of deployment. Where no mechanical failure was evident, we attribute these empty bottles to blockage at the base of the cone during the collection period

of bottle b_0 preceding the first empty bottle b_1 . Similar clogging has been reported for PARFLUX traps in the Arabian Sea (Haake et al., 1993b; Honjo et al., 1999), the Southern Ocean (Honjo et al., 2000), the Bering Sea and the central Subarctic Pacific Ocean (Takahashi et al., 2000), the western Subarctic Pacific Ocean (Honda et al., 2002) and previously at OSP (Wong et al., 1999). Clogging at OSP began after 1991 when MARK7 traps with narrow bottom orifice (28 mm) were introduced, with the exception of the clog to the MARK5 trap at 3800 m in September 1988 (Table A5). At least seven different deposition pulses caused clogs at OSP, with two events affecting traps at 1000 m and 3800 m. Nine traps thus became clogged, resulting in 306, 561 and 1273 lost days of sampling at 200 m, 1000 m and 3800 m, respectively. One clogging event occurred in the second half of April (2005) with the remaining six first detected between early-July and mid-September and arriving at 3800 m as late as October–November. Surprisingly, the traps at 3800 m were most affected. There were no clogs to MARK6 traps (30 mm orifice), which were sparingly used at OSP (1, 3 and 3 deployments at 200 m, 1000 m and 3800 m, respectively). One clog (PA13 at 3800 m) occurred to MARK5 traps (59 mm orifice), which were successfully employed 20 times (1, 4 and 14 deployments at 200 m, 1000 m and 3800 m, respectively). MARK7 traps were mechanically successful during 34 deployments (10, 12 and 12 deployments at 200 m, 1000 m and 3800 m, respectively) and clogged eight times (1, 2 and 5 clogs at 200 m, 1000 m and 3800 m, respectively) for clogging rates of 10%, 17% and 42% at progressively deeper traps. The clogging rate for MARK7 traps at 3800 m increases to 50% if the first bottle of the deep trap of moor-

Table A1
Trap schedule at 3800 m. Dates are yymmdd.

ID	Trap model	Depth (m)	Successful sampling dates			Unsuccessful or inactive dates			Cups	Days/cup	Comments
			Begin	End	# Days	Begin	End	# Days			
PA01	M5	3800	820923	830307	165				1–11	15	No poison
PA01	M5	3800	830307	830318	11				12	11	Scheduled cup duration; no poison
						830318	830327	9			Hiatus
PA02	M5	3800	830327	831005	192				1–12	16	First deployment with traps at 1000 m and 3800 m; no poison
						831005	831014	9			Hiatus
PA03	M5	3800	831014	840423	192				1–12	16	Successful deployment (previously reported as failed (Wong et al., 1999))
						840423	840429	6			Hiatus
PA04	M5	3800				840429	840513	14	1	14	handling error at recovery
PA04	M5	3800	840513	840805	84				2–7	14	
PA04	M5	3800	840805	840824	19				8–12	3–4	Scheduled cup durations
						840824	840828	4			Hiatus
PA05	M5	3800				840828	841112	76			Carousel did not rotate
						841112	841120	8			Hiatus
PA06	M5	3800	841120	850413	144				1–12	12	
						850413	850510	27			Hiatus
PA07	M5	3800	850510	851025	168				1–12	14	
						851025	851113	19			Hiatus
PA08	M5	3800	851113	860201	80				1–6	12.5–14.5	
PA08	M5	3800				860201	860423	81	7	81	Carousel stopped rotating while open on cup 7
						860423	860427	4			Hiatus
PA09	M5	3800				860427	860525	28	1–2	14	Bottles broken from carousel during rough recovery (weather)
PA09	M5	3800	860525	860706	42				3–5	14	
PA09	M5	3800				860706	860720	14	6	14	Bottle broken during deployment
PA09	M5	3800	860720	860831	42				7–9	14	
PA09	M5	3800				860831	861012	42	10–12	14	Bottles broken during deployment
						861012	861021	9			Hiatus
PA10	M5	3800	861021	870404	165				1–11	15	recovered while open to cup 12
						870404	870407	3			Hiatus
PA11	M5	3800	870407	870922	168				1–12	14	
						870922	871002	10			Hiatus
PA12	M5	3800	871002	880506	217				1–12	18–19	

						880506	880510.5	4.5			Hiatus
PA13	M5	3800	880510.5	880903	115.5				1–7	16.5	
PA13	M5	3800				880903	881124.5	82.5	8–12	16.5	Beginning of clog set at cup 8
						881124.5	881211	16.5			Hiatus
PA14	M5	3800	881211	890504	144				1–12	12	Difficult but successful recovery (weather)
						890504	890508	4			Hiatus
PA15	M5	3800	890508	890929	144				1–12	12	First deployment with traps at 200 m (M6), 1000 m (M5) and 3800 m
						890929	891016	17			Hiatus
PA16	M6	3800	891016	900502	198				1–12	16.5	First deployment without analyses on all size fractionations
						900502	900521	19			Hiatus
PA17	M6	3800	900521	901111	174				1–12	14.5	
						901111	910305	114			Hiatus
PA18	M7	3800				910305	911007	216			Mooring lost during recovery
						911007	911023	16			Hiatus
PA19	M7	3800				911023	920410	170			carousel did not rotate
						920410	920410	0			Hiatus
PA20	M7	3800				920410	920907	150			Mooring not found at time of retrieval
						920907	920926	19			Hiatus
PA21	M7	3800	920926	930510	226				1–16	14–16	Recovered while open to cup 17
						930510	930524	14			Hiatus
PA22	M7	3800	930524	931024	153				1–9	17	Traps at 250 m and 850 m on one mooring, trap at 3800 m on another 5.7 km away
						931024	940516	204	10–21	17	Beginning of clog set at cup 10
PA22	M7	3800				940516	940522	6			Hiatus
PA23	M7	3800				940522	950514	357	1–21	17	3800 m trap lost during recovery
						950514	950521	7			Hiatus
PA24	M7	3800	950521	950814	85				1–5	17	
PA24	M7	3800				950814	960512	272	6–21	17	Beginning of clog set at cup 6
						960512	960521	9			Hiatus
PA25	M7	3805	960521	970513	357				1–21	17	
						970513	970620	38			Hiatus
PA26	M7	3800	970620	980528	342				1–19	18	Recovered while open to cup 20
						980528	980615	18			Hiatus
PA27	M7	3800	980615	980702	17				1	17	
PA27	M7	3800				980702	990607	340	2–21	17	Beginning of clog set at cup 2
						990607	990904	89			Hiatus
PA28	M7	3800	990904	000603	273				1–16	16–18	Recovered while open to cup 17
						000603	000612	9			Hiatus
PA29	M7	3800	000612	000716	34				1–2	17	
PA29	M7	3800				000716	010604	323	3–21	17	Beginning of clog set at cup 3; MARK6 trap deployed at 1000 m
						010604	010622	18			Hiatus
PA30	M7	3800	010622	020614	357				1–21	17	
						020614	020709	25			Hiatus
PA31A	M6	3700	020709	021221	165				1–11	15	6.2 km from PA31; stopped rotating at cup 12 of 13; recovered with PA31 (030604)
PA31	M7	3800	020907	030604	270				1–18	15	Recovered while open to cup 19; cups 1–7 overlap with cups 5–11 of PA31A
						030604	030608	4			Hiatus
PA32	M7	3800				030608	040530	357	1–21	17	All cups empty; clog preceding bottle 1 or poor cup alignment during rotation?
						040530	040612	13			Hiatus
PA33	M7	3800	040612	050414	306				1–18	17	
PA33	M7	3800				050414	050604	51	19–21	17	Beginning of clog set at cup 19
						050604	050612	8			Hiatus
PA34	M7	3800	050612	060604	357				1–21	17	
			Total		5301.5			3353.5			

ing PA32 is deemed to have clogged during a separate event than the one that caused clogging several months later at 200 m (Table A5).

Clogs have occurred elsewhere because bottle b_0 overflowed creating a plug at the base of the cone (Honjo et al., 1999; Honjo et al., 2000). Gelatinous or fibrous organisms have been implicated

(Honda et al., 2002; Honjo et al., 1999; Honjo et al., 2000; Takahashi et al., 2000). From the total mass flux and photographic records, the bottles at OSP never filled to their capacity indicating the clogs were not caused by small bottle volume. Identifications of possible swimmers were not exceptional for the clogged bottles, as expected since the deepest traps were most affected. In February

Table A2
Trap schedule at 1000 m. Dates are yymmdd.

ID	Trap model	Depth (m)	Successful sampling dates			Unsuccessful or inactive dates			Cups	Days/cup	Comments
			Begin	End	# Days	Begin	End	# Days			
PA02	M5	1000	830327	831005	192				1–12	16	No poison
PA03	M5	1000				831005	831014	9			Hiatus
PA04	M5	1000				831014	840423	192			Carousel did not rotate
PA05	M5	1000				840423	840429	6			Hiatus
						840429	840824	117			Carousel did not rotate
						840824	840828	4			Hiatus
						840828	841112	76			Poor alignment for cups 1–3 and carousel did not rotate past cup 3
						841112	841120	8			Hiatus
PA06	M5	1000	841120	850119	60				1–5	12	
PA06	M5	1000				850119	850504	105	6	105	Battery died when carousel open to cup 6
						850504	850510	6			Hiatus
PA07	M5	1000	850510	851025	168				1–12	14	
						851025	851113	19			Hiatus
PA08	M5	1000	851113	860423	161				1–12	12.5–14.5	
						860423	860427	4			Hiatus
PA09–PA14						860427	890504	1103			Traps not deployed at 1000 m
						890504	890508	4			Hiatus
PA15	M5	1000	890508	890929	144				1–12	12	First deployment with traps at 200 m (M6), 1000 m and 3800 m (M5)
						890929	891016	17			Hiatus
PA16	M6	1000	891016	900502	198				1–12	16.5	First deployment without size fractionation
						900502	900521	19			Hiatus
PA17	M6	1000	900521	901111	174				1–12	14.5	
						901111	910305	114			Hiatus
PA18–PA21						910305	930510	797			Traps not deployed at 200 m or 1000 m except during PA20 when mooring was lost
						930510	930524	14			Hiatus
PA22	M7	850	930524	930610	17				1	17	Traps at 250 m and 850 m on one mooring, trap at 3800 m on another 5.7 km away
						930610	930627	17	2	17	Sample lost
PA22	M7	850	930627	930817	51				3–5	17	
PA22	M7	850				930817	940516	272	6–21		Beginning of clog set at cup 6
						940516	940522	6			Hiatus
PA23	M7	1000	940522	950514	357				1–21	17	
						950514	950521	7			Hiatus
PA24	M7	1000	950521	950624	34				1–2	17	
PA24	M7	1000				950624	950711	17	3	17	Bottle broken from carousel during deployment
PA24	M7	1000	950711	950728	17				4	17	
PA24	M7	1000				950728	960512	289	5–21	17	Beginning of clog set at cup 5
						960512	960521	9			Hiatus
PA25	M7	1010	960521	970513	357				1–21	17	
						970513	970620	38			Hiatus
PA26	M7	1000	970620	980528	342				1–19	18	Recovered while open to cup 20
						980528	980615	18			Hiatus
PA27	M7	1000	980615	990607	357				1–21	17	
						990607	990904	89			Hiatus
PA28	M7	1000	990904	000603	273				1–16	16–18	Recovered while open to cup 17
						000603	000612	9			Hiatus
PA29	M6	1000	000612	000716	34				1–2	17	M7 traps deployed at 200 m and 3800 m
PA29	M6	1000	000716	010414	272				3–10	34	Rotation schedule designed to match M7 traps with 21 cups
						010604	010622	18			Hiatus
PA30	M7	1000	010622	020614	357				1–21	17	
						020614	020907	85			Long hiatus due to ship obligations to Fe fertilization at OSP (SERIES)
PA31	M7	1000	020907	030604	270				1–18	15	Recovered while open to cup 19
						030604	030608	4			Hiatus
PA32	M7	1000	030608	040530	357				1–21	17	
						040530	040612	13			Hiatus
PA33	M7	1000	040612	050604	357				1–21	17	
						050604	050612	8			Hiatus
PA34	M7	1000	050612	060604	357				1–21	17	
			Total		4957			3513			

Table A3

Trap schedule at 200 m. Dates are yymmdd.

ID	Trap model	Depth (m)	Successful sampling dates			Unsuccessful or inactive dates			Cups	Days/cup	Comments	
			Begin	End	# Days	Begin	End	# Days				
PA15	M6	200	890508	890929	144				1–12	12	M5 traps at 1000 m and 3800 m Hiatus	
PA16	M5	200	891016	900502	198				1–12	16.5	M6 traps at 1000 m and 3800 m; first deployment without size fractionation Hiatus	
PA17	M5	200	900521	900816	87				1–6	14.5		
PA17	M5	200				900816	901111	87	7–12		Mechanical failure after bottle 6 Hiatus	
PA18–PA21						901111	910305	114				
						910305	930510	797			Traps not deployed at 200 m or 1000 m except during PA20 when mooring was lost Hiatus	
PA22	M7	250	930525	930610	16					1	16	Traps at 250 m and 850 m on one mooring, trap at 3800 m on another 5.7 km away;
PA22	M7	250	930610	940516	340				2–21	17		Mooring adjustment on 930526 caused duration of cup 1 (and 250 m and 850 m depths) Hiatus
PA23	M7	200				940516	940522	6				
						940522	950514	357	1–21	17		All bottles broken during deployment Hiatus
PA24						950514	950521	7				
						950521	960512	357				Traps not deployed at 200 m Hiatus
PA25	M7	230	960521	970513	357							
						960512	960521	9	1–21	17		
PA26						970513	970620	38				Hiatus
						970620	980528	342				Traps not deployed at 200 m Hiatus
						980528	980615	18				
PA27	M7	200	980615	990417	306				1–18	17		
PA27	M7	200				990417	990504	17	19	17		Bottle broken during deployment
PA27	M7	200	990504	990521	17				20	17		
PA27	M7	200				990521	990607	17	21	17		Bottle broken after retrieval Hiatus
PA28	M7	200	990904	000603	273				1–16	16–18		Recovered while open to cup 17 Hiatus
						000603	000612	9				
PA29	M7	200	000612	010604	357				1–21	17		Hiatus
						010604	010622	18				
PA30	M7	200	010622	020614	357				1–21	17		
						020614	020907	85				Long hiatus due to obligations to Fe fertilization at OSP (SERIES)
PA31	M7	200	020907	030321	195				1–13	15		
PA31	M7	200				030321	030405	15	14	15		Collection failure
PA31	M7	200	030405	030604	60				15–18	15		Recovered while open to cup 19 Hiatus
						030604	030608	4				
PA32	M7	200	030608	030729	51				1–3	17		
PA32	M7	200				030729	040530	306	4–21	17		Beginning of clog set at cup 4 Hiatus
						040530	040612	13				
PA33	M7	200	040612	050604	357				1–21	17		
						050604	050612	8				Hiatus
PA34	M7	200	050612	060604	357				1–21	17		
			Total		3472			2764				

1997, a MARK6 trap positioned at 3100 m was retrieved from station P16 (49°17'N x 134°40'W) along Line P (Fig. 1) when the carousel was on bottle 11 of 13 so seawater did not flush the cone during recovery. No sediment had collected in bottles 3–11 and a clump of material we presume arrived when bottle 2 was sampling (12 June to 7 July 1996) was intact at the base of the cone. The clump was identified as *Rhizosolenia* spp., a common genus at OSP (Section 1.2). These diatoms can form vertically-migrating mats at the surface, but are known to do so only in N-limited waters (Villareal et al., 1996; Singler and Villareal, 2005) as occur

seasonally at station P16 (Harrison et al., 2000), but not at OSP. The composition of the material in bottle b_0 (bottle 2) was BSi = 53%, CaCO₃ = 38% and POC = 2.9%. The high %BSi of the clogged bottles from OSP (Table A5) suggest these blockages also were caused by diatoms and possibly *Rhizosolenia* spp., with the exception that the clogs of traps on mooring PA22 (1000 m and 3800 m) may have been caused by gelatinous organisms since %POC was high in these bottles.

Clogs were most frequent at 3800 m, perhaps because sinking aggregates tend to consolidate and accelerate with depth (Berelson,

Table A4

Trap schedule at station AG. Dates are yymmdd.

ID	Trap model	Depth (m)	Successful sampling dates			Unsuccessful or inactive dates			Cups	Days/cup	Comments
			Begin	End	# Days	Begin	End	# Days			
AG1	M6	3700	900522	901112	174				1–12	14.5	
AG2	M7	3700	910228	911014	228	901112	910228	108	1–12	19	Hiatus 13-Cup model programmed for 12-cup rotation
AG3	M7	3700	911024	920126.5	94.5	911014	911024	10	1–7	12.5–14.5	Hiatus 21-Cup model programmed for 13-cup rotation; stopped rotating while on cup 8
AG4	M7	3500	920407	920817	132	920126.5	920407	71.5	1–11	12	Hiatus 21-Cup model programmed for 13-cup rotation; stopped rotating while on cup 12
Total			628.5			189.5					

Table A5

Failed deployments attributed to clogs at OSP with the status of all traps on the mooring when any trap clogged. Collection period, bottle number, PARFLUX trap model and composition (%) of the sediment in clogging bottle b_0 are given. PA22 traps were on two moorings separated by 5.7 km; one mooring for traps at 250 m and 850 m and another for the trap at 3800 m (Tables A1–A3). If a clog were the cause of the empty bottles of PA32, 3800 m, it must have arrived during the short period after trap deployment and before appreciable debris collected in bottle 1. No clogs were observed at station AG.

Nominal depth	1988 PA13	1993 PA22	1995 PA24	1998 PA27	2000 PA29	2003 PA32	2005 PA33
200 m	No traps	Good deployment MARK 7 High fluxes bottles 1–3 and high %POC bottles 4–5	No traps	Good deployment MARK 7 High fluxes bottles 1–4	Good deployment MARK 7 High fluxes bottles 1–2	CLOG 7/29–8/15 bottle 4 MARK 7 BSi 59 CaCO ₃ 19 POC 13	Good deployment MARK 7 Intermediate fluxes bottles 19–21
1000 m	No traps	CLOG 8/17–9/3 bottle 6 MARK 7 BSi 39 CaCO ₃ 32 POC 9.6	CLOG 7/28–8/14 bottle 5 MARK 7 BSi 58 CaCO ₃ 27 POC 6.9	Good deployment MARK 7 High fluxes bottles 2–4	Good deployment MARK 6 High fluxes bottles 1–4	Good deployment MARK 7 High fluxes bottles 3–8	Good deployment MARK 7 High fluxes bottles 18–21
3800 m	CLOG 9/3–9/20 bottle 8 MARK 5 BSi 79 CaCO ₃ 11 POC 5.0	CLOG 10/24–11/10 bottle 10 MARK 7 BSi 40 CaCO ₃ 34 POC 12	CLOG 8/14–8/31 bottle 6 MARK 7 BSi 68 CaCO ₃ 25 POC 4.0	CLOG 7/2–7/19 bottle 2 MARK 7 BSi 53 CaCO ₃ 41 POC 2.3	CLOG 7/16–8/2 bottle 3 MARK 7 BSi 50 CaCO ₃ 34 POC 2.0	CLOG? MARK 7 Fully rotated but all bottles empty	CLOG 4/14–5/1 bottle 19 MARK 7 BSi 72 CaCO ₃ 27 POC 1.8

2002) and because current speeds generally decrease with depth. We envision the horizontal approach angle at shallow traps mixing weakly consolidated aggregates within the trap's cone and spreading the arrival time of singular pulses at the base of the trap. More vertical approaches into deep traps would allow faster passage of compact aggregates through the cone, decreasing arrival duration of pulsed fluxes at the base and thus increasing the likelihood of clogs. Regardless of the cause, the possibility that some traps are pre-

disposed to clogging must be considered before deployment where moderately high or pulsed biogenic fluxes are expected.

A.3. Flux frequency distribution

Flux frequency distributions with linear (Fig. A1) and log (Fig. A2) scales. Flux climatologies based on median and log-transformed fluxes (Fig. A3).

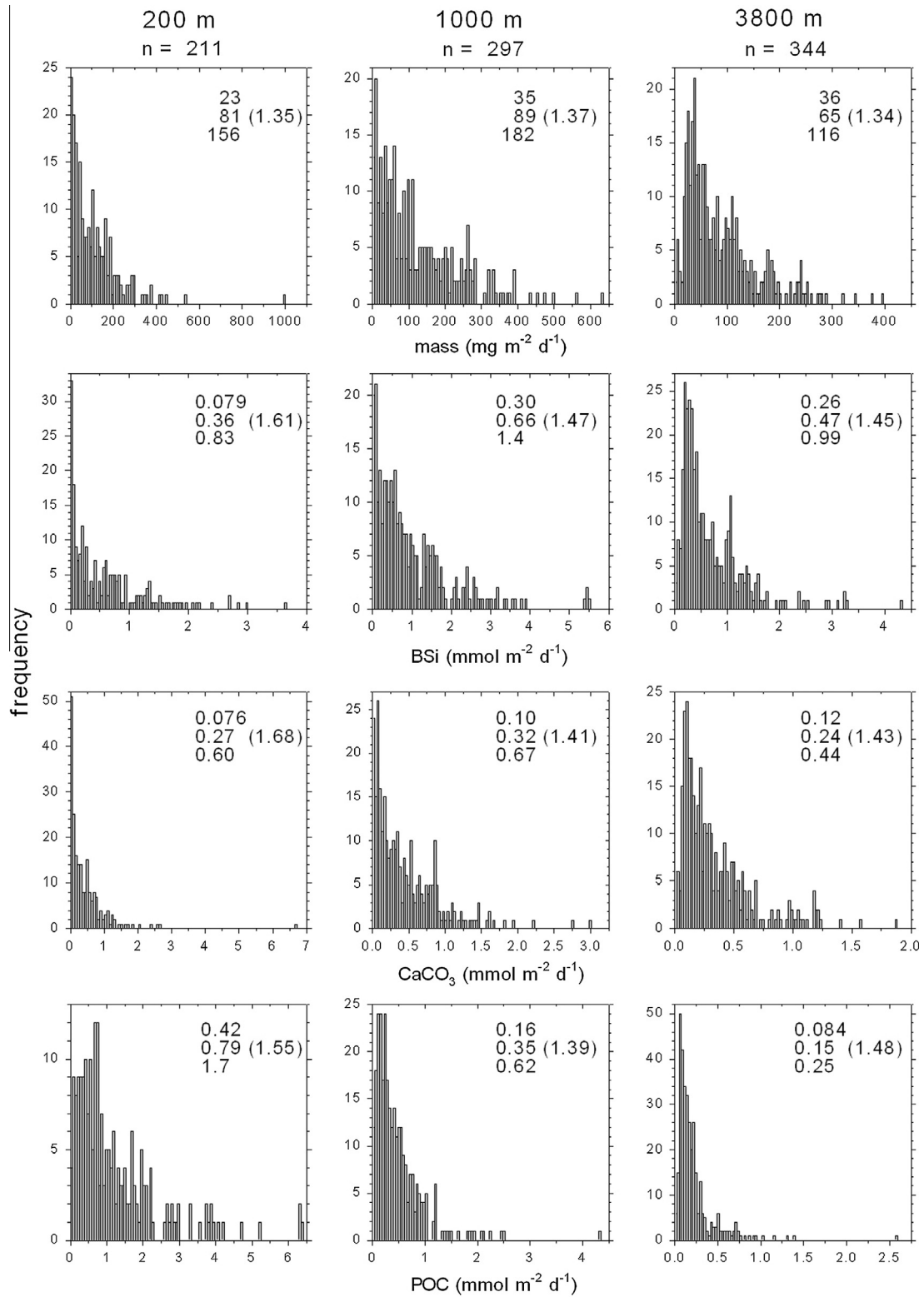


Fig. A1. Frequency distributions for mass and constituent fluxes measured at 200 m, 1000 m and 3800 m at OSP. First quartiles, medians and third quartiles are given for each distribution. Numbers in parentheses are the ratio (arithmetic mean flux):(median flux).

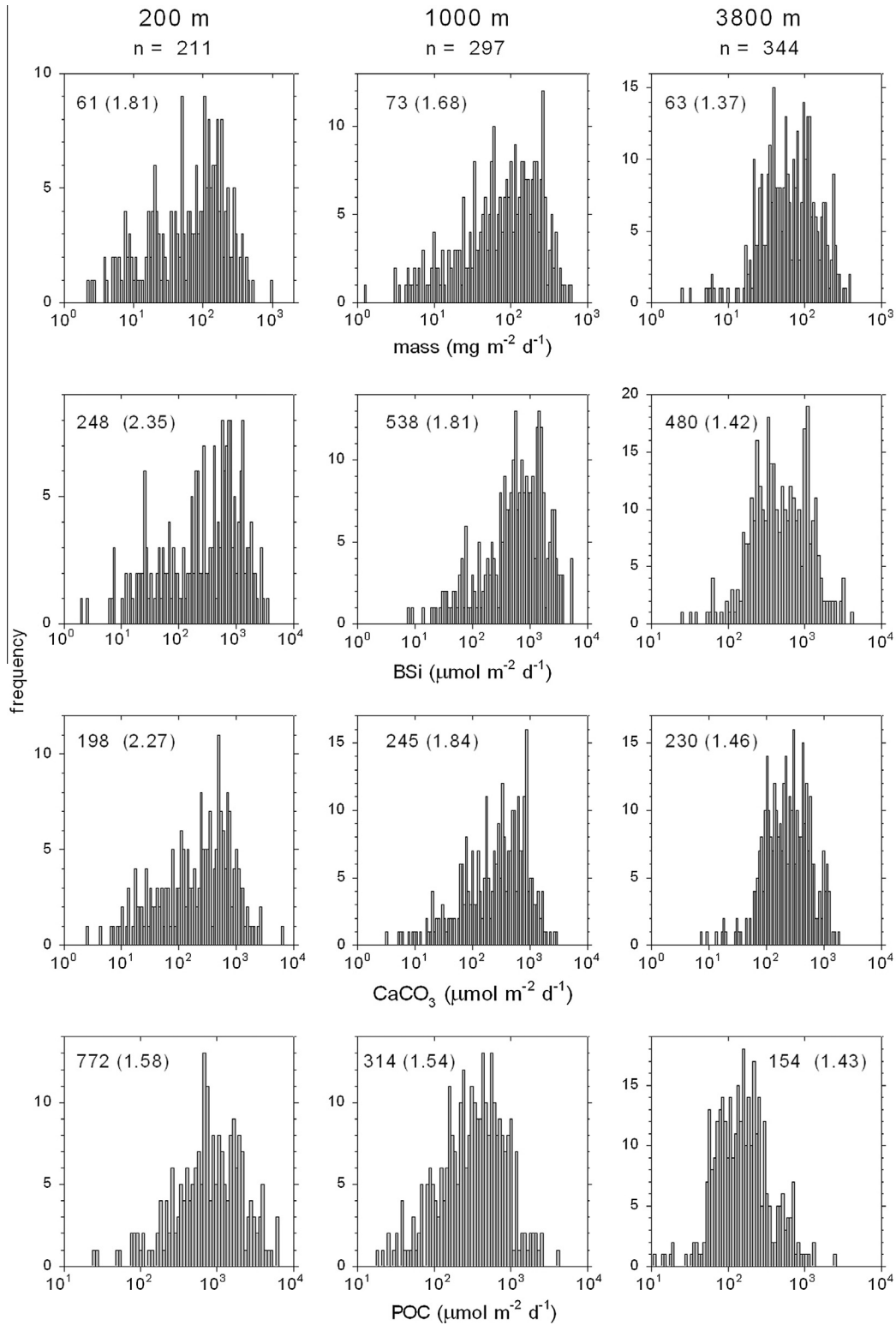


Fig. A2. Frequency distributions for log transformed mass and constituent fluxes at 200 m, 1000 m and 3800 m at OSP. Arithmetic means of the log transformed fluxes are given for each distribution. Numbers in parentheses are the ratio (arithmetic mean flux):(arithmetic mean of log transformed flux).

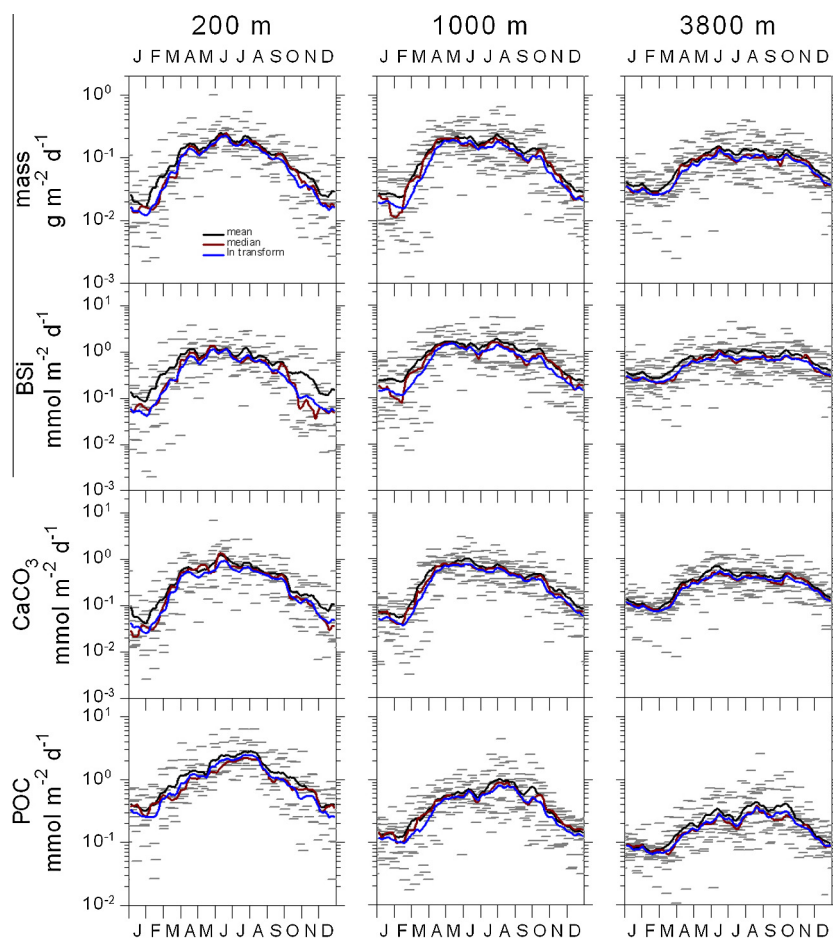


Fig. A3. Climatological curves based on arithmetic mean fluxes (Eq. (1) and Table 1), median fluxes and arithmetic means of log transformed fluxes. Reproduced from Fig. 4 with log scale showing distributions of low fluxes. Extreme events (Section 3.1.2) are plotted but not included in curves.

References

- Allison, D.G., Sutherland, I.W., 1987. The role of exopolysaccharides in adhesion of freshwater bacteria. *Journal of General Microbiology* 133, 1319–1327.
- Anderson, L.A., 1995. On the hydrogen and oxygen content of marine phytoplankton. *Deep-Sea Research I* 42, 1675–1680.
- Antia, A.N., 2005. Solubilization of particles in sediment traps: revising the stoichiometry of mixed layer export. *Biogeosciences* 2, 189–204.
- Antia, N.J., McAllister, C.D., Parsons, T.R., Stephens, K., Strickland, J.D.H., 1963. Further measurements of primary production using a large-volume plastic sphere. *Limnology and Oceanography* 8, 166–183.
- Antia, A.N., Koeve, W., Fischer, G., Blanz, T., Schulz-Bull, D., Scholten, J., Neuer, S., Kremling, K., Kuss, J., Peinert, R., Hebbeln, D., Bathmann, U., Conte, M., Fehner, U., Zeitzschel, B., 2001. Basin-wide particulate carbon flux in the Atlantic Ocean: regional export patterns and potential for atmospheric CO₂ sequestration. *Global Biogeochemical Cycles* 15, 845–862.
- Antia, A.N., Suffrian, K., Holste, L., Müller, P.J., Nejtgaard, J.C., Simonelli, P., Carotenuto, Y., Putzeys, S., 2008. Dissolution of coccolithophorid calcite by microzooplankton and copepod grazing. *Biogeosciences Discussions* 5, 1–23.
- Archer, D., Lea, D., Mahowald, N., 2000. What caused the glacial/interglacial atmospheric pCO₂ cycles? *Reviews of Geophysics* 38, 159–189.
- Armstrong, R.A., Lee, C., Hedges, J.I., Honjo, S., Wakeham, S.G., 2002. A new, mechanistic model for organic carbon fluxes in the ocean based on the quantitative association of POC with ballast minerals. *Deep-Sea Research II* 49, 219–236.
- Bacon, M.P., Anderson, R.F., 1982. Distribution of thorium isotopes between dissolved and particulate forms in the deep sea. *Journal of Geophysical Research* 87, 2045–2056.
- Bacon, M.P., Huh, C.-A., Fleer, A.P., Deuser, W.G., 1985. Seasonality in the flux of natural radionuclides and plutonium in the deep Sargasso Sea. *Deep-Sea Research* 32, 273–286.
- Barwell-Clarke, J., Whitney, F., 1996. *Institute of Ocean Sciences nutrient methods and analysis*. Institute of Ocean Sciences, Sidney, BC, p. 43.
- Benner, R., Kaiser, K., 2003. Abundance of amino sugars and peptidoglycan in marine particulate and dissolved organic matter. *Limnology and Oceanography* 48, 118–128.
- Benschop, H., 1996. Windsnelheidsmetingen op zee stations en kuststations: herleiding waarden windsnelheid naar 10-meter niveau. Koninklijk Nederlands Meteorologisch Instituut, KNMI Tech. Rapp. No. Tr-188, 16pp.
- Berelson, W.M., 2002. Particle settling rates increase with depth in the ocean. *Deep-Sea Research II* 49, 237–251.
- Berelson, W.M., Balch, W.M., Najjar, R., Feely, R.A., Sabine, C., Lee, K., 2007. Relating estimates of CaCO₃ production, export, and dissolution in the water column to measurements of CaCO₃ rain into sediment traps and dissolution on the sea floor: a revised global carbonate budget. *Global Biogeochemical Cycles* 21. <http://dx.doi.org/10.1029/2006GB002803>.
- Berger, W.H., Wefer, G., 1990. Export production: seasonality and intermittency, and paleoceanographic implications. *Palaeogeography, Palaeoclimatology, Palaeoecology (Global and Planetary Change Section)* 89, 245–254.
- Betzer, P.R., Showers, W.J., Laws, E.A., Winn, C.D., DiTullio, G.R., Kroopnick, P.M., 1984. Primary productivity and particle fluxes on a transect of the equator at 153°W in the Pacific Ocean. *Deep-Sea Research* 31, 1–11.
- Bishop, J.K.B., 1989. Regional extremes in particulate matter composition and flux: effects on the chemistry of the ocean interior. In: Berger, W.H., Smetacek, V.S., Wefer, G. (Eds.), *Productivity of the Oceans: Present and Past*. John Wiley and Sons Limited, pp. 117–137.
- Bishop, J.K.B., Wood, T.J., 2008. Particulate matter chemistry and dynamics in the twilight zone at VERTIGO ALOHA and K2 sites. *Deep-Sea Research I* 55, 1684–1706.
- Bishop, J.K.B., Calvert, S.E., Soon, M.Y.S., 1999. Spatial and temporal variability of POC in the northeast Subarctic Pacific. *Deep-Sea Research II* 46, 2699–2733.
- Blomqvist, S., Kofoed, C., 1981. Sediment trapping – a subaquatic in situ experiment. *Limnology and Oceanography* 26, 585–590.
- Bograd, S.J., Thomson, R.E., Rabinovich, A.B., LeBlond, P.H., 1999. Near-surface circulation of the northeast Pacific Ocean derived from WOCE-SVP satellite-tracked drifters. *Deep-Sea Research II* 46, 2371–2403.
- Booth, B.C., Lewin, J., Postel, J.R., 1993. Temporal variation in the structure of autotrophic and heterotrophic communities in the subarctic Pacific. *Progress in Oceanography* 32, 57–99.
- Boyd, P., Harrison, P.J., 1999. Phytoplankton dynamics in the NE subarctic Pacific. *Deep-Sea Research II* 46, 2405–2432.
- Broecker, W.S., Peng, T.H., 1982. *Tracers in the Sea*. Eldigio Press, Palisades, New York.

- Buck, K.R., Newton, J., 1995. Fecal pellet flux in Dabob Bay during a diatom bloom: contribution of microzooplankton. *Limnology and Oceanography* 40, 306–315.
- Buesseler, K.O., Livingston, H.D., Honjo, S., Hay, B.J., Konuk, T., Kempe, S., 1990. Scavenging and particle deposition in the southwestern Black Sea – evidence from Chernobyl radiotracers. *Deep-Sea Research* 37, 413–430.
- Buesseler, K.O., Steinberg, D.K., Michaels, A.F., Johnson, R.J., Andrews, J.E., Valdes, J.R., Price, J.F., 2000. A comparison of the quantity and composition of material caught in a neutrally buoyant versus surface-tethered sediment trap. *Deep-Sea Research I* 47, 277–294.
- Buesseler, K.O., Antia, A.N., Chen, M., Fowler, S.W., Gardner, W.D., Gustafsson, O., Harada, K., Michaels, A.F., van der Loeff, M.R., Sarin, M., Steinberg, D., Trull, T., 2007. An assessment of the use of sediment traps for estimating upper ocean particle fluxes. *Journal of Marine Research* 65, 345–416.
- Butman, C.A., Grant, W.D., Stolzenbach, K.D., 1986. Predictions of sediment trap biases in turbulent flows: a theoretical analysis based on observations from the literature. *Journal of Marine Research* 44, 601–644.
- Charette, M.A., Moran, S.B., 1999. Rates of particle scavenging and particulate organic carbon export estimated using ^{234}Th as a tracer in the subtropical and equatorial Atlantic Ocean. *Deep-Sea Research II* 46, 885–906.
- Chen, C.-T.A., 1990. Rates of calcium carbonate dissolution and organic carbon decomposition in the North Pacific Ocean. *Journal of the Oceanographical Society of Japan* 46, 201–210.
- Cho, B.C., Azam, F., 1988. Major role of bacteria in biogeochemical fluxes in the ocean's interior. *Nature* 332, 441–443.
- Clegg, S.L., Whitfield, M., 1990. A generalized model for the scavenging of trace metals in the open ocean-I. Particle cycling. *Deep-Sea Research* 37, 809–832.
- Clegg, S.L., Bacon, M.P., Whitfield, M., 1991. Application of a generalized scavenging model to thorium isotope and particle data at Equatorial and high-latitude sites in the Pacific Ocean. *Journal of Geophysical Research* 96, 20655–20670.
- Clemons, M.J., Miller, C.B., 1984. Blooms of large diatoms in the oceanic, subarctic Pacific. *Deep-Sea Research* 31, 85–95.
- Conte, M.H., Ralph, N., Ross, E.H., 2001. Seasonal and interannual variability in deep ocean particle fluxes at the Oceanic Flux Program (OFP)/Bermuda Atlantic Time Series (BATS) site in the western Sargasso Sea near Bermuda. *Deep-Sea Research II* 48, 1471–1505.
- Cullen, J.J., Geider, R.J., Ishizaka, J., Kiefer, D.A., Marra, J., Sakshaug, E., Raven, J.A., 1993. Toward a general description of phytoplankton growth for biogeochemical models. In: Evans, G.T., Fasham, M.J.R. (Eds.), *Towards a Model of Ocean Biogeochemical Processes*. Springer-Verlag, pp. 153–176.
- Cummins, P.F., Lagerloef, G.S.E., 2004. Wind-driven interannual variability over the northeast Pacific Ocean. *Deep-Sea Research I* 51, 2105–2121.
- De La Rocha, C.L., Passow, U., 2007. Factors influencing the sinking of POC and the efficiency of the biological carbon pump. *Deep-Sea Research II* 54, 639–658.
- De La Rocha, C.L., Nowland, N., Passow, U., 2008. Interactions between diatom aggregates, minerals, particulate organic carbon, and dissolved organic matter: further implications for the ballast hypothesis. *Global Biogeochemical Cycles* 22. <http://dx.doi.org/10.1029/2007GB003156>.
- DeMaster, D.J., 1981. The supply and accumulation of silica in the marine environment. *Geochimica et Cosmochimica Acta* 45, 1715–1732.
- Deuser, W.G., 1996. Temporal variability of particle flux in the deep Sargasso Sea. In: Ittekkot, V., Schafer, P., Honjo, S., Depetris, P.J. (Eds.), *Particle Flux in the Ocean*. John Wiley and Sons, Chichester, pp. 185–198.
- Deuser, W.G., Ross, E.H., 1980. Seasonal change in the flux of organic carbon to the deep Sargasso Sea. *Nature* 283, 364–365.
- Deuser, W.G., Muller-Kargen, F.E., Evans, R.H., Brown, O.B., Esaias, W.E., Feldman, G.C., 1990. Surface-ocean color and deep-ocean carbon flux: how close a connection? *Deep-Sea Research* 37, 1331–1343.
- Deuser, W.G., Jickells, T.D., King, P., Commeau, J.A., 1995. Decadal and annual changes in biogenic opal and carbonate fluxes to the deep Sargasso Sea. *Deep-Sea Research I* 42, 1923–1932.
- Downs, J.N., 1989. Export of Production in Oceanic Systems: Information from Phaeopigment, Carbon and Nitrogen Analyses. University of Washington.
- Dymond, J., 1984. Sediment traps, particle fluxes, and benthic boundary layer processes. In: *Global Ocean Flux Study*. U.S. National Academy Press, Woods Hole, MA, pp. 260–284.
- Emerson, S., 1987. Seasonal oxygen cycles and biological new production in surface waters of the subarctic Pacific Ocean. *Journal of Geophysical Research* 92, 6535–6544.
- Emerson, S., Hedges, J.L., 1988. Processes controlling the organic carbon content of open ocean sediments. *Paleoceanography* 3, 621–634.
- Emerson, S., Stump, C., 2010. Net biological oxygen production in the ocean: II. remote in situ measurements of O_2 and N_2 in subarctic Pacific surface waters. *Deep-Sea Research I* 57, 1255–1265.
- Emerson, S., Sabine, C., Cronin, M.F., Feely, R., Cullison Gray, S.E., DeGrandpre, M., 2011. Quantifying the flux of CaCO_3 and organic carbon from the surface ocean using in situ measurements of O_2 , N_2 , pCO_2 , and pH. *Global Biogeochemical Cycles* 25. <http://dx.doi.org/10.1029/2010GB003924>.
- Engel, A., Schartau, M., 1999. Influence of transparent exopolymer particles (TEP) on sinking velocity of *Nitzschia closterium* aggregates. *Marine Ecology Progress Series* 182, 69–76.
- Fabry, V.J., 1989. Aragonite production by pteropod molluscs in the subarctic Pacific. *Deep-Sea Research* 36, 1735–1751.
- Feely, R.A., Sabine, C.L., Lee, K., Millero, F.J., Lamb, M.F., Greeley, D., Bullister, J.L., Key, R.M., Peng, T.-H., Kozyr, A., Ono, T., Wong, C.S., 2002. In situ calcium carbonate dissolution in the Pacific Ocean. *Global Biogeochemical Cycles* 16. <http://dx.doi.org/10.1029/2002GB001866>.
- Feely, R.A., Sabine, C.L., Lee, K., Berelson, W.M., Kleypas, J., Fabry, V.J., Millero, F.J., 2004a. Impact of anthropogenic CO_2 on the CaCO_3 system in the oceans. *Science* 305, 362–366.
- Feely, R.A., Sabine, C.L., Schlitzer, R., Bullister, J.L., Mecking, S., Greeley, D., 2004b. Oxygen utilization of organic carbon remineralization in the upper water column of the Pacific Ocean. *Journal of Oceanography* 60, 45–52.
- Fiadeiro, M., 1980. The alkalinity of the deep Pacific. *Earth and Planetary Science Letters* 49, 499–505.
- Fischer, G., Futterer, D., Gersonde, R., Honjo, S., Ostermann, D., Wefer, G., 1988. Seasonal variability of particle flux in the Weddell Sea and its relation to ice cover. *Nature* 335, 426–428.
- François, R., Honjo, S., Krishfield, R., Manganini, S., 2002. Factors controlling the flux of organic carbon to the bathypelagic zone of the ocean. *Global Biogeochemical Cycles* 16. <http://dx.doi.org/10.1029/2001GB001722>.
- Fulton, J., 1983. Seasonal and Annual Variations in Net Zooplankton at Ocean Station "P", 1956–1980. Department of Fisheries and Oceans, Nanaimo, British Columbia, p. 65.
- Gardner, W.D., 1980a. Field assessment of sediment traps. *Journal of Marine Research* 38, 41–52.
- Gardner, W.D., 1980b. Sediment trap dynamics and calibration: a laboratory evaluation. *Journal of Marine Research* 38, 17–39.
- Gardner, W.D., 2000. Sediment trap technology and surface sampling in surface waters. In: Hanson, R.B., Ducklow, H.W., Field, J.G. (Eds.), *The Changing Ocean Carbon Cycle, A Midterm Synthesis of the Joint Global Ocean Flux Study*, vol. 5. Cambridge University Press, Cambridge, pp. 240–281.
- Gardner, W.D., Richardson, M.J., 1992. Particle export and resuspension fluxes in the western North Atlantic. In: Rowe, G.T., Pariente, V. (Eds.), *Deep-Sea Food Chains and the Global Carbon Cycle*. Kluwer Academic Publishers, Netherlands, pp. 339–364.
- Goes, J.L., Gomes, H.d.R., Limsakul, A., Balch, W.M., Saino, T., 2001. El Niño related interannual variations in biological production in the North Pacific as evidenced by satellite and ship data. *Progress in Oceanography* 49, 211–225.
- Goldblatt, R.H., Mackas, D.L., Lewis, A.G., 1999. Mesozooplankton community characteristics in the NE subarctic Pacific. *Deep-Sea Research II* 46, 2619–2644.
- Gust, G., Kozerski, H.-P., 2000. *In situ* sinking-particle flux from collection rates of cylindrical traps. *Marine Ecology Progress Series* 208, 93–106.
- Gust, G., Bowles, W., Giordano, S., Hüttel, M., 1996. Particle accumulation in a cylindrical sediment trap under laminar and turbulent steady flow: an experimental approach. *Aquatic Sciences* 58, 297–326.
- Haake, B., Ittekkot, V., Honjo, S., Manganini, S., 1993a. Amino acid, hexosamine and carbohydrate fluxes to the deep Subarctic Pacific (Station P). *Deep-Sea Research I* 40, 547–560.
- Haake, B., Ittekkot, V., Rixen, T., Ramaswamy, V., Nair, R.R., Curry, W.B., 1993b. Seasonality and interannual variability of particle fluxes to the deep Arabian Sea. *Deep-Sea Research I* 40, 1323–1344.
- Haake, B., Rixen, T., Reemtsma, T., Ramaswamy, V., Ittekkot, V., 1996. Processes determining seasonality and interannual variability of settling particle fluxes to the deep Arabian Sea. In: Ittekkot, V., Schäfer, P., Honjo, S., Depetris, P.J. (Eds.), *Particle Flux in the Ocean*. John Wiley & Sons Ltd., New York, pp. 251–270.
- Harrison, P.J., 2002. Station Papa time series: insights into ecosystem dynamics. *Journal of Oceanography* 58, 259–264.
- Harrison, P.J., 2006. SERIES (subarctic ecosystem response to iron enrichment study): a Canadian–Japanese contribution to our understanding of the iron-ocean-climate connection. *Deep-Sea Research II* 53, 2006–2011.
- Harrison, P.J., Boyd, P.W., Varela, D.E., Takeda, S., Shiimoto, A., Odate, T., 1999. Comparison of factors controlling phytoplankton productivity in the NE and NW subarctic Pacific gyres. *Progress in Oceanography* 43, 205–234.
- Harrison, P.J., Whitney, F.A., Tsuda, A., Saito, H., Tadokoro, K., 2004. Nutrient and plankton dynamics in the NE and NW gyres of the Subarctic Pacific Ocean. *Journal of Oceanography* 60, 93–117.
- Hawley, N., 1988. Flow in cylindrical sediment traps. *Journal of Great Lakes Research* 14, 76–88.
- Hedges, J.L., Baldock, J.A., Gélinas, Y., Lee, C., Peterson, M., Wakeham, S.G., 2001. Evidence for non-selective preservation of organic matter in sinking marine particles. *Nature* 409, 801–804.
- Hedges, J.L., Baldock, J.A., Gélinas, Y., Lee, C., Peterson, M.L., Wakeham, S.G., 2002. The biochemical and elemental compositions of marine plankton: a NMR perspective. *Marine Chemistry* 78, 47–63.
- Honda, M.C., 2003. Biological pump in Northwestern North Pacific. *Journal of Oceanography* 59, 671–684.
- Honda, M.C., Imai, K., Nojiri, Y., Hoshi, F., Sugawara, T., Kusakabe, M., 2002. The biological pump in the northwestern North Pacific based on fluxes and major components of particulate matter obtained by sediment-trap experiments (1997–2000). *Deep-Sea Research II* 49, 5595–5625.
- Honjo, S., 1978. Sedimentation of materials in the Sargasso Sea at a 5,367 m deep station. *Journal of Marine Research* 36, 469–492.
- Honjo, S., Doherty, K.W., 1988. Large aperture time-series sediment traps; design objectives construction and application. *Deep-Sea Research* 35, 133–149.
- Honjo, S., Manganini, S.J., Poppe, L.J., 1982. Sedimentation of lithogenous particles in the deep ocean. *Marine Geology* 50, 199–220.
- Honjo, S., Dymond, J., Prell, W., Ittekkot, V., 1999. Monsoon-controlled export fluxes to the interior of the Arabian Sea. *Deep-Sea Research II* 46, 1859–1902.

- Honjo, S., François, R., Manganini, S.J., Dymond, J., Collier, R., 2000. Particle fluxes to the interior of the Southern Ocean in the Western Pacific sector along 170°W. *Deep-Sea Research II* 47, 3521–3548.
- Honjo, S., Manganini, S.J., Krishfield, R.A., François, R., 2008. Particulate organic carbon fluxes to the ocean interior and factors controlling the biological pump: a synthesis of global sediment trap programs since 1983. *Progress in Oceanography* 76, 217–285.
- Ittekkot, V., Nair, R.R., Honjo, S., Ramaswamy, V., Bartsch, M., Manganini, S., Desai, B.N., 1991. Enhanced particle fluxes in Bay of Bengal induced by injection of fresh water. *Nature* 351, 385–387.
- Jacobson, D.M., Anderson, D.M., 1986. Thecate heterotrophic dinoflagellates: feeding behavior and mechanisms. *Journal of Phycology* 22, 249–258.
- Jin, X., Gruber, N., Dunne, J.P., Sarmiento, J.L., Armstrong, R.A., 2006. Diagnosing the contribution of phytoplankton functional groups to the production and export of particulate organic carbon, CaCO₃, and opal from global nutrient and alkalinity distributions. *Global Biogeochemical Cycles* 20. <http://dx.doi.org/10.1029/2005GB002532>.
- Klaas, C., Archer, D.E., 2002. Association of sinking organic matter with various types of mineral ballast in the deep sea: implications for the rain ratio. *Global Biogeochemical Cycles* 16. <http://dx.doi.org/10.1029/2001GB001765>.
- Kobari, T., Ikeda, T., 2001. Ontogenetic vertical migration and life cycle of *Neocalanus plumchrus* (Crustacea: Copepoda) in the Oyashio region, with notes on regional variations of body sizes. *Journal of Plankton Research* 23, 287–302.
- Kobari, T., Steinberg, D.K., Ueda, A., Tsuda, A., Silver, M.W., Kitamura, M., 2008. Impacts of ontogenetically migrating copepods on downward carbon flux in the western subarctic Pacific Ocean. *Deep-Sea Research II* 55, 1648–1660.
- Lam, P.J., Bishop, J.K.B., Henning, C.C., Marcus, M.A., Waychunas, G.A., Fung, I.Y., 2006. Wintertime phytoplankton bloom in the subarctic Pacific supported by continental margin iron. *Global Biogeochemical Cycles* 20. <http://dx.doi.org/10.1029/2005GB002557>.
- Lampitt, R.S., Antia, A.N., 1997. Particle flux in deep seas: regional characteristics and temporal variability. *Deep-Sea Research I* 44, 1377–1403.
- Landry, M.R., Monger, B.C., Selph, K.E., 1993. Time-dependency of microzooplankton grazing and phytoplankton growth in the subarctic Pacific. *Progress in Oceanography* 32, 205–222.
- Large, W.G., McWilliams, J.C., Niiler, P.P., 1986. Upper ocean thermal response to strong autumnal forcing of the northeast Pacific. *Journal of Physical Oceanography* 16, 1524–1550.
- Laws, E.A., 1991. Photosynthetic quotients, new production and net community production in the open ocean. *Deep-Sea Research* 38, 143–167.
- Laws, E.A., Falkowski, P.G., Smith, W.O.J., Ducklow, H., McCarthy, J.J., 2000. Temperature effects on export production in the open ocean. *Global Biogeochemical Cycles* 14, 1231–1246.
- Lee, C., Wakeham, S., Arnosti, C., 2004. Particulate organic matter in the sea: the compositional conundrum. *Ambio* 33, 565–575.
- Lipsen, M.S., Crawford, D.W., Gower, J., Harrison, P.J., 2007. Spatial and temporal variability in coccolithophore abundance and production of PIC and POC in the NE subarctic Pacific during El Niño (1998), La Niña (1999) and 2000. *Progress in Oceanography* 75, 304–325.
- Lohrenz, S.E., Knauer, G.A., Asper, V.L., Tuel, M., Michaels, A.F., Knap, A.H., 1992. Seasonal variability in primary production and particle flux in the northwestern Sargasso Sea: U.S. JGOFS Bermuda Atlantic Time-series Study. *Deep-Sea Research* 7/8, 1373–1391.
- Lomas, M.W., Steinberg, D.K., Dickey, T., Carlson, C.A., Nelson, N.B., Condon, R.H., Bates, N.R., 2009. Increased ocean carbon export in the Sargasso Sea is countered by its enhanced mesopelagic attenuation. *Biogeosciences Discussions* 6, 9547–9582.
- Mackas, D.L., Goldblatt, R., Lewis, A.G., 1998. Interdecadal variation in developmental timing of *Neocalanus plumchrus* populations at Ocean Station P in the subarctic North Pacific. *Canadian Journal of Fisheries and Aquatic Sciences* 55, 1878–1893.
- Maldonado, M.T., Boyd, P.W., Harrison, P.J., Price, N.M., 1999. Co-limitation of phytoplankton growth by light and Fe during winter in the NE subarctic Pacific Ocean. *Deep-Sea Research II* 46, 2475–2485.
- Martin, J.H., Fitzwater, S.E., 1988. Iron deficiency limits phytoplankton growth in the north-east Pacific subarctic. *Nature* 331, 341–343.
- Martin, J.H., Knauer, G.A., Karl, D.M., Broenkow, W.W., 1987. VERTEX: carbon cycling in the northeast Pacific. *Deep-Sea Research* 34, 267–285.
- Mayer, L.M., 1995. Sedimentary organic matter preservation: an assessment and speculative synthesis – a comment. *Marine Chemistry* 49, 123–126.
- McCave, I.N., Hall, I.R., Antia, A.N., Chou, L., Dehairs, F., Lampitt, R.S., Thomsen, L., vanWeering, T.C.E., Wollast, R., 2001. Distribution, composition and flux of particulate material over the European margin at 47°–50°N. *Deep-Sea Research II* 48, 3107–3139.
- McClain, C.R., Arrigo, K., Tai, K.-S., Turk, D., 1996. Observations and simulations of physical and biological processes at ocean weather station P, 1951–1980. *Journal of Geophysical Research* 101, 3697–3713.
- McDonald, D., Pedersen, T.F., Crusius, J., 1999. Multiple late Quaternary episodes of exceptional diatom production in the Gulf of Alaska. *Deep-Sea Research II* 46, 2993–3017.
- McEwen, G.F., Johnson, M.W., Folsom, T.R., 1954. A statistical analysis of the performance of the Folsom plankton sample splitter, based upon test observations. *Meteorology and Atmospheric Physics* 7, 502–527.
- McKay, R.M.L., Villareal, T.A., La Roche, J., 2000. Vertical migration by *Rhizosolenia* spp. (bacillariophyceae): implications for Fe acquisition. *Journal of Phycology* 36, 669–674.
- Michaels, A.F., Silver, M.W., Gowing, M.M., Knauer, G.A., 1990. Cryptic zooplankton “swimmers” in upper ocean sediment traps. *Deep-Sea Research* 37, 1285–1296.
- Miller, C.B., Frost, B.W., Batchelder, H.P., Clemons, M.J., Conway, R.E., 1984. Life histories of large, grazing copepods in a subarctic ocean gyre: *Neocalanus plumchrus*, *Neocalanus cristatus*, and *Eucalanus bungii* in the Northeast Pacific. *Progress in Oceanography* 13, 201–243.
- Miller, C.B., Denman, K.L., Gargett, A.E., Mackas, D.L., Wheeler, P.A., Booth, B.C., Frost, B.W., Landry, M.R., Lewin, J., Lorenzen, C.J., Perry, M.J., Dagg, M., Welschmeyer, N., 1988. Lower trophic level production dynamics in the oceanic Subarctic Pacific Ocean. In: Nemoto, T., Pearcy, W.G. (Eds.), *The Biology of the Subarctic Pacific – Proceedings of the Japan-United States of America Seminar on the Biology of Micronekton of the Subarctic Pacific*. Ocean Research Institute, University of Tokyo, Nakano, Tokyo, Japan, pp. 1–26.
- Milliman, J.D., Troy, P.J., Balch, W.M., Adams, A.K., Li, Y.-H., Mackenzie, F.T., 1999. Biologically mediated dissolution of calcium carbonate above the chemical lysocline? *Deep-Sea Research I* 46, 1653–1669.
- Moore, J.K., Villareal, T.A., 1996. Buoyancy and growth characteristics of three positively buoyant marine diatoms. *Marine Ecology Progress Series* 132, 203–213.
- Mortlock, R.A., Froelich, P.N., 1989. A simple method for the rapid determination of biogenic opal in pelagic marine sediments. *Deep-Sea Research* 36, 1415–1426.
- Müller, P.J., 1977. C/N ratios in Pacific deep-sea sediments: effect of inorganic ammonium and organic nitrogen compounds sorbed by clays. *Geochimica et Cosmochimica Acta* 41, 765–776.
- Müller, P.J., Suess, E., 1979. Productivity, sedimentation rate, and sedimentary organic matter in the oceans – I. Organic carbon preservation. *Deep-Sea Research* 26A, 1347–1362.
- Murnane, R.J., 1994. Determination of thorium and particulate matter cycling parameters at station P: a reanalysis and comparison of least squares techniques. *Journal of Geophysical Research* 99, 3393–3405.
- Murnane, R.J., Sarmiento, J.L., Bacon, M.P., 1990. Thorium isotopes, particle cycling models, and inverse calculations of model rate constants. *Journal of Geophysical Research* 95, 16195–16206.
- Nagata, T., Fukuda, H., Fukuda, R., Koibe, I., 2000. Bacterioplankton distribution and production in deep Pacific waters: large-scale geographic variations and possible coupling with sinking particle fluxes. *Limnology and Oceanography* 45, 426–435.
- Neuer, S., Ratmeyer, V., Davenport, R., Fischer, G., Wefer, G., 1997. Deep water particle flux in the Canary Island region: seasonal trends in relation to long-term satellite derived pigment data and lateral sources. *Deep-Sea Research I* 44, 1451–1466.
- Newton, P.P., Lampitt, R.S., Jickells, T.D., King, P., Boutle, C., 1994. Temporal and spatial variability of biogenic particle fluxes during the JGOFS northeast Atlantic process studies at 47°N, 20°W. *Deep-Sea Research* 41, 1617–1642.
- Parsons, T.R., Stephens, K., Strickland, J.D.H., 1961. On the chemical composition of eleven species of marine phytoplankters. *Journal of the Fisheries Research Board of Canada* 18, 1001–1025.
- Passow, U., 2004. Switching perspectives: do mineral fluxes determine particulate organic carbon fluxes or vice versa? *Geochemistry Geophysics Geosystems* 5. <http://dx.doi.org/10.1029/2003GC000670>.
- Passow, U., De La Rocha, C.L., 2006. Accumulation of mineral ballast on organic aggregates. *Global Biogeochemical Cycles* 20. <http://dx.doi.org/10.1029/2005GB002579>.
- Passow, U., French, M.A., Robert, M., 2011. Biological controls on dissolution of diatom frustules during their descent to the deep ocean: lessons learned from controlled laboratory experiments. *Deep-Sea Research I* 58, 1147–1157.
- Peña, M.A., Varela, D.E., 2007. Seasonal and interannual variability in phytoplankton and nutrient dynamics along Line P in the NE subarctic Pacific. *Progress in Oceanography* 75, 200–222.
- Platt, T., Harrison, W.G., Lewis, M.R., Li, W.K.W., Sathyendranath, S., Smith, R.E., Vezina, A.F., 1989. Biological production of the oceans: the case for a consensus. *Marine Ecology Progress Series* 52, 77–88.
- Primeau, F., 2006. On the variability of the exponent in the power law depth dependence of POC flux estimated from sediment traps. *Deep-Sea Research I* 53, 1335–1343.
- Putland, J.N., Whitney, F.A., Crawford, D.W., 2004. Survey of bottom-up controls of *Emiliania huxleyi* in the Northeast Subarctic Pacific. *Deep-Sea Research I* 51, 1793–1802.
- Redfield, A.C., Ketchum, B.H., Richards, F.A., 1963. The influence of organisms on the composition of sea-water. In: Hill, M.N. (Ed.), *The Sea*, vol. 2. John Wiley & Sons, New York, pp. 26–77.
- Reynolds, L., Thunell, R.C., 1985. Seasonal succession of planktonic foraminifera in the subpolar North Pacific. *Journal of Foraminiferal Research* 15, 282–301.
- Reynolds, L., Thunell, R.C., 1986. Seasonal production and morphologic variation of *Neoglobobulimina pachyderma* (Ehrenberg) in the northeast Pacific. *Micropaleontology* 32, 1–18.
- Richardson, T.L., Cullen, J.J., 1995. Changes in buoyancy and chemical composition during growth of a coastal marine diatom: ecological and biogeochemical consequences. *Marine Ecology Progress Series* 128, 77–90.
- Rivkin, R.B., Putland, J.N., Anderson, M.R., Deibel, D., 1999. Microzooplankton bacterivory and herbivory in the NE subarctic Pacific. *Deep-Sea Research II* 46, 2579–2618.
- Sakshaug, E., 1993. The relationship between phytoplankton growth rate and production with emphasis on respiration and excretion. In: Li, W.K.W.,

- Maestrini, S.Y. (Eds.), Measurement of Primary Production from the Molecular to the Global Scale, vol. 197. La Rochelle, pp. 63–68.
- Sarmiento, J.L., Dunne, J., Gnanadesikan, A., Key, R.M., Matsumoto, K., Slater, R., 2002. A new estimate of the CaCO₃ to organic carbon export ratio. *Global Biogeochemical Cycles* 16. <http://dx.doi.org/10.1029/2002GB001919>.
- Sarmiento, J.L., Simeon, J., Gnanadesikan, A., Gruber, N., Key, R.M., Schlitzer, R., 2007. Deep ocean biogeochemistry of silicic acid and nitrate. *Global Biogeochemical Cycles* 21. <http://dx.doi.org/10.1029/2006GB002720>.
- Sautter, L.R., Thunell, R.C., 1989. Seasonal succession of planktonic foraminifera: results from a four-year time-series sediment trap experiment in the Northeast Pacific. *Journal of Foraminiferal Research* 19, 253–267.
- Savidge, G., Boyd, P., Pomroy, A., Harbour, D., Joint, I., 1995. Phytoplankton production and biomass estimates in the northeast Atlantic Ocean, May–June 1990. *Deep-Sea Research I* 42, 599–617.
- Schlitzer, R., 2004. Export production in the Equatorial and North Pacific derived from dissolved oxygen, nutrient and carbon data. *Journal of Oceanography* 60, 53–62.
- Schmidt, M., Botz, R., Rickert, D., Bohrmann, G., Hall, S.R., Mann, S., 2001. Oxygen isotopes of marine diatoms and relations to opal-A maturation. *Geochimica et Cosmochimica Acta* 65, 201–211.
- Schneider, B., Schlitzer, R., Fischer, G., Nöthig, E.-M., 2003. Depth-dependent elemental compositions of particulate organic matter (POM) in the ocean. *Global Biogeochemical Cycles* 17, 1032. [10.1029/2002GB001871](http://dx.doi.org/10.1029/2002GB001871).
- Schnetzler, A., Steinberg, D.K., 2002. Active transport of particulate organic carbon and nitrogen by vertically migrating zooplankton in the Sargasso Sea. *Marine Ecology Progress Series* 234, 71–84.
- Siegel, D.A., Fields, E., Buesseler, K.O., 2008. A bottom-up view of the biological pump: modeling source funnels above ocean sediment traps. *Deep-Sea Research I* 55, 108–127.
- Singler, H.R., Villareal, T.A., 2005. Nitrogen inputs into the euphotic zone by vertically migrating *Rhizosolenia* mats. *Journal of Plankton Research* 27, 545–556.
- Smayda, T.J., 1970. The suspension and sinking of phytoplankton in the sea. *Oceanography and Marine Biology Annual Review* 8, 353–414.
- Smetacek, V.S., 1985. Role of sinking in diatom life-history cycles: ecological, evolutionary and geological significance. *Marine Biology* 84, 239–251.
- Smith Jr., K.L., Kaufmann, R.S., 1999. Long-term discrepancy between food supply and demand in the deep eastern North Pacific. *Science* 284, 1174–1177.
- Smith Jr., K.L., Baldwin, R.J., Ruhl, H.A., Kahru, M., Mitchell, B.G., Kaufmann, R.S., 2006. Climate effect on food supply to depths greater than 4,000 meters in the northeast Pacific. *Limnology and Oceanography* 51, 166–176.
- Solomon, S., Qin, D., Manning, M., Marquis, M., Averyt, K.B., Tignor, M., Miller, H.L., Chen, Z. (Eds.), 2007. *Climate Change 2007: The Physical Science Basis*. Cambridge University Press, Cambridge, United Kingdom and New York, NY, USA.
- Stanley, R.H.R., Buesseler, K.O., Manganini, S.J., Steinberg, D.K., Valdes, J.R., 2004. A comparison of major and minor elemental fluxes collected in neutrally buoyant and surface-tethered sediment traps. *Deep-Sea Research I* 51, 1387–1395.
- Strom, S.L., Welschmeyer, N.A., 1991. Pigment-specific rates of phytoplankton growth and microzooplankton grazing in the open subarctic Pacific Ocean. *Limnology and Oceanography* 36, 50–63.
- Strom, S.L., Postel, J.R., Booth, B.C., 1993. Abundance, variability, and potential grazing impact of planktonic ciliates in the open subarctic Pacific Ocean. *Progress in Oceanography* 32, 185–203.
- Suess, E., 1980. Particulate organic carbon flux in the oceans – surface productivity and oxygen utilization. *Nature* 288, 260–263.
- Tabata, S., 1961. Temporal changes of salinity, temperature, and dissolved oxygen content of the water at Station “P” in the Northeast Pacific Ocean, and some of their determining factors. *Journal of the Fisheries Research Board of Canada* 18, 1073–1124.
- Tabata, S., 1991. Annual and interannual variability of baroclinic transports across Line P in the northeast Pacific Ocean. *Deep-Sea Research* 38, S221–S245.
- Tabata, S., Weichselbaumer, W.E., 1992. An Update of the Statistics of Hydrographic/CTD Data Taken at Ocean Station P (May 1956–September 1990). *Institute of Ocean Sciences, Sidney, BC*, p. 75.
- Takahashi, K., 1986. Seasonal fluxes of pelagic diatoms in the subarctic Pacific, 1982–1983. *Deep-Sea Research* 33, 1225–1251.
- Takahashi, K., 1987a. Radiolarian flux and seasonality: climatic and El Niño response in the subarctic Pacific, 1982–1984. *Global Biogeochemical Cycles* 1, 213–231.
- Takahashi, K., 1987b. Response of Subarctic Pacific diatom fluxes to the 1982–1983 El Niño disturbance. *Journal of Geophysical Research* 92, 14387–14392.
- Takahashi, K., 1987c. Seasonal fluxes of silicoflagellates and Actiniscus in the subarctic Pacific during 1982–1984. *Journal of Marine Research* 45, 397–425.
- Takahashi, K., 1989. Silicoflagellates as productivity indicators: evidence from long temporal and spatial flux variability responding to hydrography in the northeastern Pacific. *Global Biogeochemical Cycles* 3, 43–61.
- Takahashi, K., 1997a. Siliceous microplankton fluxes in the Eastern Subarctic Pacific, 1982–1986. *Journal of Oceanography* 53, 455–466.
- Takahashi, K., 1997b. Time-series fluxes of Radiolaria in the eastern subarctic Pacific Ocean. *News of Osaka Micropaleontologists* 10, 299–309.
- Takahashi, K., Honjo, S., Tabata, S. (1989). Siliceous phytoplankton flux: interannual variability and response to hydrographic changes in the Northeastern Pacific. In: Peterson, D. (Ed.), *Aspects of Climate Variability in the Pacific and Western Americas*. Geophysical Monographs, vol. 55. AGU, pp. 151–160.
- Takahashi, K., Billings, J.D., Morgan, J.K., 1990. Oceanic province: assessment from the time-series diatom fluxes in the northeastern Pacific. *Limnology and Oceanography* 35, 154–165.
- Takahashi, K., Fujitani, N., Yanada, M., Maita, Y., 2000. Long-term biogenic particle fluxes in the Bering Sea and the central subarctic Pacific Ocean, 1990–1995. *Deep-Sea Research I* 47, 1723–1759.
- Taylor, G.T., Karl, D.M., 1991. Vertical fluxes of biogenic particles and associated biota in the eastern North Pacific: implications for biogeochemical cycling and productivity. *Global Biogeochemical Cycles* 5, 289–303.
- Taylor, S.R., McClennan, S.M., 1985. *The Continental Crust: Its Composition and Evolution*. Blackwell Scientific.
- Thibault, D., Roy, S., Wong, C.S., Bishop, J.K., 1999. The downward flux of biogenic material in the NE Subarctic Pacific: importance of algal sinking and mesozooplankton herbivory. *Deep-Sea Research II* 46, 2669–2697.
- Thomas, B.R., Kent, E.C., Swail, V.R., 2005. Methods to homogenize wind speeds from ships and buoys. *International Journal of Climatology*, 979–995.
- Thunell, R.C., Honjo, S., 1987. Seasonal and interannual changes in planktonic foraminiferal production in the North Pacific. *Nature*, 335–337.
- Timothy, D.A., 2004. Organic matter remineralisation and biogenic silica dissolution in a deep fjord in British Columbia, Canada: a regression analysis of upper ocean sediment-trap flux. *Deep-Sea Research I* 51, 439–456.
- Timothy, D.A., Pond, S., 1997. Describing additional fluxes to deep sediment traps and water-column decay in a coastal environment. *Journal of Marine Research* 55, 383–406.
- Toth, D.J., Lerman, A., 1977. Organic matter reactivity and sedimentation rates in the ocean. *American Journal of Science* 277, 465–485.
- Tsurumi, M., Mackas, D.L., Whitney, F.A., DiBacco, C., Galbraith, M.D., Wong, C.S., 2005. Pteropods, eddies, carbon flux, and climate variability in the Alaska Gyre. *Deep-Sea Research II* 52, 1037–1053.
- Varela, D.E., Harrison, P.J., 1999. Seasonal variability in nitrogenous nutrition of phytoplankton assemblages in the northeastern subarctic Pacific Ocean. *Deep-Sea Research II* 46, 2505–2538.
- Verity, P.G., Williams, S.C., Hong, Y., 2000. Formation, degradation, and mass:volume ratios of detritus derived from decaying phytoplankton. *Marine Ecology Progress Series* 207, 53–68.
- Villareal, T.A., Woods, S., Moore, J.K., Culver-Rymsza, K., 1996. Vertical migration of *Rhizosolenia* mats and their significance to NO₃ fluxes in the central North Pacific gyre. *Journal of Plankton Research* 18, 1103–1121.
- Waite, A.M., Nodder, S.D., 2001. The effect of in situ iron addition on the sinking rates and export flux of Southern Ocean diatoms. *Deep-Sea Research II* 48, 2635–2654.
- Waite, A.M., Thompson, P.A., Harrison, P.J., 1992. Does energy control the sinking rates of marine diatoms? *Limnology and Oceanography* 37, 468–477.
- Wakeham, S.G., Hedges, J.L., Lee, C., Pease, T.K., 1993. Effects of poisons and preservatives on the composition of organic matter in a sediment trap experiment. *Journal of Marine Research* 51, 669–696.
- Wakeham, S.G., Lee, C., Hedges, J.L., Hernes, P.J., Peterson, M.L., 1997. Molecular indicators of diagenetic status in marine organic matter. *Geochimica et Cosmochimica Acta* 61, 5363–5369.
- Walsh, I., Fischer, K., Murray, D., Dymond, J., 1988. Evidence for resuspension of rebound particles from near-bottom sediment traps. *Deep-Sea Research* 35, 59–70.
- Wang, W.-y., Shao, Q.-q., 2008. Remote sensing of sea surface features: implications of fisheries in the North Pacific Ocean. *The International Archives of the Photogrammetry, Remote Sensing and Spatial Information Sciences* 37, 659–664.
- Waniek, J., Koeve, K., Prien, R.D., 2000. Trajectories of sinking particles and the catchment areas above sediment traps in the northeast Atlantic. *Journal of Marine Research* 58, 983–1006.
- Welschmeyer, N., Goericke, R., Strom, S., Peterson, W., 1991. Phytoplankton growth and herbivory in the subarctic Pacific: a chemotaxonomic analysis. *Limnology and Oceanography* 36, 1631–1649.
- Welschmeyer, N.A., Strom, S., Goericke, R., DiTullio, G., Belvin, M., Petersen, W., 1993. Primary production in the subarctic Pacific Ocean: Project SUPER. *Progress in Oceanography* 32, 101–135.
- Wheeler, P.A., Kokkinakis, S.A., 1990. Ammonium recycling limits nitrate use in the oceanic subarctic Pacific. *Limnology and Oceanography* 35, 1267–1278.
- Whitney, F.A., Freeland, H.J., 1999. Variability in upper-ocean water properties in the NE Pacific Ocean. *Deep-Sea Research II* 46, 2351–2370.
- Wong, C.S., Crawford, D.W., 2002. Flux of particulate inorganic carbon to the deep subarctic Pacific correlates with El Niño. *Deep-Sea Research II* 49, 5705–5715.
- Wong, C.S., Matear, R.J., 1999. Sporadic silicate limitation of phytoplankton productivity in the subarctic NE Pacific. *Deep-Sea Research II* 46, 2539–2555.
- Wong, C.S., Whitney, F.A., Iseki, K., Page, J.S., Zeng, J., 1995. Analysis of trends in primary productivity and chlorophyll-a over two decades at Ocean Station P (50°N 145°W) in the Subarctic Northeast Pacific Ocean. *Canadian Journal of Fisheries and Aquatic Sciences* 121, 107–117.
- Wong, C.S., Whitney, F.A., Crawford, D.W., Iseki, K., Matear, R.J., Johnson, W.K., Page, J.S., Timothy, D., 1999. Seasonal and interannual variability in particle fluxes of carbon, nitrogen and silicon from time series of sediment traps at Ocean Station P, 1982–1993: relationship to changes in subarctic primary productivity. *Deep-Sea Research II* 46, 2735–2760.

- Wong, C.S., Waser, N.A.D., Nojiri, Y., Whitney, F.A., Page, J.S., Zeng, J., 2002. Seasonal cycles of nutrients and dissolved inorganic carbon at high and mid latitudes in the North Pacific Ocean during the *Skaugran* cruises: determination of new production and nutrient uptake ratios. *Deep-Sea Research II* 49, 5317–5338.
- Zhou, J., Mopper, K., Passow, U., 1998. The role of surface-active carbohydrates in the formation of transparent exopolymer particles by bubble adsorption of seawater. *Limnology and Oceanography* 43, 1860–1871.